NORTHWESTERN UNIVERSITY

Synaptic integration in excitable CA1 pyramidal neuron dendrites

A DISSERTATION

SUBMITTED TO THE GRADUATE SCHOOL

IN PARTIAL FULFILLMENT OF THE REQUIREMENTS

for the degree

DOCTOR OF PHILOSOPHY

Field of Neuroscience

By

Yael Katz

EVANSTON, ILLINOIS

December 2008

ABSTRACT

Synaptic integration in excitable CA1 pyramidal neuron dendrites

Yael Katz

A pyramidal neuron receives thousands of inputs spread throughout its dendritic tree, which it must integrate into a decision about whether or not to fire action-potential output. Since action potentials are the primary means by which these neurons communicate with their network partners, understanding this input-output relationship is critical for understanding information processing in the cerebral cortex.

Using a combined approach of computational modeling and experimentation, we find that voltage attenuation reduces EPSPs generated at many distal synapses to negligible levels at the soma in CA1 pyramidal neurons. Distance-dependent conductance scaling is insufficient to overcome attenuation for these inputs; instead, they are predicted to communicate using dendritic spikes. Experiments corroborate this prediction: AMPA receptor density increases with distance from the soma, but decreases in the most distal region of the cell.

Dendrites are more excitable near their terminal ends than near their branch points, so in the absence of compensatory mechanisms, dendritic spikes would be preferentially

initiated at distal locations. Using serial-section electron microscopy to reconstruct apical oblique dendrites of CA1 pyramidal neurons, we find that synapse density and strength is greater near branch points than near terminal ends. Incorporating this result into our computational model, we find that synapses are organized to normalize the contribution of inputs to dendritic spike initiation and optimize the contribution of each branch to axonal output.

Both the initiation and propagation of dendritic spikes are affected by inhibition. Using experimentally-constrained computational models to investigate the effect of inhibition targeting different somato-dendritic domains of pyramidal cells, we show how the dynamics of CA1 microcircuits depend on the location, magnitude, timing, and biophysical properties of inhibitory relative to excitatory inputs.

In order to understand how the biophysical properties of CA1 pyramidal neuron dendrites contribute to the ability of the hippocampus to navigate space, we directly simulate the spatial alternation task using a network consisting of biophysically realistic model neurons. In the model, the integration of place and temporal context information arriving on the distal and more proximal apical dendrites of CA1 pyramidal neurons respectively make them splitter cells, cells which fire selectively based on a combination of place and temporal context. These cells store a memory of the previous path through the environment, which the animal uses to navigate to a reward site.

Acknowledgements

First, I would like to thank Nelson Spruston for the time, advice, support, and many insights he has given me over the past four years. His door was always open and I was truly fortunate to have him as an advisor. Nelson taught me to demand perfection in every aspect of research, and I hope I can live up to his high standard.

Bill Kath, my second advisor, is a rare combination of brilliance and modesty. I could ask him any question, big or small, and I thank him for our many discussions both about work and life.

Dan Nicholson had exceptional patience in training me in the art of serial-section EM. His unwavering optimism is the reason I got through the experiment, and I am grateful.

I thank Mike Hasselmo for his hospitality when I spent a quarter in his lab at BU.

Members of my thesis committee, David Ferster and Indira Raman, provided me with their guidance, and I appreciate it.

I thank Krutika Lakhoo, Betsy Piekarz, and Annie Liu for their technical support, conscientiousness, and positive attitude.

To my labmates: Vilas Menon, Rachel Trana, Michael Rempe, Catherine Kaczorowski, Shannon Moore, Jason Hardie, and Stefan Remy, thanks for the science, the friendship and the fun times.

To the NU presidential fellows and to the NICO reading group: thank you for keeping me interested and maintaining my faith in academia.

I could not have made it through grad school without my family. I would like to express my heartfelt thanks to:

My father, Avi, for teaching me to love learning, to be an optimist, and to try anything.

My mother, Chava, for her devotion to her children.

Above all, Aryeh, my colleague, my friend, and the best husband anyone could want, for his humor, love, and constant support.

Finally, my baby, Ilana, for helping me keep things in perspective.

I acknowledge the National Science Foundation (NSF-IGERT, DGE 9987577) and Northwestern University (Presidential Fellowship) for supporting this work.

Dedication

This thesis is dedicated to my grandfather, Frank Katz. A model of perseverance, his hard work is the reason I got to where I am today.

Table of Contents

List of Tables

List of Figures

CHAPTER 1

Introduction

Ever since Democrites identified the brain as the organ that controls behavior in the 5^{th} century BCE, it has intrigued scientists, philosophers, and lay people alike, and how the biophysics of neurons contributes to behavior remains at the heart of neuroscience today. Addressing this issue benefits from a combination of experimentation and quantitative modeling: experiments to determine the detailed properties of neurons and the connections between them, and models to fit together these details, because bridging events across multiple spatial and temporal scales is difficult to do by intuition alone.

This thesis focuses on understanding the input-output functions of individual pyramidal neurons. How do these neurons integrate information from thousands of inputs to produce binary output? An experimentally-constrained computational model of a CA1 pyramidal neuron is developed and used to study ways in which inputs at locations all throughout the dendritic tree communicate with the neuron's output site in the axon. Quantitative predictions about the organization of synapses along CA1 dendrites are formulated, and tested using serial-section electron microscopy. The experimental findings are incorporated back into the model to assess their functional implications. Finally, a network model of the hippocampus consisting of biophysically-realistic reduced model neurons is constructed, and the output of the network is used to guide a virtual rat in a simulated behavioral task.

1.1. Pyramidal neuron morphology and synaptic integration

Pyramidal neurons (reviewed in Spruston, 2008) are a major type of excitatory neuron in the cerebral cortex. They are found in fish, reptiles, birds, and mammals in many forebrain structures including the hippocampus, cortex, and amygdala (Ramon y Cajal,

1897). The fact that these cells are conserved across a large evolutionary distance is evidence for their adaptive value and their presence in brain structures associated with higher cognitive function suggests that pyramidal neurons are important for the instantiation of these functions.

Although there are important differences between pyramidal neurons in different species and in different brain structures, they all have extended, branched morphologies (Ramon y Cajal, 1897) (Figure 1.1a,b). Pyramidal neuron cell bodies are shaped like pyramids, giving these neurons their names. They have a primary apical dendrite emanating from the apex of their somata with many oblique apical side branches extending from it. The primary apical dendrite bifurcates, culminating in an apical tuft. Pyramidal neurons also have distinct basal dendritic trees extending from the base of their somata. Output is generated from a single axon that arborizes extensively (Bannister & Larkman, 1995; DeFelipe & Farinas, 1992; Ramon y Cajal, 1897). The signature branched morphologies of pyramidal neurons both provide opportunities for increased computing power and create challenges that must be overcome.

Figure 1.1. Computer reconstruction of a CA1 pyramidal neuron from rat hippocampus. Distinct apical and basal dendritic trees emanate from the apex and base of the soma, respectively. The primary apical dendrite bifurcates and culminates in an apical tuft. B. Biocytin-filled CA1 pyramidal neurons in a brain slice from rat hippocampus. CA1 pyramidal neuron tufts reside in stratum lacunosum moleculare (slm), their apical dendrites are in stratum radiatum (sr), their somata are in stratum pyramidale (sp), and their basal dendrites are in stratum oriens (so). C. Two inputs to CA1 apical dendrites. The perforant-path input from entorhinal cortex (purple) selectively innervates CA1 apical tufts and the Schaffer collaterals from CA3 (green) targets their apical dendrites. Figures courtesy of the Spruston laboratory.

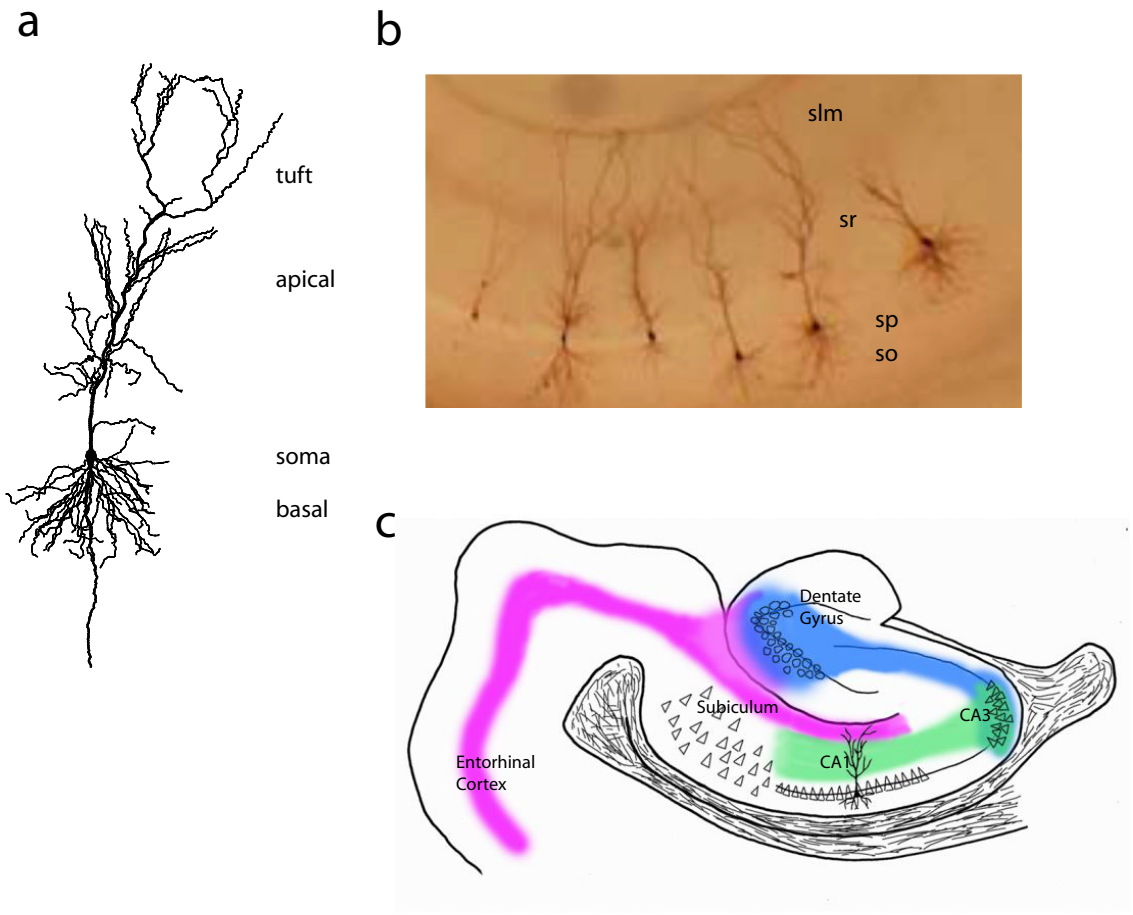
a
tuft
apical
soma
basal
b
slm
sr
sp
so
c
Dentate
Gyrus
Subiculum
CA3
CA1
Entorhinal
Cortex

Figure 1.1.

Fundamentally, pyramidal neurons are input-output devices, and inputs have two ways of influencing neuronal output. They can trigger voltage signals that spread passively from input site to output site and depolarize the axon directly, or they can activate voltage-gated channels locally and trigger dendritic spikes, which can then propagate forward under certain conditions (Jarsky et al., 2005). In either case, the outcome is profoundly shaped by neuronal morphology. First, inputs that enter a cell through synapses located far away from the action-potential initiation zone attenuate greatly due to the high axial resistance and leakiness of the dendritic tree, and thus, in the absence of compensatory mechanisms, are less efficacious than inputs that enter the cell closer to the soma (Golding et al., 2005; Rall, 1967). Second, dendritic spikes are predicted to be much more easily generated when synapses are located on the terminal portion of a branch than when they are located near the branch point with the main apical dendrite, owing to differences in excitability along oblique dendrites. The load of the neuron to which the branch is attached and the characteristically large diameters of dendritic segments near branch points give them a relatively low input impedance rendering them inexcitable, while the effect of a sealed end and the characteristically small diameters of segments near terminal ends give them a relatively high input impedance, making them highly excitable. These issues affect information processing in all pyramidal neurons, although different types of pyramidal neurons deal with them in different ways. How pyramidal neurons, and in particular hippocampal CA1 pyramidal neurons, overcome these challenges and take advantage of the increased computing power available to them is the subject of this thesis.

1.2. Inputs to pyramidal neurons

Pyramidal neurons are constantly bombarded by inputs. A single CA1 pyramidal neuron receives an estimated 30,000 excitatory and 1700 inhibitory inputs (Megias et al., 2001). The properties and distributions of these inputs shape action potential firing in these neurons.

1.2.1. Excitatory Inputs

Excitatory inputs to pyramidal neurons are spatially segregated; axons from different areas of the brain selectively innervate different regions of pyramidal-neuron dendrites. Pyramidal neurons tend to receive long-range connections from far-away brain areas such as the thalamus and distant layers of cortex at their tufts and inputs from more local locations at their proximal dendrites (Spruston, 2008). For example, CA1 pyramidal neurons receive two distinct inputs (in addition to a thalamic projection), the first is the perforant-path input from entorhinal cortex that targets their apical tufts, and the second is the Schaffer-collateral input from the CA3 region of the hippocampus that targets their more proximal apical dendrites and their basal dendritic trees (Amaral & Witter, 1989) (Figure 1.1c). The perforant-path input may be especially important because the entorhinal cortex contains a grid-like representation of space (Hafting et al., 2005) and information about the spatial environment must be received by the CA1 pyramidal neurons in order for an animal to perform many navigational tasks (O'Keefe & Dostrovsky, 1971). Therefore it is important to understand how inputs arriving at all dendritic locations, including the apical tuft, contribute to neuronal output.

1.2.2. Spines

Excitatory synaptic inputs contact pyramidal neurons on thousands of spines, protrusions of the neuronal cell membrane that house glutamatergic synapses. The function of spines is not well understood: they may provide biochemical compartmentalization by limiting the diffusion of intracellular molecules (Koch & Zador, 1993), and they may contribute to the neuron's electrical properties as well (Tsay & Yuste, 2004).

Spines consist of a spine head, ranging in volume from 0.003 to 0.55 μm^3, and a spine neck, ranging in diameter from 0.038 to 0.46 μm in area CA1 of the hippocampus, (Harris & Stevens, 1989) so they are at the limits of what can be resolved with light microscopy. Most studies of spine morphology rely on serial-section electron microscopy (Sorra & Harris, 2000). Spines have been classified on the basis of size (large and small) (Matsuzaki et al., 2004) and shape (Peters & Kaiserman-Abramof, 1969). Classifying spines according to shape is important, because spines of particular shapes always contain particular types of synapses (Harris et al., 1992; Harris & Kater, 1994). For example, mushroom spines always contain perforated synapses, which contain a high density of synaptic receptors (Ganeshina et al., 2004b). Studying spine and synapse morphology is an important tool for learning about the integrative properties of dendrites. Many thin dendritic branches are inaccessible to electrophysiological recording, so synaptic integration in these branches cannot be studied directly. Since characteristics of spines and synapses that can be seen with an electron microscope can be correlated with receptor number, a measure of synaptic strength, one can instead use observations about spine and synapse anatomy on a dendrite to make inferences about function.

Spine taxonomy according to shape was first proposed by Peters & Kaiserman-Abramof (1969), and more recently, spine shapes have been defined based on the relative dimensions of their heads and necks (Nimchinsky et al., 2002; Sorra & Harris, 2000). Thin spines have a thin neck, which expands into a rounded head; their head and neck diameters are similar, and their total length is much greater than this diameter. Stubby spines are as wide or wider than they are short and lack a well-defined neck. Sessile spines lack a neck constriction and bulbous head and are longer than their diameters. Mushroom spines have large, irregularly shaped heads with their head diameters much larger than their neck diameters. Whether spines actually fall into distinct categories is debated, with one study indicating that their geometries lie on a continuum (Trommald & Hulleberg, 1997), and another indicating that they can be divided into shape classes based only on the basis of the ratio of head volume to neck diameter (Harris et al., 1992). Most spines contain single synapses, but a few are composed of two or more branches, which often take different shapes (Sorra et al., 1998).

Spines are not static; their actin cytoskeletons enable them to readily change shape both during development and with activity in the mature brain (Matus, 2000). Spines undergo a life cycle where they begin as thin, long filipodia and mature into spines (Cline & Haas, 2008; Fiala et al., 1998). In the adult, many spines are transient, emerging and disappearing from their parent dendrite, but there are subpopulations that are stable over long periods of time (Grutzendler et al., 2002; Holtmaat et al., 2006, 2005). Transient spines are exclusively thin and may be used for learning, while persistent spines are mushroom shaped and may be the substrate of stored memories (Bourne & Harris, 2007; Kasai et al., 2003).

1.2.3. Excitatory Synapses

Postsynaptic densities (PSDs) can only be seen at the electron microscopic level (Figure 1.2). If the postsynaptic density appears as thick as the presynaptic thickening, (symmetric synapse), the synapse is inhibitory, whereas if the PSD is thicker than the presynaptic thickening (asymmetric synapse), the synapse is excitatory. In pyramidal neurons, excitatory synapses are typically found on spines, although some reside directly on the dendritic shaft (Megias et al., 2001).

Figure 1.2. Serial section electron micrographs showing perforated and nonperforated axospinous synapses. The two small synapses between axon terminals labeled AT1 and AT2 and dendritic spines labeled SP1 and SP2 show continuous PSD profiles and are thus nonperforated. The large synapse between axon terminal AT3 and spine SP3 is perforated because it shows a discontinuous PSD profile. Figure courtesy of Dan Nicholson.

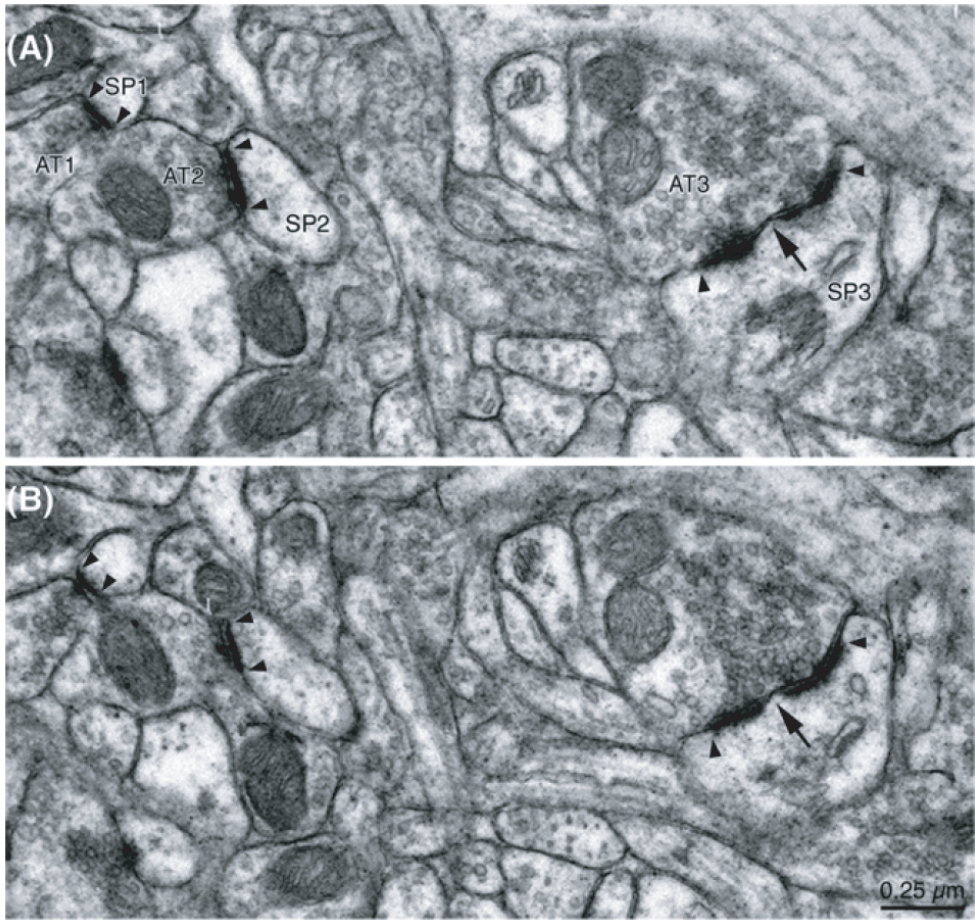

Figure 1.2.

Serial-sections cut perpendicular to the synaptic cleft reveal that axospinous excitatory synapses can be divided into two categories according to the shape of their PSDs (Geinisman, 1993; Peters & Kaiserman-Abramof, 1969). Perforated synapses show a discontinuity in their PSD profiles, which can have a fenestrated (like a donut), horseshoe, or segmented shape and are also contacted by multiple presynaptic release zones. Non-perforated synapses have continuous PSD profiles that are shaped like a disc. Perforated synapses contain many more receptors (both AMPA and NMDA) than non-perforated synapses of the same volume, (Ganeshina et al., 2004a,b) although the function of the perforation is not known.

AMPA and NMDA receptors mediate glutamatergic synaptic transmission in pyramidal neurons. AMPA receptors are permeable to sodium and potassium with a reversal potential around 0 mV, but when they open, the net effect is to admit sodium into the cell, causing a rapid depolarization (Hille, 2001). NMDA channels are permeable to calcium, and to a lesser extent sodium and potassium, and have a reversal potential around 5 mV. They are also voltage dependent: at rest they are blocked by magnesium ions that occlude the channel pore, but depolarization removes this block, bringing calcium and sodium into the cell. NMDA receptors have slow kinetics compared to AMPA receptors, which reach peak activation in hundreds of microseconds (Hille, 2001). Some non-perforated synapses called "silent synapses" completely lack AMPA receptors (Isaac et al., 1995; Liao et al., 1995). Like spines, synapses undergo plasticity, in which small nonperforated synapses become larger perforated synapses with the activity-dependent addition of AMPA receptors (Nicholson & Geinisman, 2006).

Several forms of plasticity have been observed in pyramidal neurons: traditional Hebbian plasticity in which synapses become stronger as a function of activity (Bliss & Lomo, 1973), spike-timing dependent plasticity where synapses become stronger or weaker depending on the timing of spikes in the pre- and post- synaptic cell (Bi & Poo, 1998), and homeostatic plasticity in which synaptic strength is maintained in a stable range (Turrigiano, 1999). Synapses are also modulated by a wide array of neurotransmitters, enabling neurons to respond differently depending on the behavioral state (Egorov et al., 2002; Hasselmo & Schnell, 1994). These properties of synapses may make them the substrates of learning and memory (Hebb, 1949).

1.2.4. Inhibitory Inputs

Pyramidal neurons receive inhibition to their perisomatic regions via basket cells and to their dendrites via a diversity of GABAergic interneurons (reviewed in (McBain & Fisahn, 2001) and (Somogyi & Klausberger, 2005)) that selectively target different parts of their dendritic trees. Different classes of interneurons targeting different somato-dendritic domains are predicted to have different functions with respect to synaptic integration (Miles et al., 1996). For example, perisomatic inhibition is positioned to inhibit firing indiscriminately because it acts as a current shunt near the site of action potential initiation. Inhibition targeting the proximal apical dendrites shunts current propagating down the primary apical dendrite and may prevent distally generated dendritic spikes from reaching the soma. Inhibition to the most distal dendrites may stop the initiation of dendritic spikes in the apical tuft. In addition to limiting action potential firing, inhibitory inputs generate and modulate rhythmic output of pyramidal neurons (Buzsaki et al., 1992).

Two types of inhibition can be distinguished, and pyramidal neurons receive both of them. The first is feedforward inhibition, where an input activates both the pyramidal neuron and the interneurons targeting the pyramidal neuron. In CA1 pyramidal neurons, both excitatory pathways, the perforant path and the Schaffer-collaterals, activate feedforward inhibition. Feedforward inhibition can modulate the time window for summation of excitatory inputs because it does not depend on spiking in the target cell (Pouille & Scanziani, 2001).

The second type of inhibition is feedback inhibition, where pyramidal neurons activate interneurons that then inhibit the pyramidal neurons. Feedback inhibition can modulate repetitive firing because it is activated by spiking in the target cell. "Onset-transient" feedback inhibition targets the soma and proximal apical dendrites and turns both on and off quickly. "Late-persistent" feedback inhibition targets the distal dendrites and turns on more slowly and is prolonged (Pouille & Scanziani, 2004). In CA1, feedback inhibition targeting the apical tufts of pyramidal neurons is mediated by OLM interneurons (McBain & Fisahn, 2001) and in the neocortex it is achieved by Martinotti cells (Silberberg & Markram, 2007).

1.2.5. Inhibitory Synapses

Inhibitory synapses are present on the soma, axons and dendrites of pyramidal neurons, and occasionally on their spine necks (Megias et al., 2001). Their conductance is not scaled with distance from the soma, suggesting that they are important for modulating local rather than global activity (Andrasfalvy & Mody, 2006). They contain GABA receptors, which come in two forms: $GABA_A$ receptors have fast kinetics and contain

chloride channels, which have a reversal potential near rest. If the $GABA_A$ reversal potential is at or above rest, these receptors are predicted to mediate shunting inhibition, which is effective only when it overlaps in time with an EPSP. If the $GABA_A$ reversal potential is below rest, they can provide hyperpolarization, which can be effective for the entire time course of the inhibition (Farrant & Nusser, 2005). $GABA_B$ receptors are slower and contain potassium channels with a reversal potential below rest, so are capable of hyperpolarizing the cell during the time course of the IPSP (Kaupmann et al., 1997).

1.3. Excitability

Action potential generation is an example of excitability in which a cell responds in a highly nonlinear fashion to supra-threshold inputs. Fundamentally, excitability results from the interplay between fast positive and slow negative feedback (Borisyuk & Rinzel, 2003). The positive feedback produces a large and sudden spiking behavior, which is then damped out by the slower negative feedback. In the Hodgkin-Huxley model, the regenerative activation of sodium channels provides the fast autocatalysis, and the subsequent inactivation of sodium channels and activation of potassium channels provide the slow negative feedback.

Three basic types of excitability were first identified by Hodgkin based on studies of the squid giant axon (Hodgkin, 1948; Izhikevich, 2007). In Class 1 excitability, the frequency of action potentials varies with the amplitude of the applied current. In Class 2 excitability, action potential generation is insensitive to the amplitude of the applied current, and they only occur in a narrow frequency band. Class 3 excitability is characterized by the generation of single action potentials in response to applied current with tonic

spiking being difficult or impossible to generate. Each of these different classes of neurons has different functional properties. Class 1 excitable cells ("integrators") can smoothly encode an input into an output spike train. Class 2 excitable cells ("resonators") act as threshold detectors that report when the overall strength of an input exceeds a particular value. Pyramidal neurons are class 1 excitable, and fast spiking cortical interneurons are class 2 excitable. Class three cells remains stable for all biophysically relevant values of applied current. Such behavior has been observed in some mesV cells in the brainstem (Izhikevich, 2003).

Pyramidal neurons contain many types of ion channels that are differentially distributed in their cell membranes. The properties and distributions of ion channels as well as their morphologies give these neurons their wide array of firing properties.

1.3.1. Ion channels and firing properties

The following is an outline of the ion channels demonstrated to be important to pyramidal neuron excitability and their contribution to their firing properties. Only ion channels that have been included in our models will be discussed in detail; the rest will be reviewed briefly.

1.3.1.1. Sodium channels. Voltage-gated sodium channels are uniformly distributed in pyramidal neuron dendrites (Magee, 2008), and drive membrane depolarization and action potentials. They are relatively homogeneous as they all derive from a single family of SCN genes (Yu & Catterall, 2003). Sodium channels activate with depolarization, typically with fast activation and inactivation kinetics. Inactivation can be slowed or prevented, as in the case of the persistent sodium current (Crill, 1996). Persistent sodium currents

can influence subthreshold excitability and support high frequency action potential firing. Subthreshold sodium channel activation can amplify synaptic inputs (Stuart & Sakmann, 1995) and sodium channels in the axon can sometimes amplify somatic EPSPs (Stuart & Sakmann, 1995).

There is one important difference between the sodium channel population in the soma and dendrites of CA1 pyramidal neurons: the dendritic membrane contains a much larger fraction of sodium channels that inactivate on a time scale of seconds rather than milliseconds than the somatic membrane does (Colbert et al., 1997; Jung et al., 1997). A consequence of this is that high frequency action potential firing can activate sodium channels with prolonged inactivation, increasing attenuation of backpropagating action potentials and propagation failure through dendritic branch points.

1.3.1.2. Potassium channels. Pyramidal neurons contain all four types of potassium channels: leak, voltage-gated, calcium activated, and inward rectifying potassium channels, some of which are non-uniformly distributed in their dendrites. These channels help set the resting potential, stabilize the cell by opposing depolarizing voltage changes, and shape subthreshold voltage properties (Hille, 2001).

Leak channels, so called because they are constitutively open, were recently shown to be a type of potassium channel in molecular studies (Lesage & Lazdunski, 2000). These channels give neurons a resting potential close to the equilibrium potential of potassium.

Voltage-gated potassium channels are the most heterogeneous of all channels, with eight subfamilies resulting from the expression of KCN genes and additional variants that

result from the heteromeric combination of these (Coetzee et al., 1999). The voltage-gated potassium channels that have been shown to be particularly prominent in pyramidal neurons are delayed rectifyer, M-type, A-type, and D-type and are briefly discussed here.

Delayed-rectifier potassium channels are a class of functionally similar channels that "keep short action potentials short" by activating rapidly and not inactivating, repolarizing the membrane potential after an action potential (Hille, 2001). Another type of non-inactivating potassium channel important in pyramidal neurons are M-type channels. These channels are both voltage-gated and modulated by acetylcholine binding G-protein coupled muscarinic acetylcholine receptors (Brown & Yu, 2000) which blocks the channel causing increased excitability. These channels are partially on at rest and have a very low threshold for activation. They modulate a neuron's firing rate since action potentials turn on this current, thus raising voltage threshold.

A-type potassium channels are mostly inactivated at rest, but at relatively hyperpolarized potentials they activate and inactivate rapidly. Thus they raise voltage threshold, increase the latency to action potential firing, and reduce firing frequency (Connor & Stevens, 1971). In CA1 pyramidal neurons, A-type potassium channel density increases with distance from the soma (Hoffman et al., 1997). This serves to limit the amplitude of backpropagating action potentials and decrease the size of EPSPs triggered in the dendrites. D-type potassium channels (Storm, 1987) are similar to A-type potassium channels in that they produce transient outward current, but they have a lower threshold for activation, and inactivate more slowly and have a slower recovery from inactivation.

Fast calcium-activated potassium channels, also known as BK channels, open when both the internal calcium concentration and voltage increase, with the internal calcium

modulating the channel's voltage dependence (Hille, 2001). BK channels contribute to spike repolarization and the fast afterhyperpolarization (AHP). Slow calcium-activated potassium channels, also known as SK channels produce a current called the IAHP. These channels open with moderate increases in the internal calcium concentration and contribute to spike frequency accomodation, the slow afterhyperpolarization, and inter-burst intervals (Hille, 2001).

Inward rectifying potassium channels are a class of channels that open with hyperpolarization and close with depolarization. They act as a diode or a latch: (Hille, 2001) when the voltage is a few millivolts positive to EK, they allow entry of potassium, maintaining a resting potential near EK (door is latched), but once other depolarizing influences act on the cell, the IRK channels close and the membrane potential is again free to change (door is unlatched).

1.3.1.3. Calcium channels. All three families of voltage-gated calcium channels are represented in CA1 pyramidal neurons, and although the total calcium conductance is relatively uniform, different regions of the neuron preferentially express different channel subtypes (Magee, 1998). L- and N-type calcium channels dominate the proximal region of the cell, and T- and R-types are expressed at higher density in the distal dendrites, which may result in a decreasing gradient in intracellular calcium concentration along the somato-dendritic axis.

L-type, N-type (which can be divided into P/Q and R subtypes) and T-type calcium channels have high, intermediate, and low activation thresholds respectively and have

large, intermediate, and small single-channel conductances, respectively (Hille, 2001). L-type calcium channels inactivate very slowly, over a time course of 500 ms, N-type channels inactivate a factor of 10 more quickly, and T-type channels show strong inactivation.

In CA1 pyramidal neurons, the L-type current has a component that is partially on at rest (Magee, 1998). EPSPs can further activate L-type channels, locally increasing calcium concentration and boosting voltage amplitude. T-type channels are partly inactivated at rest, but when deinactivated by hyperpolarization can also mediate calcium entry (Magee, 1998; Magee & Johnston, 1995). In addition to their role in synaptic transmission, R-type calcium channels underlie the ADP and contribute to action potential bursting (Metz et al., 2005).

1.3.1.4. H-Channels. The density of hyperpolarization-activated cation channels (H channels) increases in apical dendrites with distance from the soma in both neocortical layer V and CA1 hippocampal pyramidal cells (Berger et al., 2001; Lorincz et al., 2002; Magee, 1998, 1999; Williams & Stuart, 2000). H channels conduct both sodium and potassium ions, with a reversal potential of approximately -30 mV. H channels are largely on at rest, so they lower input resistance, cause a more depolarized resting potential, and add to voltage attenuation because they make the membrane leakier. They activate upon hyperpolarization with a significant delay, producing a depolarizing current, and do not inactivate. The effect of these channels is to oppose changes in membrane potential: they damp out hyperpolarizing stimuli by producing a depolarizing current, so H channels reduce IPSP duration and produces a slight depolarization following the IPSP (Williams & Stuart, 2003). However, depolarization turns Ih off, reducing EPSP duration and resulting in a slight hyperpolarization following the EPSP (Magee, 1999; Williams & Stuart, 2000).

In layer 5 and CA1 pyramidal neurons, Ih serves to equalize the window for temporal summation of EPSPs at the soma for inputs coming in at all locations (Magee, 1999; Williams & Stuart, 2000). In CA1 pyramidal neurons, differences in the properties of the H conductance along the somato-dendritic axis give the dendrite location-dependent resonance frequencies in the theta range (Narayanan & Johnston, 2007, 2008).

1.3.2. Dendritic excitability: Backpropagation and dendritic spikes

The ion channels described above contribute to neurons' array of firing properties. The presence of these channels in dendrites means that the dendrites are not passive conduits of synaptic current but have their own active properties.

Action potentials initiated in the axon of pyramidal neurons backpropagate into their dendrites (Hausser et al., 2000; Stuart et al., 1997b). These action potentials attenuate significantly as they backpropagate through the apical dendritic arbor (Frick et al., 2003; Gasparini et al., 2007) and the basal dendrites of layer V pyramidal cells (Nevian et al., 2007). There are two reasons for this attenuation: the neuron's morphology causes action potentials to attenuate or fail through branch points (Vetter et al., 2001), and the increasing gradient of A-type potassium channels in CA1 dendrites (Hoffman et al., 1997; Migliore et al., 1999) and other types of potassium channels in layer V pyramidal neurons dendrites oppose membrane depolarization. Backpropagation can be enhanced by depolarization, which opens sodium and inactivates potassium channels (Gasparini et al., 2007; Migliore et al., 1999; Stuart & Hausser, 2001) and reduced by inactivation of sodium channels (Colbert et al., 1997; Jung et al., 1997; Mickus et al., 1999). CA1 pyramidal

neurons fall into two populations depending on whether action potentials backpropagate strongly or weakly into the dendritic tree (Golding et al., 2001).

Strong, synchronous inputs can activate both sodium and calcium voltage-gated channels in the dendrite and lead to spikes initiated in the dendrites. Several types of dendritic spikes have been observed: brief sodium spikes were observed in both apical (Hausser et al., 2000; Stuart et al., 1997a) and basal (Nevian et al., 2007) dendrites. Larger and broader calcium spikes were observed in apical dendrites only (Golding et al., 1999; Schiller et al., 1997), and regenerative activation of NMDA receptors by relief of the magnesium block was observed in basal dendrites only (Schiller et al., 2000). The propagation of these spikes is limited to depolarized areas where glutamate is present (Schiller & Schiller, 2001).

In a conductance-based model of a CA1 pyramidal neuron, it was shown that "traveling wave attractors" determine the extent of both forward and back propagation of action potentials in apical dendrites, and these are effected by both I(A) channels and dendritic morphology (Acker & White, 2007). In CA1 pyramidal neurons, distally generated dendritic spikes often fail to reach the axon on their own, but their propagation can be facilitated by depolarization entering more proximally enabling these neurons to act as coincidence detectors (Jarsky et al., 2005).

1.3.3. Modeling framework

The biophysics of neurons is quite complex, so it is sometimes useful to think about action potential generation in more general terms with limited reference to the underlying biophysical mechanisms (Izhikevich, 2007). The earliest biophysical models of the action potential were formulated by Hodgkin and Huxley (Hodgkin & Huxley, 1952), and

contained only sodium and potassium channels, but even these were too complicated to provide much geometrical insight. Fitzhugh and Nagumo simplified the Hodgkin-Huxley model to a two dimensional system which allowed for easy visualization of the model solutions (FitzHugh, 1961). Other simplified models of action potentials have also been considered (Morris & Lecar, 1981). These two dimensional models can have stable states corresponding to only the resting state, only the firing state, or both. In these models, the onset of firing can only be generated in four ways, which differ in whether the resting state and the firing state coexist and whether the firing state corresponds to sustained or transient oscillations (Izhikevich, 2007).

Much can be learned from these simple models, but an important part of pyramidal neurons is their dendrites, which shape information processing. In order to assess the role of dendrites in synaptic integration, detailed models that incorporate the neuron's geometry and biophysical properties are required.

In this thesis, we develop three-dimensional morphological models of CA1 pyramidal neurons constrained by experimental data. Our goal is to create a model neuron that faithfully replicates many aspects of the physiology of a real neuron so it can be used to conduct in-silico experiments on synaptic integration. Models are particularly important to address the role of dendrites in synaptic integration because many regions of the dendritic tree are inaccessible to direct experimentation due to their small diameters. In order to probe these dendrites, models must be constructed that are constrained by experimental data so information can be extrapolated from these models. A brief outline of our modeling approach follows.

In previous work, CA1 pyramidal neurons from rat hippocampus were kept alive in brain slices and visualized using differential interference contrast imaging. Using a technique called patch-clamp recording (Neher et al., 1978), a glass micropipette containing an electrode was used to form a gigaohm seal on the neuronal membrane, so when the membrane was ruptured, an accurate reading of voltage across the neuronal membrane could be obtained. Current was injected into the cell or synapses were stimulated, and the resulting voltage response curves were used to constrain the model parameters.

After the recording experiment, the neuron was filled with a biocytin stain and visualized using a camera-microscope system. The three dimensional structure of the neuron was manually traced and its coordinates are entered into a computer. The realistic neuronal morphology obtained from this procedure was used as the geometry within which to solve the model equations.

The propagation of voltage through the neuronal geometry is modeled using a second order partial differential equation (Rall, 1964):

$$\frac{\partial V}{\partial t} = \frac{\lambda^2}{\tau}\frac{\partial^2 V}{\partial x^2} + \frac{I}{C}$$

Where τ is the membrane time constant, λ is the space constant, C is the capacitance per unit area of the neuronal membrane, and I represents the ionic, synaptic, and injected current densities. This equation, called the cable equation, is a reaction-diffusion-like equation where the first term on the right hand side represents diffusion through the neuronal morphology and the currents act as reactions.

The ionic currents depend on the voltage and concentration differences of ions across the neuronal membrane. The time course of these currents is shaped by ion-channel conductances, which have complicated dependencies on voltage and time.

$$I_{ion} = G_{channel}(V,t)(V - E_{ion})$$

This current is modeled using a Hodgkin-Huxley-like formalism. For example:

$$I_{ion} = -G_{Na}m(V)^3h(V)(V - E_{Na} - G_{Kdr}n(V)^4(V - E_K) + \ldots$$

with

$$\frac{dm}{dt} = \frac{m_\infty V - m}{\tau_m}; \quad \frac{dh}{dt} = \frac{h_\infty V - h}{\tau_h}; \quad \frac{dn}{dt} = \frac{n_\infty V - n}{\tau_n};$$

Where C is the membrane capacitance per unit area, G_{Na} and G_{Kdr} are the maximal values for the sodium and delayed-rectifyer potassium conductance densities, m and h are the sodium-channel activation and inactivation gating variables, and n is the potassium-channel activation gating variable. m_∞, h_∞, and n_∞ are the steady state values of m, n, and h, and τ_m, τ_h, and τ_n are the time constants for the activation and inactivation of the channels.

Our model includes sodium, delayed rectifier potassium, A-type potassium, and sometimes H channels because these are prominent in CA1 pyramidal neurons. The kinetics of these channels as well as their distributions in the cell membrane are obtained from the literature and from our own experiments (Golding et al., 2005; Hoffman et al., 1997; Magee, 1998; Migliore et al., 1999). We solve the model by discretizing the neuronal morphology into a series of compartments sufficiently small so that the voltage can be

considered uniform in each compartment, and taking into account the coupling between compartments. We estimate the parameters by fitting to experimental data. There are approximately fifty free parameters, but sufficient experimental data to constrain the fits have been obtained. Programming is done in the NEURON simulation environment (Hines & Carnevale, 1997). Equations are integrated using a backward Euler method with a time step of .025 ms.

Synaptic currents are modeled as a difference of exponentials: when the presynaptic cell fires, the synaptic conductance of the postsynaptic cell exponentially rises and exponentially falls, mimicking the fast conductance change characteristic of AMPA synapses. The injected currents are chosen to match experimental procedures.

There are many ion-channel types known to be present in pyramidal neurons that are not included in our models that are present in other pyramidal-neuron models (Poirazi et al., 2003). Our models are minimal models in the sense that we include only the ion channels necessary to reasonably match experimental data or that are known to be important for the particular phenomenon being investigated. An alternative approach would be to develop more comprehensive models (Poirazi et al., 2003). We did not do that, however, because then the number of free parameters explodes and the model could exhibit more complex behavior that we would have less confidence is accurate. Thus we omitted further details from our model so we would be able to attribute specific responses to specific actions of ion channels. Despite the simplicity of our models, they reproduce a wide variety of measured behaviors, including passive voltage responses to hyperpolarizing current steps, spiking responses to depolarizing current injections, and the amplitudes of forward and back- propagating action potentials along the main apical dendrite.

1.3.4. Work presented: Voltage attenuation and the limits of synaptic scaling

The degree to which an input can influence neuronal output depends upon how much voltage attenuates through the dendritic cable from input site to the action potential initiation zone in the axon hillock. For locations on the main apical dendrite, attenuation could be measured directly using simultaneous dendritic and somatic patch-clamp recording (Golding et al., 2005). However, most dendrites are inaccessible to this technique due to their small diameters. To quantify the attenuation of an individual input arriving at an arbitrary dendritic location, we constructed computational models of CA1 pyramidal neurons constrained by the amount of attenuation recorded in the main apical dendrite, and then used the models to assess the attenuation of individual inputs from arbitrary synaptic locations and resolve the different factors contributing to the observed voltage attenuation.

Using this method, our models predicted that distal inputs attenuate many-fold from synapse to soma, and that the high axial resistance and the fact that many ion channels are on at rest (particularly the H-conductance) act together to produce the observed voltage attenuation through the dendritic cable (Golding et al., 2005). This implied that it would be difficult for many distal inputs to influence neuronal output and that, in the absence of compensatory mechanisms, inputs are weighted according to their locations, where inputs entering a cell at locations close to the action potential initiation zone would exert greater control over output than those entering more distally.

Magee and Cook (2000) showed that synapses on the first several hundred microns of the main apical dendrite compensate for the effect of voltage attenuation by increasing their strength with distance from the soma. We examined whether the ability of synaptic

scaling to normalize synaptic efficacy extends to all synapses or whether synapses at some locations would be unable to overcome the effect of voltage attenuation. Using our pyramidal cell models, we found that synaptic scaling is not effective for the most distal synapses. This is because there is a theoretical limit to the local size of an input imposed by the synapse reversal potential: as the local membrane potential approaches the reversal potential, successive increases in conductance draws less further charge into the cell. Dendrites are sufficiently leaky that for many distal locations, no value of synaptic conductance could make the local inputs large enough to exert an appreciable influence on the somatic voltage (Nicholson et al., 2006).

We corroborated these predictions experimentally by using immuno-gold electron microscopy to determine the density of AMPA receptors, a correlate of synapse strength, at synapses in the different layers of CA1 (Nicholson et al., 2006). AMPA receptor density increased in synapses in distal stratum radiatum relative to proximal stratum radiatum, but was not highest in stratum lacunosum moleculare, where the most distal synapses are situated. This is in agreement with the theoretical result that synaptic scaling can only normalize synaptic efficacy for synapses at limited distances from the soma. Beyond that we did not expect to see synapse size increase because there would be no associated functional gain.

Since it would be difficult for distal inputs to influence neuronal output via EPSPs, we hypothesized that they communicate with the soma primarily by activating voltage-gated conductances to produce dendritic spikes. We constructed a model with active channels and showed that dendritic spikes are readily generated in distal dendrites (Nicholson et al., 2006).

1.3.5. Work presented: Normalization of dendritic spike initiation

If dendritic spikes are an important means by which distal synapses communicate with the soma, an additional issue arises. According to cable theory (Rall, 1964) portions of a dendrite near its terminal end would be more excitable than portions of a dendrite near its branch point with the parent branch. This is because the effect of a sealed end and the characteristically small diameters of segments near terminal ends give them a relatively high input impedance, while the load of the rest of the cell and the characteristically large diameters of segments near branch points give them a relatively low input impedance. Therefore, in the absence of compensatory mechanisms, synapses located near terminal ends would exert a disproportionate influence over local dendritic spike initiation relative to synapses located near branch points.

There is increasing evidence that individual dendritic branches may behave as independent computational subunits in which inputs are locally summated before being globally summated by the neuron (Polsky et al., 2004). Therefore it may be important for inputs to normalize their contributions to the output of a dendritic branch as well as to the soma directly (Hausser, 2001; Magee & Cook, 2000; Nicholson et al., 2006). However, normalization of synaptic efficacy for these two cases leads to competing predictions about the strength of individual synapses along individual dendritic branches. Normalization of somatic EPSPs suggests that synapses should be stronger at more distal locations, in order to compensate for attenuation of synaptic current. Normalization of dendritic spike initiation suggests that synapses should be weaker at more distal locations, in order to compensate for the larger local EPSPs associated with smaller dendrites.

To determine whether synapses scale in such a way as to normalize for dendritic spike initiation or somatic EPSP amplitude, we used serial-section EM to reconstruct oblique dendrites and compare spines and synapses on dendritic segments near and far from the main apical dendrite. We found that spines and synapses were both larger and more numerous on low-excitability segments near branch points, arguing that synapses are distributed to normalize dendritic spike initiation. We incorporated this experimental finding back into the pyramidal cell model and found that the observed distribution also increases the contribution of each dendritic branch to the somatic depolarization. This is because the largest synapses are closer to the soma minimizing the attenuation of the largest inputs, and the propagation of distally generated EPSPs and dendritic spikes is facilitated by inputs to the large synapses situated close to the branch point.

1.3.6. Work presented: Inhibition and CA1 microcircuit dynamics

Synaptic integration in pyramidal neurons is profoundly shaped by inhibition (Pouille & Scanziani, 2001, 2004). To determine how the relative location, amplitude, and timing of excitatory and inhibitory inputs affect dendritic spike initiation and propagation in CA1 pyramidal neurons, we performed simulations in which we distributed excitatory and inhibitory synapses in different regions of the cell according to experimental data (Megias et al., 2001), fixed the excitatory input, and randomly activated different percentages of inhibitory synapses and measured the resulting voltage at all points on the neuron.

We looked at four cases: perforant-path inhibition and excitation, perforant path inhibition and Schaffer-collateral exciation, Schaffer collateral inhibition and excitation, and Schaffer-collateral inhibition and perforant-path excitation. We found that dendritic

spikes activated by the perforant-path can be gated by inhibition. When excitation and inhibition spatially overlap, the probability of both dendritic spike initiation and propagation is reduced.

We looked at two different types of inhibition: shunting and hyperpolarizing inhibition. Distal shunting inhibition is not effective in stopping spikes initiated in the apical dendrite from propagating forward toward the soma or spreading backward toward the tuft, but modest amounts of distal hyperpolarizing inhibition can prevent the spread of these spikes. We also varied the timing of inhibition relative to excitation. Shunting inhibition is effective when the IPSC is coincident with an EPSP, while hyperpolarizing inhibition is effective for the entire time course of the IPSP.

1.4. Pyramidal neurons in vivo

These studies of pyramidal neurons can yield insights into the function of the brain structures in which they are found. Here we focus on the hippocampus, which has been shown to responsible for types of spatial learning and episodic memory and how the integrative properties of hippocampal pyramidal neurons relate to these functions.

1.4.1. The function of the hippocampus in humans

Modern interest in the hippocampus goes back to 1953 when a man in Hartford Connecticut known as patient H.M. became profoundly amnesiac following surgery involving the bilateral removal of his hippocampi and parts of his medial temporal lobe (Scoville, 1954). Since that time, nearly one hundred researchers have studied H.M to elucidate his precise memory deficits (Corkin, 2002).

H.M. is severely impaired in his ability to form new memories and is unable to recall events immediately prior to his surgery, but he retains memories of his childhood. From studying patient HM and others like him it was concluded that the hippocampus is required for the formation and consolidation of new declarative memories (Milner & Penfield, 1955; Squire, 1992), memories of "what, when and where" (episodic memories), and memories of facts not connected to autobiographical experience (semantic memory) (Eichenbaum, 2000). Recent work has suggested that the hippocampus is particularly important for episodic memories, while other parts of the medial temporal lobe are important for semantic memory (Tulving & Markowitsch, 1998) Since the hippocampus is generally not required for the retrieval of old memories, it must pass information along to other brain structures for long-term storage.

Patient H.M. is able to learn new skills (Cohen & Squire, 1980; Corkin, 1968). This provides experimental evidence for the century-old idea that conscious memories can be distinguished from unconscious habits (James, 1890). He is also intelligent and sociable, indicating that these are not functions of the hippocampus (Corkin, 2002).

1.4.2. The function of the hippocampus in rats

To further explore the role of the hippocampus in episodic memory, several animal studies have been conducted. In rats, a function of the hippocampus that can be readily assayed is spatial learning and memory (O'Keefe & Dostrovsky, 1971; O'Keefe & Nadel, 1978). In humans, spatial learning and memory also appears to be a function of the hippocampus (Maguire et al., 2000, 2006).

Whether animals have episodic memory as experienced by humans is controversial (Tulving, 2002), but animals can be said to have episodic-like memory, memory of "what, when, and where", without the requirement of autonoesis (Eichenbaum & Cohen, 2001; Morris, 2001). Although hippocampal neuron types and connections are conserved between rats and humans, the extent to which we can learn about human episodic memory from studying rats is debated. One hypothesis is that the hippocampus performs the same essential computations in both species, but there are elements of the inputs to these computations in the humans that are not present in rats (Eichenbaum & Cohen, 2001).

1.4.3. Neural correlates of hippocampal function

When an animal explores an environment, some neurons fire predominantly when it is in a particular location (O'Keefe & Dostrovsky, 1971). These neurons, dubbed place cells, are found in the hippocampus and are thought to be the substrates of cognitive maps (O'Keefe & Nadel, 1978). Place cells are not static, but dynamically remap with experience (Wilson & McNaughton, 1993).

During performance of the spatial alternation task, in which an animal must take alternate paths through a T maze in order to obtain rewards, some place cells take on an additional property. They fire selectively when the animal is in a particular location on the stem of the maze, but only after it comes from either the left or the right. Thus they are thought to be neural correlates of temporal context (Wood et al., 2000). Most of these cells, called "splitter cells" or "episodic cells," fire based on the animal's recent history, although some predict future action (Ferbinteanu & Shapiro, 2003).

1.4.4. Work presented: Coincidence and spatial navigation

Relating the biophysical properties of CA1 pyramidal-neuron dendrites to hippocampus-dependent spatial navigation requires a model that spans a wide range of spatial and temporal scales. To make this connection, we simulated the spatial alternation task using a network of biophysically realistic model neurons. Our model was the first to use biophysically realistic elements to consider the observed context-dependent properties of hippocampal neurons and relate them to behavior.

Due to the high computational cost of simulating a network of full-morphological model neurons, we first constructed a reduced CA1 pyramidal neuron model consisting of four nodes electrically coupled together, representing the apical tuft, more-proximal apical dendrites, soma, and basal dendrites. The reduced model had weakly excitable dendrites and reproduces the phenomenon of gating, the ability of subthreshold proximal inputs to enable a distally generated dendritic spike to propagate forward (Jarsky et al., 2005).

We used these reduced models to construct a network model of the hippocampus. Single-compartment entorhinal cortical neurons projected to the apical tufts of the CA1 neurons and conveyed information about the animal's location in the environment. Single-compartment CA3 neurons projected to the more proximal apical dendrites of the CA1 neurons and conveyed the memory of the animal's previous path through the environment, the temporal context. The CA1 neurons were coincidence detectors of place and temporal context, firing only when both inputs were active.

In the model, the integration of place and temporal context information in CA1 pyramidal neurons representing the stem of the maze made them "splitter cells", cells which

fire selectively based on a combination of place and temporal context. The animal used the information stored by the splitter cells to choose correct paths through the maze.

1.5. Overview

To achieve the goal of understanding how the hippocampus encodes memory, we must understand how components within hippocampal circuits function. Synaptic integration in excitable dendrites is crucial to understanding this. Here we address fundamental biophysical issues about pyramidal neurons, the interaction between excitation and inhibition in CA1 dendrites, and finally how these issues are integrated to produce observed firing behavior in awake behaving animals.

CHAPTER 2

Distance-dependent differences in synapse number and AMPA receptor expression in hippocampal CA1 pyramidal neurons

Published in Neuron 50, 431-442 (2006).

By: Daniel A. Nicholson, Rachel Trana, Yael Katz, Wiliam L. Kath, Nelson Spruston, and Yuri Geinisman.

Author contributions: I wrote all code for the computer simulations leading to the prediction that there are limits to the effectiveness of conductance scaling. Rachel Trana ran simulations with different parameters and produced the figures. Daniel Nicholson performed all electron microscopy experiments that corroborated our prediction and wrote the paper. Bill Kath, Nelson Spruston, and Yuri Geinisman guided the research.

Note that in this chapter, the supplementary material has been integrated into the text, so the figure numbering is different from the original publication in Neuron.

2.1. Abstract

The ability of synapses throughout the dendritic tree to influence neuronal output is crucial for information processing in the brain. Synaptic potentials attenuate dramatically, however, as they propagate along dendrites toward the soma. To examine whether excitatory axospinous synapses on CA1 pyramidal neurons compensate for their distance from the soma to counteract such dendritic filtering, we evaluated axospinous synapse number and receptor expression in three progressively distal regions: proximal and distal stratum radiatum (SR), and stratum lacunosum-moleculare (SLM). We found that the proportion of perforated synapses increases as a function of distance from the soma, and that their AMPAR, but not NMDAR, expression is highest in distal SR and lowest in SLM. Computational models of pyramidal neurons derived from these results suggest that they arise from the compartment-specific use of conductance scaling in SR and dendritic spikes in SLM to minimize the influence of distance on synaptic efficacy.

2.2. Introduction

The excitatory synaptic inputs onto a single neuron often originate in different areas of the brain and are distributed throughout a branched dendritic tree that can extend hundreds of microns from the soma. Activation of these synapses generates potentials that propagate toward the soma and axon, where all electrical signaling from the dendrites converges. In order to influence activity in these final integration zones, however, synaptic potentials must overcome severe filtering and attenuation caused by the cable properties of dendrites (Rall, 1977; Williams & Stuart, 2003). Because of the size and complexity of dendrites, the impact of dendritic filtering increases with distance from the soma and substantially reduces the influence of distal synapses on neuronal output. Recent studies suggest, however, that CA1 pyramidal neurons can counteract this voltage attenuation with two different mechanisms, both of which are capable of effectively and reliably depolarizing the soma and axon: distance-dependent conductance scaling (Magee & Cook, 2000; Smith et al., 2003). and dendritic spikes (Gasparini & Magee, 2006; Gasparini et al., 2004; Golding & Spruston, 1998).

Conductance scaling has been studied among the CA3_CA1 synapses of stratum radiatum (SR), where locally generated synaptic potentials in distal dendritic regions are larger than those generated more proximally. When these same potentials are recorded at the soma, however, their average amplitudes are virtually indistinguishable, imparting location independence to synapses in SR. Dendritic spikes also have been studied in detail within apical dendritic regions, where they are triggered locally by synaptic activity and propagate with variable reliability toward the soma. Dendritic spikes likely play an integral role in relaying synaptic signals from stratum lacunosum-moleculare (SLM) because,

in the absence of dendritic action potentials, inputs in this region have only a minor effect at the soma (Cai et al., 2004; Golding & Spruston, 1998; Jarsky et al., 2005; Wei et al., 2001). Additionally, the forward-propagation of dendritic spikes originating in SLM, and their effectiveness at driving axonal action potentials, are facilitated dramatically by very modest synaptic activity in SR (Jarsky et al., 2005). Such findings suggest that, through the gating action of SR synapses, dendritic spikes are the principal form of communication between SLM and the soma/axon. These studies have contributed to the emerging view that CA1 pyramidal neurons employ both conductance scaling and dendritic spikes to ensure that synapses throughout the apical dendrite influence neuronal output. Virtually nothing is known, however, regarding the cellular substrates of synaptic distance compensation. In addition, the likelihood that SR and SLM synapses use the same or different mechanisms to reduce the impact of their dendritic location has never been addressed.

To characterize the extent to which synapses are regulated in a distance-dependent manner, especially in SLM where such a role may be masked by the technical limitations of recording from the small-diameter dendritic tufts, we used conventional and postembedding immunogold electron microscopy to examine the number, as well as the AMPAR and NMDAR expression, of synapses throughout the apical dendrite of CA1 pyramidal neurons. At least within SR, the number or density of AMPARs appears to be the major determinant of synaptic strength because various other parameters that influence excitatory postsynaptic potential (EPSP) amplitude – including cleft glutamate concentration, the size of the readily releasable pool of vesicles, probability of release, maximum channel open probability, single channel current, and NMDAR-mediated current – do not vary with distance from the soma, yet synapses in this region exhibit conductance scaling

(Smith et al., 2003). Accordingly, we used the number and density of immunogold particles for AMPARs projected onto the postsynaptic density (PSD) as an estimate of the relative strength of synapses. We then derived computational models of CA1 pyramidal neurons from these data to determine how distance-dependent differences in synaptic strength affect dendritic integration. Taken together, our results suggest that synapses on the apical dendrites of CA1 pyramidal neurons minimize voltage attenuation by utilizing conductance scaling in SR and the generation of dendritic spikes in SLM.

2.3. Results

2.3.1. Distance-dependent regulation of synapse number

The vast majority of excitatory synapses on CA1 pyramidal neurons are located on dendritic spines (Geinisman et al., 2004; Sorra & Harris, 2000), and can be either perforated or nonperforated (Carlin et al., 1980; Peters & Kaiserman-Abramof, 1969), depending on the configuration of their PSD. When viewed in serial sections, perforated synapses exhibit discontinuous PSD profiles (Figures 2.1A-C), while nonperforated synapses show continuous PSD profiles (Figure 2.1D-F). Importantly, perforated synapses have a higher number of immunogold particles for both AMPARs and NMDARs compared to their nonperforated counterparts (Desmond & Weinberg, 1998; Ganeshina et al., 2004a,b). Such findings are consistent with the idea that perforated synapses, when activated, will generate larger synaptic currents than nonperforated synapses. To clarify the role of these two synaptic subtypes in distance compensation, we first asked whether the number or proportion of perforated synapses changes with distance from the soma. If conductance

scaling is used throughout the apical dendrite, then perforated synapses might be more prevalent in distal regions, compared to locations closer to the soma/axon.

Figure 2.1. Ratio of perforated-to-nonperforated synapses increases with distance from the soma in CA1 pyramidal neurons

(A-C) A perforated synapse between a presynaptic axon terminal (at) and a postsynaptic spine (sp), characterized by discontinuities (arrows) in its postsynaptic density profiles (arrowheads). Scale bar, 0.25 μm. **(D-F)** Nonperforated synapses between two presynaptic axon terminals (at1 and at2) and two postsynaptic spines (sp1 and sp2) display continuous postsynaptic density profiles (arrowheads) in all sections. Scale bar, 0.25 μm. **(G)** A pyramidal neuron in the hippocampal CA1 region (arrows). **(H)** Location of the pSR, dSR, and SLM depicted on a CA1 pyramidal neuron. **(I)** Total number of perforated (triangles) and nonperforated (circles) synapses in pSR, dSR, and SLM. pSR has fewer perforated synapses than dSR and SLM (*); SLM has fewer nonperforated synapses than pSR and dSR (**). **(J)** The perforated-to-nonperforated synapse ratio is higher in dSR than in pSR (*) and highest in SLM (**). All values are based on pooled data from three rats (1,032 perforated synapses; 7,569 nonperforated synapses) and are presented $\pm$ SEM.

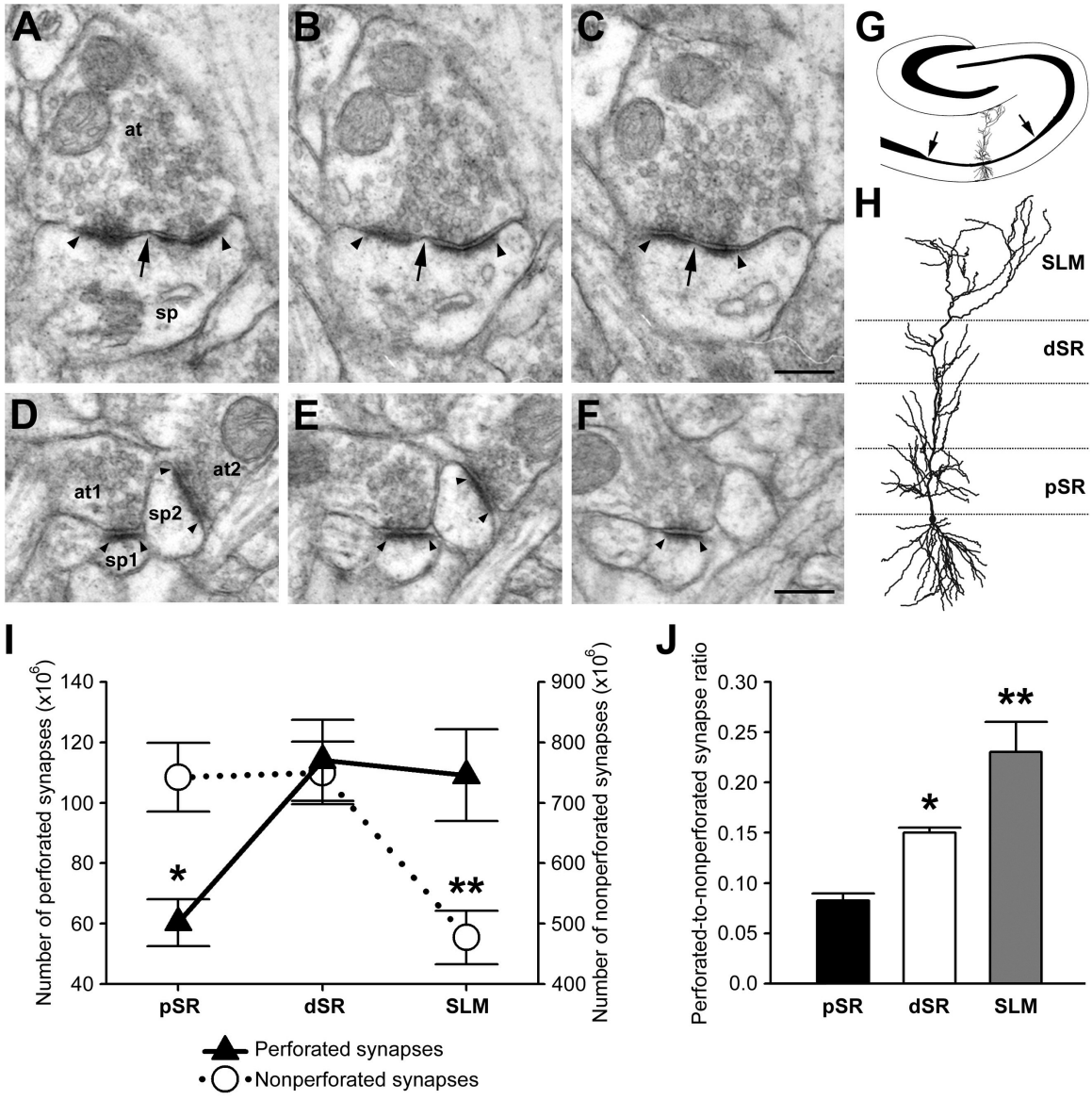
A
B
C
at
sp
D
E
F
at1
at2
sp2
sp1
G
H
SLM
dSR
pSR
I
Number of perforated synapses (x10^6)
Number of nonperforated synapses (x10^6)
140
120
100
80
60
40
900
800
700
600
500
400
pSR
dSR
SLM
*
**
Perforated synapses
Nonperforated synapses
J
Perforated-to-nonperforated synapse ratio
0.30
0.25
0.20
0.15
0.10
0.05
0.0
pSR
dSR
SLM
*
**

Figure 2.1.

We used unbiased stereological sampling and counting procedures combined with serial section analyses to characterize the incidence of axospinous synapses on CA1 pyramidal neurons in three progressively distal zones of the apical dendritic tree (Figure 2.1G and H): the proximal one-third of the SR (pSR), the distal one-third of the SR (dSR), and the SLM, the most distal synaptic region. Our estimates of the total number of perforated and nonperforated synapses in the three zones revealed that their numbers varied in a distance-dependent manner. Specifically, there are more perforated synapses in dSR and SLM than in pSR, and there are fewer nonperforated synapses within SLM than in pSR and dSR (Figure 1I). Together, these differences in synaptic subtype number progressively increase the proportion of perforated synapses with distance from the soma (Figure 2.1J).

That the number of perforated synapses is increased in the dSR, and then maintained at the same elevated level in SLM (Figure 1I), suggests that perforated synapses play a pivotal role in distance-dependent synaptic scaling. Because of the exceptionally high level of AMPAR immunoreactivity in perforated synapses (Ganeshina et al., 2004a,b), the increase in their proportion might underlie the higher incidence of large-amplitude miniature excitatory postsynaptic currents (mEPSCs) in dSR (Magee & Cook, 2000; Smith et al., 2003). A parallel augmentation in perforated synapse strength would account for the electrophysiological finding that the dSR contains a subpopulation of synapses 2-3 times more powerful than any synapse in pSR (Magee & Cook, 2000; Smith et al., 2003). Furthermore, perforated synapse strength might be expected to surpass that in dSR if conductance scaling extends to SLM. To examine these ideas, we assessed the AMPAR and NMDAR immunoreactivity of axospinous synapses from the pSR, dSR, and SLM.

2.3.2. Synaptic AMPARs exhibit distance-dependent regulation

Currently, the best available method for localizing and quantifying neurotransmitter receptors is postembedding immunogold electron microscopy (Nusser, 2000; Ottersen & Landsend, 1997; Petralia et al., 1999). By applying the antibodies directly to ultrathin sections, this method restricts labeling to the epitopes present on the cut surface of the tissue, permitting high-resolution localization and quantification of receptors by examining immunogold particle number and density. We combined stereological sampling techniques, serial section analyses, and postembedding immunogold electron microscopy to evaluate whether the AMPAR and NMDAR immunoreactivity of perforated and nonperforated synapses changes with distance from the soma. We first examined AMPAR expression because AMPARs mediate the majority of fast synaptic transmission, and previous electrophysiological studies have provided evidence that distance-dependent synaptic scaling is accomplished via an increase in synaptic AMPAR conductance (Andrasfalvy & Magee, 2001; Magee & Cook, 2000; Smith et al., 2003). In serial ultrathin sections, perforated synapses are invariably immunopositive for AMPARs and exhibit an abundance of immunogold particles associated with their PSD (Figure 2.2A-E). In contrast, nonperforated synapses can be either immunonegative or immunopositive (Figure 2.2A and F-H), with the latter typically containing only a few immunogold particles (Ganeshina et al., 2004a,b; Nusser et al., 1998a; Petralia et al., 1999; Racca et al., 2000; Takumi et al., 1999).

Figure 2.2. AMPAR expression in perforated and nonperforated synapses throughout the apical dendritic tree in CA1 pyramidal neurons

(A) Low magnification electron micrograph showing profiles of a perforated synapse (black arrow) and two nonperforated synapses (white arrows) in a section immunostained for AMPARs. These profiles of the perforated and nonperforated synapses are seen at a higher magnification in panels **D** and **F**, respectively. **(B-E)** A perforated synapse (labeled in **B** by at and sp) immunostained for AMPARs, with postsynaptic density (PSD) profiles (arrowheads) exhibiting discontinuities (arrows) in some sections. **(F-H)** Two nonperforated synapses immunostained for AMPARs with continuous PSD profiles (arrowheads) in all sections. One (labeled in **F** by at1 and sp1) is immunopositive, while the other (labeled in **F** by at2 and sp2) lacking immunogold particles is immunonegative. Scale bars, upper panels = 0.2 μm, lower panels = 0.12 μm. **(I)** Mean number of immunogold particles for AMPARs per perforated (triangles) and nonperforated (circles) synapse. Perforated synapses in dSR have the highest particle number (*), whereas those in SLM have the lowest (**). **(J)** Mean density of immunogold particles for AMPARs per PSD unit area (μm^2). Among perforated synapses, those in dSR have the highest particle density (*), and those in SLM have the lowest (**). Nonperforated synapses in dSR have a higher particle density than those in both pSR and SLM (#). **(K)** Percentage (bars) and cumulative percentage (lines) of perforated and immunopositive nonperforated synapses with a given number of immunogold particles for AMPARs. **(L)** Superimposed cumulative percentages of perforated and nonperforated synapses with a given number of immunogold particles for AMPARs. All values are based on pooled data from three

rats (431 perforated synapses; 1,306 immunopositive nonperforated synapses) and are presented ± SEM.

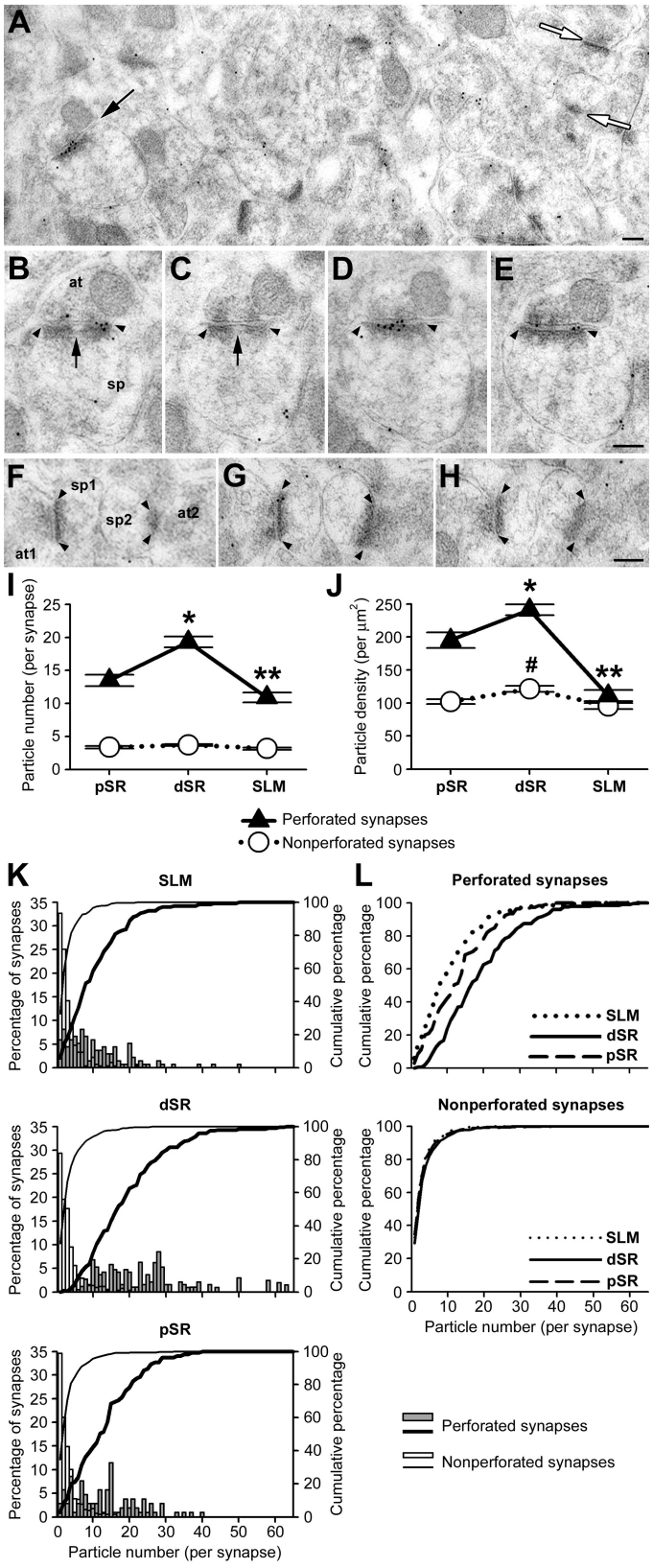
A
B
at
sp
C
D
E
F
sp1
sp2
at2
at1
G
H
I
Particle number (per synapse)
pSR
dSR
SLM
J
Particle density (per μm²)
Perforated synapses
Nonperforated synapses
K
SLM
Percentage of synapses
Cumulative percentage
dSR
pSR
L
Perforated synapses
Nonperforated synapses
Particle number (per synapse)

Figure 2.2.

We found that perforated synapses had more immunogold particles for AMPARs than immunopositive nonperforated synapses, regardless of whether they were in the pSR, dSR, or SLM (Figure 2.2I). However, distance-dependent differences in AMPAR immunoreactivity were seen almost exclusively among perforated synapses. Perforated synapses in the dSR had the highest particle number and density, whereas those in SLM had the lowest particle number and density (Figure 2.2I and J). Among nonperforated synapses, neither the particle number (Figure 2.2I) nor the percentage of immunopositive nonperforated synapses (69, 71 and 69% in the pSR, dSR and SLM, respectively) changed with distance from the soma. The only difference seen among nonperforated synapses was a slightly higher particle density in those from the dSR (Figure 2.2J).

Plots of the percentage of perforated and immunopositive nonperforated synapses with a given number of immunogold particles for AMPARs illustrate that perforated synapses represent a powerful synaptic subtype throughout the apical dendritic tree (Figure 2.2K). Additionally, there is a substantially higher proportion of perforated synapses with > 30 immunogold particles in dSR (13%) compared to both pSR (4%) and SLM (3%). Furthermore, the cumulative frequency plots for perforated synapses with a given number of immunogold particles suggest the possibility that, relative to the pSR, there is a shift toward stronger synapses in dSR, and weaker synapses in SLM (Figure 2.2L). No such pattern is observed among nonperforated synapses (Figure 2.2L). These results provide the first cellular evidence that conductance scaling may be achieved by an increase in the number and density of AMPARs, and they extend this view by demonstrating that the upregulation of AMPARs is limited to perforated synapses. Additionally, this particular form of conductance scaling does not appear to extend to SLM.

2.3.3. Synaptic NMDARs do not scale with distance from the soma

Although a previous study provided compelling evidence that NMDAR-mediated currents do not change with distance from the soma in SR (Andrasfalvy & Magee, 2001), there is evidence that the NMDAR-to-AMPAR ratio is highest in SLM (Otmakhova et al., 2002). Moreover, synaptic currents mediated by NMDARs have slower kinetics than those mediated by AMPARs (Hestrin et al., 1990; Spruston et al., 1995), which, through a variety of mechanisms, can be expected to decrease the impact of voltage attenuation on potentials from very distal synapses such as those in dSR and SLM (Rall, 1977; Schiller & Schiller, 2001; Williams & Stuart, 2003). To determine whether NMDARs play a role in distance compensation we examined NMDAR immunoreactivity in synapses from the pSR, dSR, and SLM.

Figure 2.3. NMDAR expression in perforated and nonperforated synapses throughout the apical dendritic tree in CA1 pyramidal neurons

(A) Low magnification electron micrograph showing a profile of a perforated synapse (black arrow) immunostained for NMDARs. This synaptic profile is seen at a higher magnification in panel **D**. **(B-E)** A perforated synapse (labeled in **B** by at and sp) immunostained for NMDARs, with postsynaptic density (PSD) profiles (arrowheads) exhibiting discontinuities (arrows) in some sections. **(F-H)** A nonperforated synapse immunostained for NMDARs with continuous PSD profiles (arrowheads) in all sections. Scale bars, upper panels = 0.2 μm, lower panels = 0.12 μm. **(I)** Mean number of immunogold particles for NMDARs per perforated (triangles) and nonperforated (circles) synapse. Perforated synapses have more immunogold particles than nonperforated ones in all dendritic regions studied (*), but there are no distance-dependent differences. **(J)** Mean density of immunogold particles for NMDARs per PSD unit area (μm^2). Nonperforated synapses have a higher particle density than their perforated counterparts, but this pattern does not change with distance from the soma (*). **(K)** Percentage (bars) and cumulative percentage (lines) of perforated and nonperforated synapses with a given number of immunogold particles for NMDARs. **(L)** Superimposed cumulative percentages of perforated and nonperforated synapses with a given number of immunogold particles for NMDARs. All values are based on pooled data from three rats (356 perforated synapses; 2,025 nonperforated synapses) and are presented ± SEM.

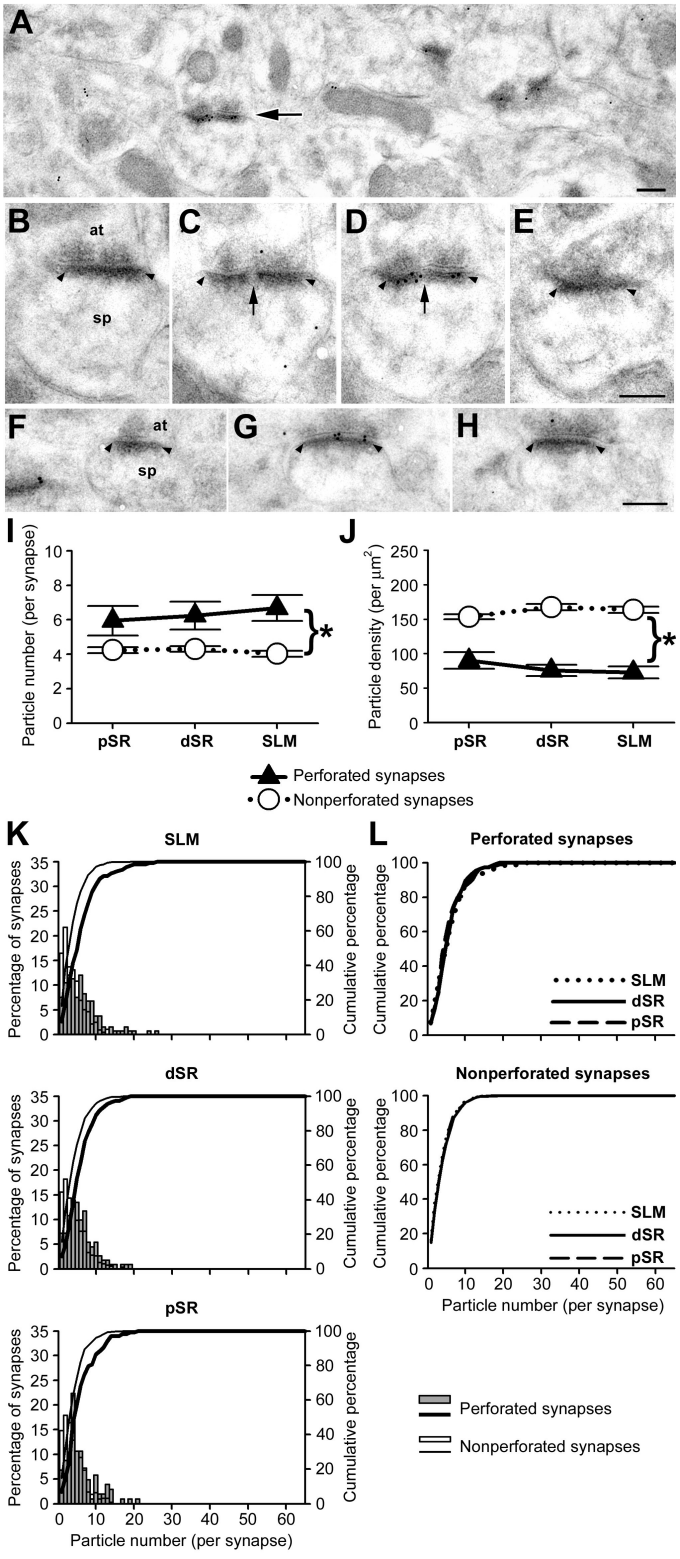
A
B
at
sp
C
D
E
F
at
sp
G
H
I
Particle number (per synapse)
pSR
dSR
SLM
J
Particle density (per μm²)
pSR
dSR
SLM
Perforated synapses
Nonperforated synapses
K
SLM
dSR
pSR
Percentage of synapses
Cumulative percentage
Particle number (per synapse)
L
Perforated synapses
Nonperforated synapses
SLM
dSR
pSR
Cumulative percentage
Particle number (per synapse)
Perforated synapses
Nonperforated synapses

Figure 2.3.

When viewed in serial sections, all perforated (Figures 2.3A-E) and nonperforated (Figures 2.3A and F-H) synapses are immunopositive for NMDARs (Ganeshina et al., 2004b). We found that perforated synapses had a higher number, but a lower density, of immunogold particles for NMDARs than their nonperforated counterparts (Figures 3I and 3J). In stark contrast to synaptic AMPARs, however, NMDAR expression among synapses did not exhibit any distance-dependent differences (Figures 2.3I-L).

Nonspecific labeling might be expected to have a larger proportional effect on nonperforated synapses, which have fewer immunogold particles for AMPARs and NMDARs projected onto their PSD, than on perforated synapses, which have many immunogold particles. When we excluded immunopositive synapses (both perforated and nonperforated) with 1 immunogold particle from the analyses, however, we found the exact same pattern of results for both the AMPAR and NMDAR experiments (Table 2.1 for more information).

2.3.4. Perforated synapses reduce location-dependence in stratum radiatum

The results from our electron microscopic studies show that CA1 pyramidal neurons regulate the number of both perforated and nonperforated synapses as a function of distance from the soma, but adjust synaptic strength only among the perforated subtype, and even then only by modifying the number of AMPARs. The selective involvement of perforated synapses in distance-dependent synaptic scaling suggests that they are the only synaptic subtype capable of reducing their location dependence. To provide insight into the possible functional consequences of such compartment-specific differences in synapse number

and receptor content, we used computer simulations of a morphologically reconstructed pyramidal neuron with passive membrane properties (Golding et al., 2005).

Figure 2.4. Simulating somatic EPSPs generated by nonperforated and perforated synapses at different locations on CA1 pyramidal neuron dendrites

(A) Synaptic conductances (g_{syn}) for perforated (P) and nonperforated (NP) synapses located in stratum oriens (SO), pSR, middle stratum radiatum (mSR), dSR, and SLM in our simulations. All g_{syn} values are relative to a reference conductance (0.3 nS) necessary for a nonperforated synapse located in the most proximal region of pSR to generate a 0.2 mV somatic EPSP. The values for perforated and nonperforated g_{syn} in pSR, dSR, and SLM derive from the results of our AMPAR immunogold electron microscopy experiment. The value for the nonperforated synapse g_{syn} at all dendritic locations was 0.3 nS, whereas the g_{syn} value for perforated synapses changed with distance from the soma (pSR: 1.2 nS; dSR: 1.8 nS; SLM: 1.0 nS). **(B)** Color-coded display of the somatic EPSP generated by synaptic conductances (g_{syn}) characteristic of nonperforated (left) or perforated synapses (right) throughout various locations of the apical dendrite. Color map of somatic EPSP (dV_{soma}) is on a log-scale. **(C)** Percentage and cumulative percentage of perforated (gray bars, thick lines) and nonperforated (white bars, thin lines) synapses located in pSR, dSR, or SLM that produced somatic EPSPs within the ranges of amplitudes displayed in **B**. **(D)** Cumulative percentages of perforated (top panel) and nonperforated (bottom panel) synapses in pSR, dSR, and SLM plotted as a function of the depolarization (in mV) achieved in the soma. **(E)** Average amplitude of somatic EPSPs caused by perforated (P) and nonperforated (NP) synaptic conductances originating in pSR, dSR, or SLM. **(F)** The percentage of EPSPs in pSR, dSR, and SLM that exceeded 0.16 mV. Values for average somatic EPSP amplitudes in **E** are presented ± SD.

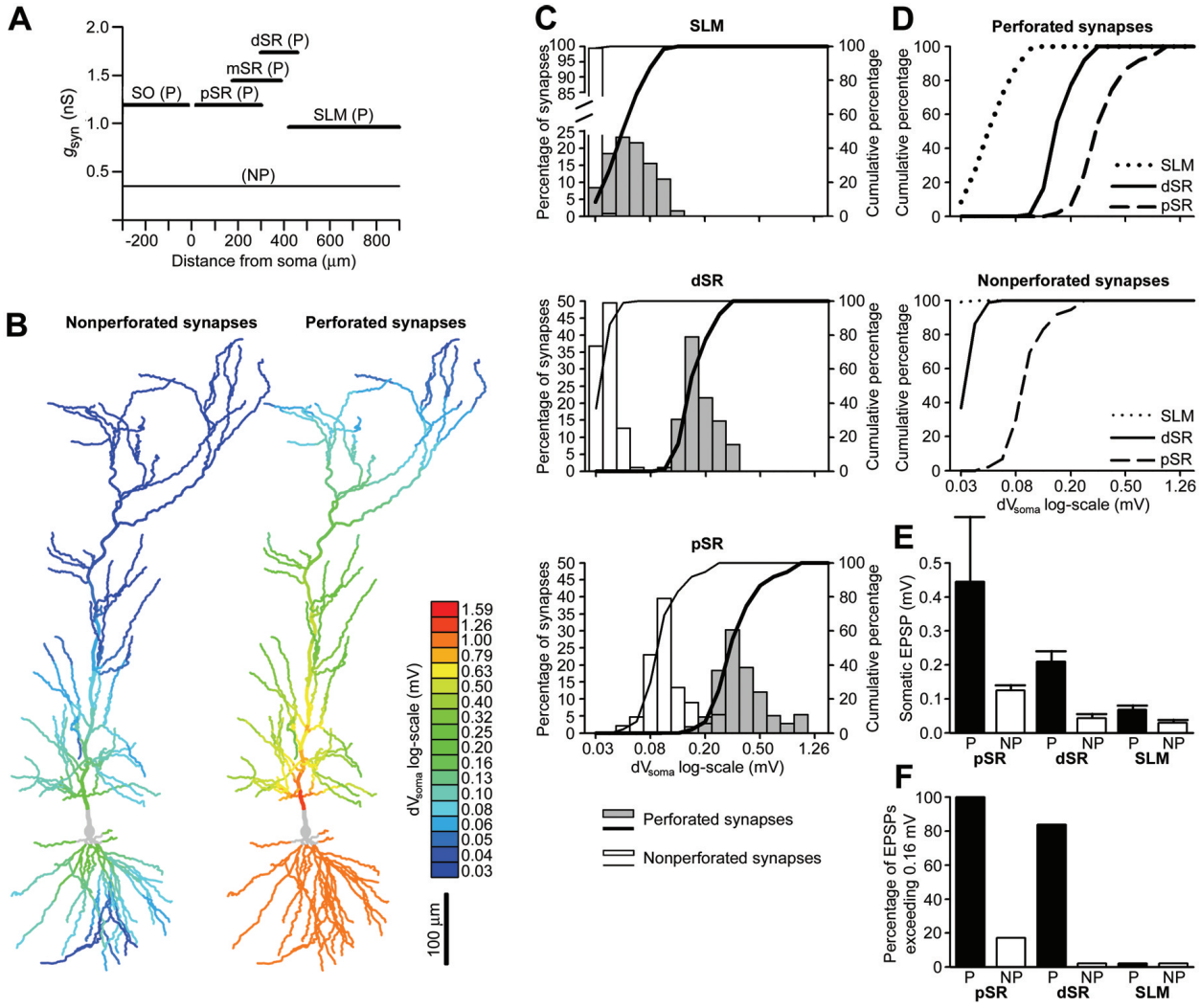
A
2.0
1.5
1.0
0.5
g_{syn} (nS)
dSR (P)
mSR (P)
SO (P)
pSR (P)
SLM (P)
(NP)
-200
0
200
400
600
800
Distance from soma (µm)
B
Nonperforated synapses
Perforated synapses
1.59
1.26
1.00
0.79
0.63
0.50
0.40
0.32
0.25
0.20
0.16
0.13
0.10
0.08
0.06
0.05
0.04
0.03
dV_{soma} log-scale (mV)
100 µm
C
SLM
dSR
pSR
Percentage of synapses
Cumulative percentage
0.03
0.08
0.20
0.50
1.26
dV_{soma} log-scale (mV)
Perforated synapses
Nonperforated synapses
D
Perforated synapses
Nonperforated synapses
SLM
dSR
pSR
E
Somatic EPSP (mV)
P
NP
pSR
dSR
SLM
F
Percentage of EPSPs exceeding 0.16 mV

Figure 2.4.

We first used the computer simulations to model the somatic EPSPs that perforated and nonperforated synapses located throughout the apical dendrite would produce. We used synaptic conductances (g_{syn}) based on the known properties of somatic EPSPs and the relative number of immunogold particles for AMPARs in the two synaptic subtypes (Figure 2.4A). The average amplitude of miniature EPSPs (mEPSPs) in SR is approximately 0.2 mV (Magee and Cook, 2000). We incorporated this into our model by assuming a g_{syn} of 0.3 nS for nonperforated synapses, which resulted in somatic EPSPs of 0.2 mV from the most proximal dendritic synapse locations. Based on the AMPAR immunoreactivity of nonperforated synapses, this value was kept constant at all dendritic locations. The g_{syn} value for perforated synapses was based on their relative level of AMPAR expression compared to nonperforated synapses, and was therefore dependent on dendritic location. We assigned identical g_{syn} values to perforated synapses in stratum oriens (SO) and pSR, given their similar distance from the soma; and extrapolated g_{syn} of perforated synapses in middle stratum radiatum (mSR) to a value intermediate to those in pSR and dSR.

Using these values for g_{syn}, only the most proximal nonperforated synapses produced somatic EPSPs near 0.2 mV (i.e. exceeding 0.16 mV), whereas somatic EPSPs from all other locations were considerably smaller because of the lack of conductance scaling (Figures 2.4B-E). Importantly, nonperforated synapses in dSR and SLM produced EPSPs that were on average 3 to 6 times smaller than those in pSR (pSR: 0.13 mV; dSR: 0.04 mV; SLM: 0.02 mV), suggesting that many nonperforated synaptic potentials originating in distal dendritic regions attenuate to nearly undetectable amplitudes. When perforated synapses were simulated, most synapses throughout SR (100% in pSR, 85% in dSR)

caused somatic EPSPs that exceeded 0.16 mV and produced relatively uniform somatic EPSP amplitudes over a large range of dendritic locations (Figures 2.4B-E). The average somatic EPSP amplitude for perforated synapses in pSR (0.45 mV) exceeded that of perforated synapses in dSR (0.21 mV), but our simulations suggest that somatically-recorded pSR EPSPs are likely to originate from a mixture of both perforated and nonperforated synapses whereas dSR EPSPs would be produced predominantly by perforated synapses (Figures 2.4C-4F). This would result in average pSR EPSPs being intermediate to that of the nonperforated and perforated EPSPs (0.28 mV), and average dSR EPSPs being derived from perforated EPSPs only (0.21 mV). Values based on such assumptions are consistent with recording studies (Magee & Cook, 2000; Smith et al., 2003). On the other hand, EPSPs originating in SLM (average = 0.068 mV) never exceeded 0.2 mV, with > 90% producing somatic EPSPs below 0.1 mV and none above 0.16 mV (Figure 2.4B-E).

The simulations of perforated and nonperforated synapses complement the electron microscopy studies, and together they show that an increase in the proportion (Figure 2.1I,J) and strength (Figures 2I, 2J) of perforated synapses in dSR provides a plausible cellular basis for synaptic location independence throughout SR. These results also show that, despite having the highest proportion of perforated synapses (Figure 2.1J), SLM synapses do not effectively counteract dendritic filtering. Rather, synaptic potentials originating in SLM attenuate so severely that they produce much smaller average somatic EPSPs than SR EPSPs, consistent with previous recording studies (Jarsky et al., 2005).

2.3.5. Evidence for compartment-specific mechanisms of distance compensation

Our studies clearly show that conductance scaling does not extend into SLM, implying that some other mechanism must operate in this region to reduce synaptic location dependence. Dendritic spikes may represent such a mechanism because they are prevalent in SLM, and can be triggered relatively easily by brief bursts of synaptic activity (Gasparini et al., 2004; Golding & Spruston, 1998; Golding et al., 2002; Jarsky et al., 2005). Recent evidence suggests that SLM synapses indeed rely heavily on dendritic spikes because, in their absence, SLM inputs appear to only have minimal impact on neuronal output (Golding et al., 2005; Jarsky et al., 2005). These studies suggest that synapses in SLM are capable of effectively counteracting dendritic filtering only via a two-stage process: (1) SLM synaptic conductances trigger a dendritic spike; and (2) this dendritic spike then propagates toward the soma under some conditions (see Discussion).

Figure 2.5. Modeling of the synaptic conductance required to achieve a normalized somatic EPSP or a large local depolarization

(A) The synaptic conductance required to achieve a somatic EPSP of 0.2 mV throughout the dendritic tree (blue), or a local depolarization to -30 mV (red). Synaptic conductance (g_{syn}) values were normalized relative to the reference conductance (g_{ref}) used for simulations of nonperforated synapses in pSR (0.3 nS; Figure 2.4), and are plotted on a log-scale. **(B)** Plots, as a function of dendritic location, of the g_{syn} required to achieve either a somatic EPSP of 0.2 mV (blue) or a local depolarization to -30 mV (red) first. **(C)** The percentage of synaptic locations that achieved a somatic EPSP of 0.2 mV first (blue) or a local depolarization to -30 mV first (red) in pSR, dSR, and SLM. **(D)** Average values of the synaptic conductances (g_{syn}) required to achieve either a somatic EPSP of 0.2 mV (blue) or a local depolarization to –30 mV (red) for synaptic locations in pSR, dSR, and SLM. Number of immunogold particles for AMPARs per perforated synapse (black) in pSR, dSR, and SLM is superimposed with a separate ordinate. The axis for immunogold particle number is aligned such that the average particle number per immunopositive nonperforated synapse in pSR (3.38) is level with the average value required to achieve a 0.2 mV somatic EPSP in pSR (0.58 nS). All values are presented ± SEM.

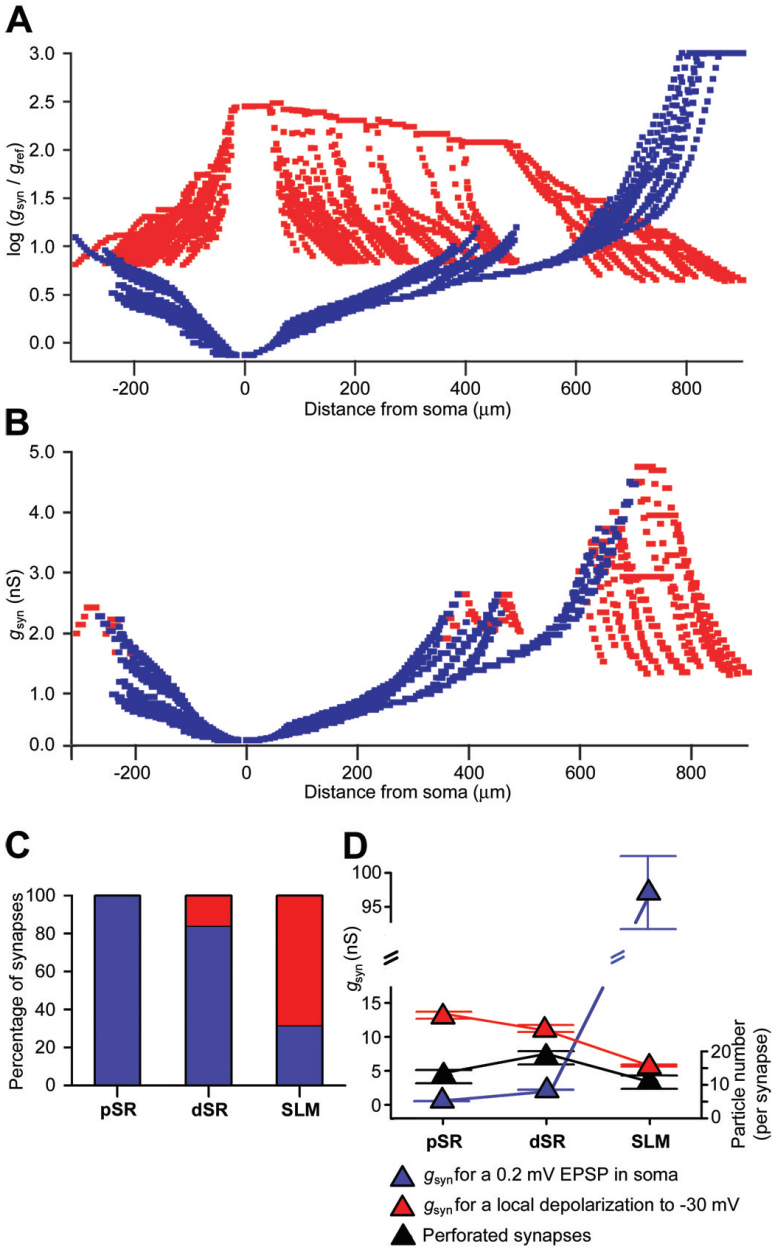
A
log (g_{syn} / g_{ref})
Distance from soma (µm)
B
g_{syn} (nS)
Distance from soma (µm)
C
Percentage of synapses
pSR
dSR
SLM
D
g_{syn} (nS)
Particle number (per synapse)
pSR
dSR
SLM
g_{syn} for a 0.2 mV EPSP in soma
g_{syn} for a local depolarization to -30 mV
Perforated synapses

Figure 2.5.

To explore the possibility that SLM synapses preferentially use dendritic spikes rather than conductance scaling, we used the computational model to compare the conductances necessary to achieve two different conditions: (1) a unitary EPSP of 0.2 mV at the soma; and (2) a local depolarization to 30 mV, which can be considered sufficient to generate a local dendritic spike (Gasparini et al., 2004; Golding & Spruston, 1998). We incrementally increased the value of g_{syn} for synaptic locations throughout the dendritic tree until each of the two conditions was achieved. We then examined whether the g_{syn} necessary to achieve these two different conditions varied with distance from the soma. A unitary somatic EPSP of 0.2 mV could be achieved with relatively moderate increases in synaptic strength throughout pSR and dSR (Figure 2.5A, blue). Consistent with the previous electrophysiological studies and our electron microscopic experiments showing an increase in the number and AMPAR immunoreactivity of perforated synapses in dSR, g_{syn} of these synapses needed to be increased up to 10-fold relative to the reference conductance (g_{ref}) in pSR (0.3 nS) to normalize the somatic EPSP. Much larger g_{syn} values were required for synapses in SLM. Specifically, synaptic conductances ranging from 100 to over 1000 times that of more proximal synaptic locations were required to effectively counteract dendritic filtering and produce a somatic EPSP of 0.2 mV (Figure 5A, blue). Thus the pattern of resulting conductances is consistent with our electron microscopic data from SR, but not from SLM, where perforated synapses have the lowest level of AMPAR expression. When we simulated the g_{syn} necessary to depolarize the local membrane potential to -30 mV, the highest values were observed for the large diameter main apical dendrite (Figure 2.5A, red). Much smaller values were required in the smaller diameter apical oblique and tuft branches (Figure 2.5A, red). For most synapses in SLM, the conductance required to reach

-30 mV was substantially lower than the conductance required to achieve a 0.2 mV somatic EPSP (Figure 2.5A, red). That is, when the most distal synapses – primarily within SLM – were activated, they achieved our dendritic spike threshold before they generated a 0.2 mV somatic EPSP (Figures 5A-5D). Importantly, this observation is opposite to that seen in SR, where most synaptic locations produced the normalized somatic EPSP at lower g_{syn} values than those required to produce a local depolarization to -30 mV (Figures 2.5A-D). Taken together our studies indicate that perforated synapses in SR scale their strength to produce somatic EPSPs near 0.2 mV, whereas those in SLM are governed by different rules, perhaps depending on their ability to recruit dendritic spikes, rather than their ability to depolarize the soma (Figure 2.5D).

2.4. Discussion

How synapses on the most remote dendritic locations influence neuronal output remains a critical question. In the absence of compensatory mechanisms, a distance-dependent gradient would be imposed on synaptic potentials in the soma/axon. Here we provide cellular and computational evidence that synapses located in different dendritic regions employ distinct mechanisms to diminish any such gradients and mitigate the effects of dendritic filtering. First, we show that perforated and nonperforated synapse number is different in pSR, dSR, and SLM (Figure 2.6A). The major result of these differences is that the proportion of perforated synapses increases with distance from the soma. Second, we show that AMPAR, but not NMDAR, expression varies across dendritic compartments (Figure 2.6A). AMPAR content is highest in dSR and lowest in SLM, and these compartment-specific differences are found only within the perforated synaptic

subtype. Third, we used computer simulations to examine the somatic EPSPs that a perforated or nonperforated synapse located throughout the apical dendrite would produce and found that perforated synapses are the only subtype capable of effectively reducing their location dependence, and that such success is confined to the SR. Finally, using computer simulations, we incrementally strengthened synaptic conductances at locations throughout the apical dendrite and found that synapses in SR achieve a somatic EPSP criterion before they achieve a local depolarization criterion, whereas SLM synapses cause the large local depolarization first (i.e. at lower synaptic conductances). These results are consistent with the idea that the strength of synapses in SR is determined by their ability to depolarize the soma/axon, whereas synaptic strength in SLM is governed by the ability to cause large local depolarizations. Moreover, they provide strong evidence that only perforated synapses in SR use conductance scaling to achieve location independence, whereas those in SLM need to first trigger dendritic spikes to successfully counteract dendritic filtering.

Figure 2.6. Summary of the differences in the proportion of perforated and nonperforated PSDs, PSD size, and receptor-content of axospinous synapses located on CA1 apical dendrites. Synapse number and receptor content are depicted in proportion to their relative numbers as determined in Experiments 1-3. There are twice as many perforated synapses in dSR and SLM as in pSR. In addition, perforated synapses in dSR have the most AMPARs. AMPAR immunoreactivity of nonperforated synapses is not different at the various dendritic locations, but there are fewer of these synapses in SLM. Although perforated synapses have more NMDARs than nonperforated synapses, this difference does not change with distance from the soma. Additionally, the PSD sizes of nonperforated synapses immunopositive for AMPARs were larger than immunonegative ones, and PSD size among perforated synapses increased with distance from the soma. See Figure 2.7 and Table 2.2 for further information.

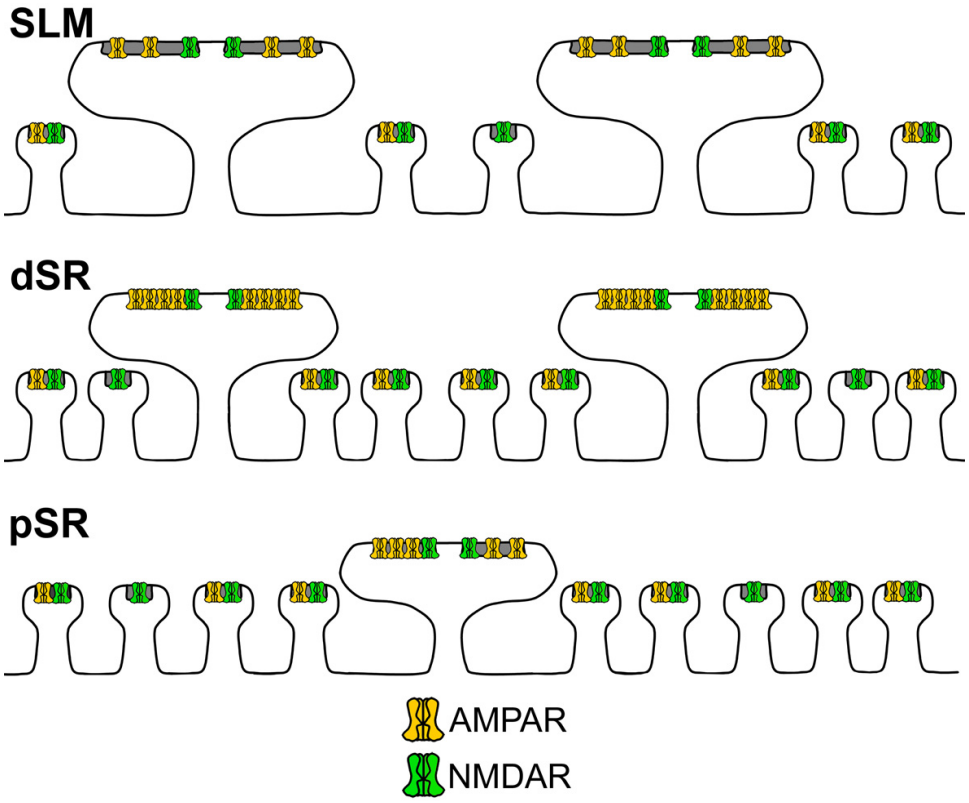

Figure 2.6.

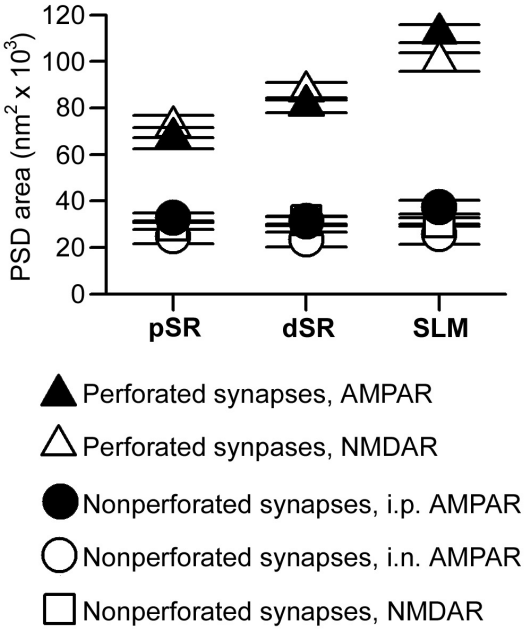

Figure 2.7.

Figure 2.7. Changes in PSD correlate with AMPAR immunoreactivity, PSD configuration, and distance from the soma. Nonperforated synapses that were immunonegative for AMPARs (i.n.) were significantly smaller than immunopositive nonperforated synapses (i.p.), and both are significantly smaller than perforated synapses. PSD area among nonperforated synapses does not change with distance from the soma. In contrast, perforated synapses in dSR are significantly larger than those in pSR (double asterisks). Perforated synapses in SLM are significantly larger than perforated synapses in both pSR and dSR (triple asterisks). Differences and post hoc comparisons were considered statistically significant at $P < 0.05$.

Antigen	Dendritic region	Synaptic subtype	Particle number and range	Particle number Individual means (rat1, rat2, rat3)	Particle number CV	Particle density and range (per μm²)	Particle density CV	Particle density Individual means (rat1, rat2, rat3)
AMPAR	pSR	NP	3.38 (1-39)	3.0, 2.9, 4.14	1.14	102.1 (7-616)	0.82	90, 97, 119
AMPAR	dSR	NP	3.70 (1-28)	3.8, 3.2, 4.01	1.01	121.2 (15-856)	0.85	110, 117, 135
AMPAR	SLM	NP	3.15 (1-22)	2.7, 2.6, 3.6	0.96	94.9 (9-593)	0.82	66, 80, 116
AMPAR	pSR	P	13.45 (1-40)	11.2, 12.9, 17.1	0.65	195.7 (18-571)	0.62	169, 177, 228
AMPAR	dSR	P	19.30 (2-63)	17.2, 18.1, 24.8	0.58	241.9 (42-631)	0.47	206, 223, 302
AMPAR	SLM	P	10.93 (1-50)	7.4, 8.6, 16.8	0.80	110.8 (10-480)	0.89	65, 62, 112
Antigen	**Dendritic region**	**Synaptic subtype**	**Particle number (range)**	**Particle number Individual means (rat1, rat2, rat3)**	**Particle number CV**	**Particle density and range (per μm²)**	**Particle density CV**	**Particle density Individual means (rat1, rat2, rat3)**
NMDAR	pSR	NP	4.23 (1-19)	3.7, 4.2, 5.0	0.68	153.4 (14-635)	0.64	127, 168, 167
NMDAR	dSR	NP	4.30 (1-17)	3.9, 4.2, 4.5	0.68	167.3 (11-853)	0.94	134, 177, 187
NMDAR	SLM	NP	4.02 (1-19)	3.5, 4.1, 4.4	0.69	163.7 (12-608)	0.71	140, 166, 187
NMDAR	pSR	P	5.95 (1-21)	5.1, 5.9, 7.0	0.65	90.0 (12-323)	0.66	78, 95, 97
NMDAR	dSR	P	6.24 (1-19)	5.7, 5.5, 7.4	0.63	75.5 (13-276)	0.61	72, 77, 77
NMDAR	SLM	P	6.68 (1-26)	5.7, 7.1, 7.4	0.73	72.7 (6-273)	0.71	68, 81, 68

Mean values for immunogold particle number and density when immunopositive synapses with 1 particle are excluded

Antigen	Dendritic region	Synaptic subtype	n	n (excluded)	Particle number	Particle density (per μm²)
AMPAR	pSR	NP	338	182	4.65	135.6
AMPAR	dSR	NP	363	151	4.95	150.2
AMPAR	SLM	NP	185	90	4.1	122.3
AMPAR	pSR	P	101	1	13.51	199.1
AMPAR	dSR	P	190	0	19.3	241.9
AMPAR	SLM	P	128	8	11.25	118.1
NMDAR	pSR	NP	528	96	4.75	170.1
NMDAR	dSR	NP	641	118	4.8	188.5
NMDAR	SLM	NP	542	105	4.6	185.2
NMDAR	pSR	P	87	1	5.96	94.1
NMDAR	dSR	P	136	1	6.24	78.7
NMDAR	SLM	P	118	8	7.04	79.4

Table 2.1. Immunogold quantification of AMPARs and NMDARs

Though not directly proven by our experiments, the compartment-specific use of conductance scaling and dendritic spikes to reduce synaptic location dependence is also supported by evidence from other studies. Previous electrophysiological work has shown that SR synapses can increase their conductance to compensate for their distance from the soma/axon (Magee & Cook, 2000; Smith et al., 2003). These studies found that the amplitudes of somatically-recorded mEPSPs are relatively independent of their location of origin within SR, while the distribution of dendritically recorded mEPSCs contained substantially more large-amplitude events in dSR than in pSR. These data are consistent with our results. For example, the increase we found in the number and AMPAR immunoreactivity of perforated synapses in dSR might account for the findings that there is a higher incidence of large-amplitude mEPSCs in dSR, with some mEPSCs being 2-3 times larger than any seen in pSR (Magee & Cook, 2000; Smith et al., 2003). That is, these findings suggest that conductance scaling in SR is achieved by increases in the number of perforated synapses, as well as increases in their AMPAR content. In SLM, however, the AMPAR immunoreactivity of perforated synapses was significantly lower than that in both pSR and dSR. This suggests that perforated synapses in SLM actually may be the weakest of all such synapses on the apical dendrites, thereby indicating that conductance scaling does not extend to SLM.

Several studies indicate that dendritic spikes, rather than conductance scaling, may be used by SLM synapses to influence neuronal output. Although EPSPs originating in SLM attenuate the most, the small diameter of these branches (Megias et al., 2001) will cause local EPSPs to be larger (Rall, 1977) and therefore more likely to trigger local dendritic spikes. This idea is consistent with our study, which suggests that synaptic

strength in SLM is actually scaled down as a result of the ease with which large local depolarizations could be achieved in this region. Moreover, in the absence of dendritic spikes, SLM synapses are unable to generate axonal action potentials and have only minimal impact on somatic depolarization (Golding et al., 2005; Golding & Spruston, 1998; Jarsky et al., 2005; Wei et al., 2001). Though the propagation of dendritic spikes in SLM can be restricted to the apical tuft (Cai et al., 2004; Golding & Spruston, 1998; Wei et al., 2001), such spatial confinement is dramatically reduced by modest synaptic activity in SR (Jarsky et al., 2005). In other words, synapses in SR actively gate the propagation of dendritic spikes originating in SLM, conferring to dendritic spikes the ability to propagate to the soma, and allowing dendritic spikes to act as a reliable mechanism of distance compensation for SLM synapses. Together, these findings strengthen the notion that perforated synapses in SR can communicate directly with the soma/axon in a relatively location independent manner by use of conductance scaling, but that SLM synapses first need to trigger dendritic spikes, which then propagate toward and ultimately depolarize the final integration zones in the soma and axon. Importantly, dendritic spikes are not a mechanism of distance compensation exclusive to SLM synapses. Rather, SR synapses can influence activity in the soma and axon with or without dendritic spikes (Gasparini & Magee, 2006), whereas SLM synapses are unlikely to impact neuronal output in their absence (Jarsky et al., 2005). Even if SLM synaptic potentials summate with EPSPs in dSR to trigger local spikes in SR (Jarsky et al., 2005), the available data are consistent with the notion that SLM synapses rely on dendritic spikes to drive axonal action potentials, whereas SR synapses do not.

2.4.1. Synaptic subtypes and neuronal output

Since their initial description (Carlin et al., 1980; Peters & Kaiserman-Abramof, 1969), perforated and nonperforated synapses were thought to differ functionally, but the nature of any such differences has remained elusive. Because perforated synapse number and proportion is increased during development, learning, and after long-term potentiation (reviewed in (Bailey & Kandel, 1993; Geinisman, 2000; Greenough & H., 1988; Harris et al., 1992; Jones & Harris, 1995; Nikonenko et al., 2002; Nimchinsky et al., 2002)), one view is that they represent a synaptic subtype capable of generating large synaptic conductances. Recent work using postembedding immunogold electron microscopy for AMPARs and NMDARs has supported this idea (Desmond & Weinberg, 1998; Ganeshina et al., 2004a,b). The present study not only provides further support for such a notion, but also extends it by showing that perforated synapses are likely to play an integral role in allowing multiple dendritic compartments of CA1 pyramidal neurons to contribute to action potential output regardless of their distance from the soma. If we assume that AMPAR immunoreactivity is proportional to the actual number of AMPARs present at synapses, and that g_{syn} is proportional to AMPAR number, then the argument can be made that the contribution of single synapses to neuronal output is dichotomous: single perforated synapses can communicate effectively with the soma, but most single nonperforated synapses cannot. One major consequence of such differences in synaptic efficacy is that the contribution of these two synaptic subtypes to neuronal activity is likely to be very different.

Given their small g_{syn} and somatic EPSP, the synchronous activation of many (> 100) nonperforated synapses would be required to trigger axonal action potentials or

dendritic spikes. And because they do not exhibit conductance scaling, the number of coincidentally activated nonperforated synapses required to produce an axonal action potential would increase progressively with distance from the soma. Considering the high level of AMPAR expression in perforated synapses, they are more likely to contribute to both axonal and dendritic spikes than their nonperforated counterparts throughout SR and SLM. Our simulations indicate, however, that dendritic filtering of EPSPs originating in SLM is so severe that even perforated synapses may not contribute substantially to somatic depolarization. Rather, these synapses may instead operate together to trigger dendritic spikes. Given their abundance of AMPARs, the relative frequency of perforated synapses may be highest in SLM to increase the probability that synaptic input causes a local depolarization sufficient to trigger a dendritic spike.

2.4.2. Perforated synapses and synaptic transmission

The probabilistic nature of vesicular release and the lack of saturation of AMPARs and NMDARs during quantal transmission (Liu et al., 1999; Mainen et al., 1999; McAllister & Stevens, 2000) suggest that two mechanisms might operate in favor of increasing the strength of transmission at perforated synapses. First, the high number of AMPARs at perforated synapses might increase the number of channels activated, independent of changes in single channel current or presynaptic parameters. With these parameters being equal throughout SR (Smith et al., 2003), increasing the number of perforated synapses or the number of AMPARs per synapse each represents a relatively straightforward means of increasing synaptic strength in dSR. An analogous mechanism involving insertion of $GABA_A$ receptors and augmentation of inhibitory postsynaptic currents might operate

at inhibitory synapses onto cerebellar stellate cells (Nusser et al., 1997) and hippocampal granule cells (Nusser et al., 1998a). An increase in the relative frequency of perforated synapses in dSR, with their high AMPAR content, would increase the number of synapses operating under conditions of high receptor activation, resulting in local mEPSPs with large amplitudes. The increased number of activated AMPARs at perforated synapses may also decrease the number of transmission failures due to unbound glutamate, thereby enhancing the reliability of information transfer across the synaptic cleft.

Second, because the presynaptic active zone co-localizes with the PSD (Harris & Sultan, 1995), and the extent of both organelles along the synaptic cleft is much larger in perforated synapses than in nonperforated ones, multivesicular release may occur at perforated synapses. Multiquantal release onto CA1 pyramidal neuron synapses (Christie & Jahr, 2006) would result in the summation of multiple postsynaptic quantal responses (Conti & Lisman, 2003; Raghavachari & Lisman, 2004), and generate large local mEPSPs, such as those seen in dSR, but not pSR (Magee & Cook, 2000; Smith et al., 2003). If these notions regarding synaptic transmission at perforated synapses are accurate, then the progressive increase in the proportion of perforated synapses with distance from the soma may enhance postsynaptic reliability and potency in both SR and SLM. Moreover, such large EPSPs would confer to perforated synapses throughout SR relative equivalence in influencing axonal action potential output, and would make synaptic activation in SLM more likely to cause local depolarizations beyond the dendritic spike threshold.

It is important to note that we are assuming that synaptic transmission *per se* is fundamentally similar within SR and SLM, and at perforated and nonperforated synapses. While many of the parameters that influence synaptic strength are indeed similar in pSR

and dSR (Smith et al., 2003), essentially nothing is known about them in SLM due to the technical limitations of patching onto the small-diameter dendritic tufts in this region, and no study has ever explicitly compared synaptic transmission at perforated versus nonperforated synapses. Future studies combining optical or electrophysiological measurements of transmission at single synapses and subsequent serial section electron microscopic analyses of the activated synapses (e.g. (Mackenzie et al., 1999) are necessary to further address the validity of our assumptions.

Our study indicates that the contribution of synapses to neuronal output differs with regard to their subtype and dendritic location, and that location dependence among synapses is reduced only for the perforated subtype, which utilizes conductance scaling in SR and the generation of dendritic spikes in SLM. Regardless of its functional significance, many questions remain concerning the distance-dependent regulation of synaptic ultrastructure and receptor content. For example, one important question is whether there are differences in the glutamate receptor subunit composition of the different synaptic subtypes, and whether this composition changes with distance from the soma. Of further interest is whether the content of other PSD-bound proteins, such as those involved in signal transduction and structural stability (Ehlers, 2002; Kennedy, 2000; Li et al., 2004; Peng et al., 2004), differs between perforated and nonperforated synapses in the various dendritic regions, particularly within SLM, where perforated PSDs are significantly larger than those in SR, despite having the lowest number of AMPARs. Also unknown is whether perforated and nonperforated synapses differ in their relative levels of stability. Considering that perforated synapses are typically much larger than nonperforated ones, recent evidence suggests that synaptic subtype-specific variation in activity-dependent plasticity

may indeed exist (Geinisman, 2000; Lang et al., 2004; Matsuzaki et al., 2004; Noguchi et al., 2005). In addition, the forms of synaptic plasticity underlying distance-dependent regulation of synapse number and AMPAR content, although unknown, are probably different because the number of both perforated and nonperforated synapses changes with distance from soma, whereas synaptic strength is changed exclusively within the perforated subtype. These and other questions will need to be addressed in future experiments to fully catalog the effects that such regulation has on synaptic integration at the various dendritic locations.

2.5. Experimental Procedures

2.5.1. Experimental animals

Six young adult (6-month-old) male F_1 hybrid Fischer344xBrown Norway rats (Harlan, Indianapolis, Indiana) were used in the studies performed either with conventional (n = 3) or postembedding immunogold (n = 3) electron microscopy. All experiments were conducted following the procedures approved by the Animal Care and Use Committee of Northwestern University.

2.5.2. Unbiased quantitative electron microscopy

Tissue samples prepared for conventional electron microscopy were used to assess the total number of axospinous perforated and nonperforated synapses in the dorsal half of the hippocampus with unbiased stereological sampling and counting procedures combined with serial section analyses (Geinisman et al., 2004). Briefly, the rats were intracardially perfused with a mixture of paraformaldehyde and glutaraldehyde, the right hippocampal formation was dissected free and its dorsal half cut into 5-7 consecutive transverse slabs. The location of the first cut was chosen randomly within the first (most rostral) 0.8 mm interval, and subsequent cuts were made systematically at 0.8 mm intervals. From the rostral face of slab, a 2μm-thick histological section was prepared and stained with azure II/methylene blue. In such sections, CA1 was distinguished from adjacent CA2 and subiculum by a relatively narrow stratum pyramidale formed by tightly packed pyramidal cell bodies of a homogenously small size (Amaral & Witter, 1995; Ishizuka et al., 1995). Within CA1, SLM was delineated from SR by the abundance of myelinated fibers and the absence of pyramidal cell dendrites running perpendicular to the hippocampal fissure

as in the pSR and dSR (Ishizuka et al., 1995; Megias et al., 2001). Outlines of the SR and SLM sectional profiles were drawn, and their areas estimated in each section by point counting. The total volume of CA1 SR and SLM in the dorsal hippocampus was calculated as the product of their profile areas and the thickness of the tissue slabs. pSR and dSR were each assigned the volume that was equal to one-third of the total SR volume. From these slabs, five were chosen in a systematic random manner and used for obtaining 27 – 35 serial ultrathin sections from each slab (5 slabs per rat; 15 slabs total). Each section spanned the extent of the apical dendritic region of CA1 pyramidal neurons, from the pyramidal cell layer to the hippocampal fissure. The borders of the pSR, dSR, and SLM were determined from measurements performed on histological sections using the field delineator of the electron microscope. Subsequently, electron micrographs (final magnification of 21,900x) of a systematic randomly selected sampling field were obtained from each apical dendritic zone on the same set of serial sections. The synaptic numerical density was estimated using the physical disector method on micrographs of adjacent serial sections (24 disectors were examined in each dendritic zone per slab). In each rat, the total number of perforated and nonperforated synapses was estimated separately for the pSR, dSR, and SLM as the product of the volume of the dendritic region (in μm^3) and its average synaptic numerical density (synapses/ μm^3) obtained from the 5 slabs. The ratio of perforated to nonperforated synapses was calculated from their total numbers. The data were derived from analyses of 1,032 perforated synapses and 7,569 nonperforated synapses (340, 316, and 376 perforated synapses; 2,463, 2,584, and 2,522 nonperforated synapses from three rats).

2.5.3. Quantification of AMPAR and NMDAR immunoreactivity

Expression of postsynaptic AMPARs and NMDARs was assessed with postembedding immunogold electron microscopy as specified previously (Ganeshina et al., 2004a,b). The sampling design indicated above was used with the following modifications. The dorsal half of the right hippocampal formation was cut into transverse 0.3 mm-thick slabs. In 5 slabs selected in a systematic random manner, the CA1 region was divided along its medio-lateral extent into 3 blocks, each of 0.5-1 mm in width. Following plunge-freezing, freeze-substitution, and low temperature embedding in Lowicryl (Electron Microscopy Sciences), one block from each slab was used to prepare 17 – 33 serial ultrathin sections (5 blocks per rat; 15 blocks total). The latter were immunostained with a mixture of primary antibodies (Chemicon) specific either to AMPAR subunits (GluR1, GluR2, GluR2/3, and GluR4) or NMDAR subunits (NR1 and NR2A/B) and then with secondary antibodies conjugated to 10-nm gold particles (British BioCell International). Electron micrographs (final magnification of 37,800x) were obtained from systematic randomly selected fields of the pSR, dSR, and SLM in the same serial sections. From each field, synapses were sampled with 24 disectors. The number of particles per synapse, PSD area, and particle concentration per PSD unit area (μm^2) were estimated on these electron micrographs. PSD area was calculated for each synapse as the product of the total linear length of its PSD profiles measured on serial sections (in μm) and the average section thickness (0.068 μm). For the AMPAR immunostaining, the data were derived from a total of 431 perforated synapses and 1,306 immunopositive nonperforated synapses (165, 131, and 135 perforated synapses and 476, 324, 506 immunopositive nonperforated synapses from three rats). NMDAR immunoreactivity was estimated from analyses of 356 perforated synapses

and 2,025 nonperforated synapses, all of which were immunopositive (117, 134, and 105 perforated synapses and 659, 728, and 638 nonperforated synapses from three rats). See Table 2.1 for data from individual rats.

2.5.4. Data analyses

The variance of the data from individual rats was compared statistically using Hartley's F-max test and Cochran's C-test. There were no statistical differences in any of the three experiments, and analyses were therefore performed on the pooled data. The total number of synapses and the perforated-to-nonperforated synapse ratio were evaluated statistically using analysis of variance. AMPAR and NMDAR immunoreactivity was compared with multivariate analysis of covariance, using PSD area as the covariate. Differences and post hoc comparisons (Tukey's Honestly Significant Difference) were considered statistically significant at $P < 0.05$.

2.5.5. Computational modeling

The CA1 pyramidal neuron model used for all simulations was reconstructed from a stained neuron in a hippocampal slice as described previously (Golding et al., 2005). All simulations were performed using the neuronal simulator NEURON (Hines & Carnevale, 1997). The model included only passive membrane properties, which were constrained by direct recording of voltage attenuation from the soma to a dendritic recording in the same neuron (Golding et al., 2005). Addition of a hyperpolarization-activated conductance to the model increased the voltage attenuation for all synapses, but did not appreciably change the results of the presented simulations (Figure 2.8 and 2.9). Similar results were

obtained in a second model of a CA1 pyramidal neuron derived in the same way as the first model (Figures 2.10, 2.10, 2.10, and 2.10), and two additional models with multiple active conductances (Figures 2.14 and 2.15). NEURON code for all simulations is available online at http://www.northwestern.edu/dendrite.

Figure 2.8.Simulation of somatic EPSPs generated by nonperforated and perforated synapses at different locations on CA1 pyramidal neuron dendrites after adding a hyperpolarization-activated conductance. **(A)** g_{syn} for synapses located in stratum oriens (SO), pSR, middle stratum radiatum (mSR), dSR, and SLM in our simulation. All g_{syn} values are relative to the reference conductance (g_{ref} ; 0.33 nS) necessary for a nonperforated synapse located in pSR to generate a 0.2 mV somatic EPSP (see text for details). **(B)** Color-coded display of the somatic EPSP generated by synaptic conductances (g_{syn}) located throughout the apical dendrite for a fixed g_{syn} characteristic of nonperforated synapses (left), or by a variable g_{syn} scaled according to the results for perforated synapses in our immunogold electron microscopy experiment (right).

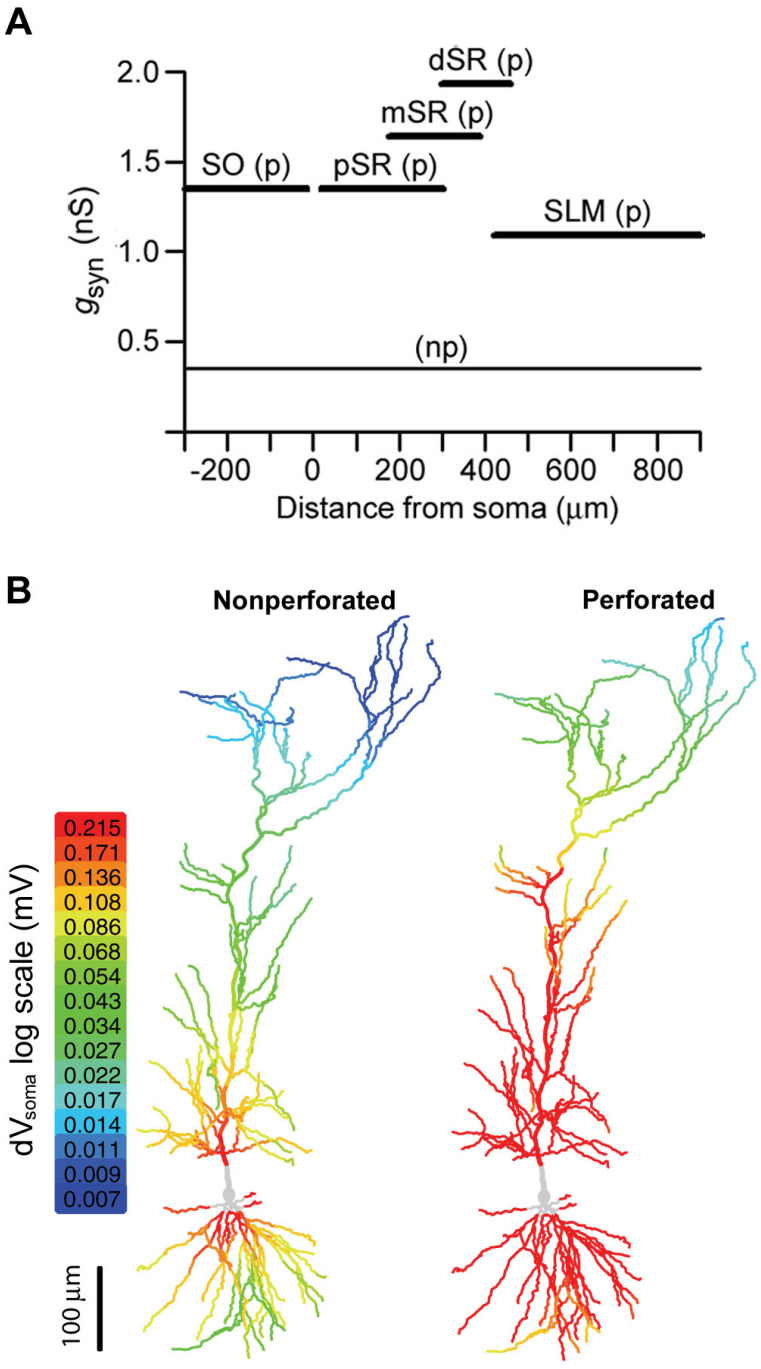
A
2.0
1.5
1.0
0.5
g_{syn} (nS)
dSR (p)
mSR (p)
SO (p)
pSR (p)
SLM (p)
(np)
-200
0
200
400
600
800
Distance from soma (µm)
B
Nonperforated
Perforated
dV_{soma} log scale (mV)
0.215
0.171
0.136
0.108
0.086
0.068
0.054
0.043
0.034
0.027
0.022
0.017
0.014
0.011
0.009
0.007
100 µm

Figure 2.8.

Figure 2.9. Modeling of the synaptic conductance required to achieve a somatic EPSP or a large local depolarization after adding a hyperpolarization-activated conductance. **(A)** The synaptic conductance (g_{syn}) required to achieve a somatic EPSP of 0.2 mV throughout the dendritic tree (blue), or a local depolarization to -30 mV (red). **(B)** Plots of the g_{syn} that achieved either a somatic EPSP of 0.2 mV (blue) or a local depolarization to -30 mV (red) first. **(C)** The percentage of synaptic locations that achieved a somatic EPSP of 0.2 mV first (blue) or a local depolarization to -30 mV first (red) in pSR, dSR, and SLM.

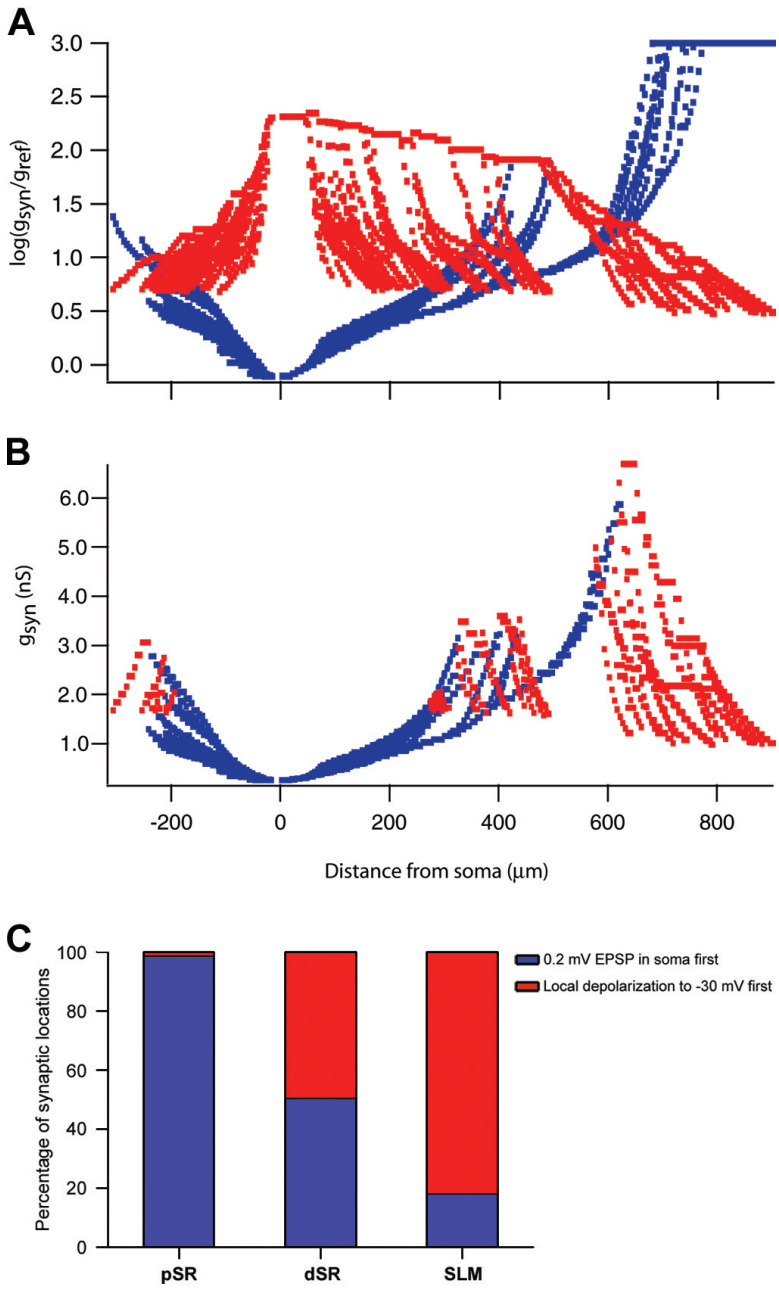
A
3.0
2.5
2.0
1.5
1.0
0.5
0.0
log(gsyn/gref)
B
6.0
5.0
4.0
3.0
2.0
1.0
gsyn (nS)
-200
0
200
400
600
800
Distance from soma (µm)
C
100
80
60
40
20
0
Percentage of synaptic locations
pSR
dSR
SLM
0.2 mV EPSP in soma first
Local depolarization to -30 mV first

Figure 2.9.

Figure 2.10. Simulation of somatic EPSPs generated by nonperforated and perforated synapses at different dendritic locations in a second model of a CA1 pyramidal neuron. **(A)** g_{syn} for synapses located in stratum oriens (SO), pSR, middle stratum radiatum (mSR), dSR, and SLM in our simulation. All g_{syn} values are relative to the reference conductance (g_{ref} ; 0.44 nS) necessary for a nonperforated synapse located in pSR to generate a 0.2 mV somatic EPSP (see text for details). **(B)** Color-coded display of the somatic EPSP generated by synaptic conductances (g_{syn}) located throughout the apical dendrite for a fixed g_{syn} characteristic of nonperforated synapses (left), or by a variable g_{syn} scaled according to the results for perforated synapses in our immunogold electron microscopy experiment (right).

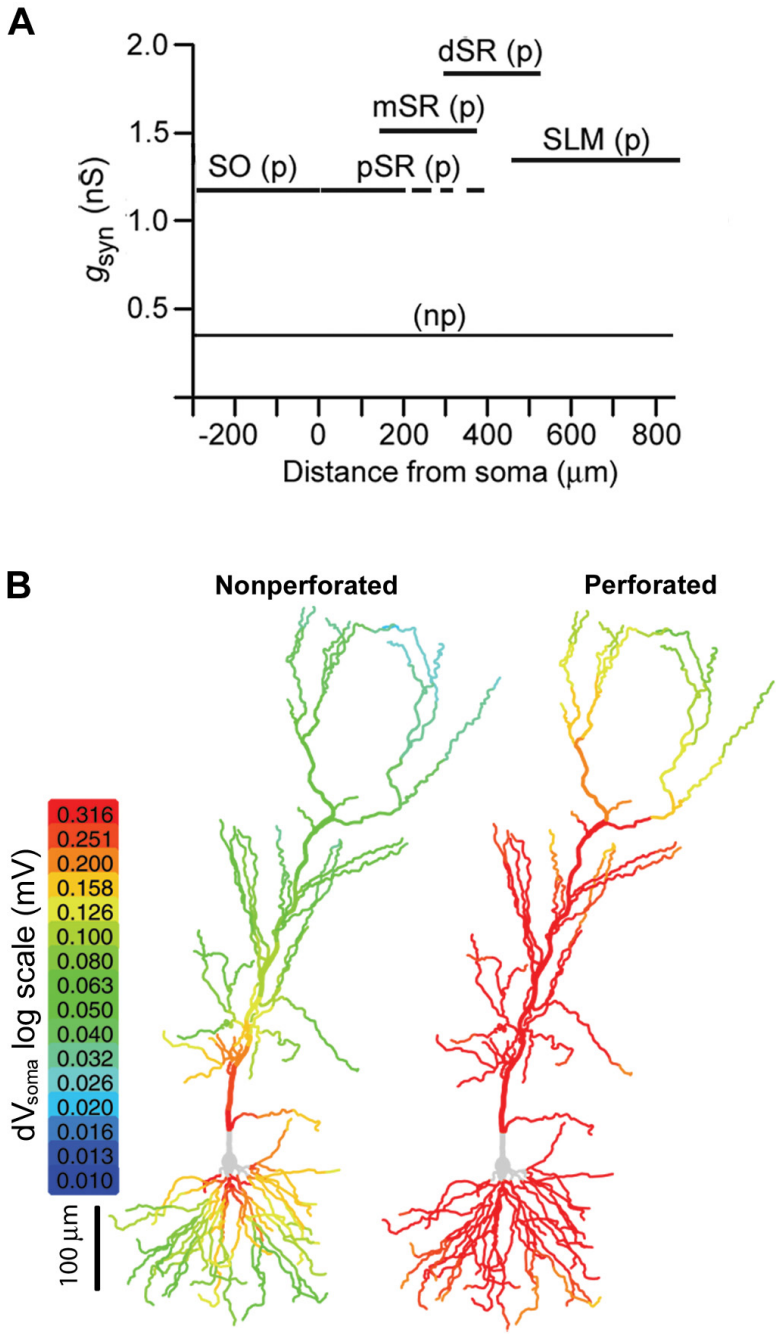
A
2.0
1.5
1.0
0.5
g_{syn} (nS)
dSR (p)
mSR (p)
SLM (p)
SO (p)
pSR (p)
(np)
-200
0
200
400
600
800
Distance from soma (µm)
B
Nonperforated
Perforated
dV_{soma} log scale (mV)
0.316
0.251
0.200
0.158
0.126
0.100
0.080
0.063
0.050
0.040
0.032
0.026
0.020
0.016
0.013
0.010
100 µm

Figure 2.10.

Figure 2.11. Modeling of the synaptic conductance required to achieve a somatic EPSP or a large local depolarization in a second model of a CA1 pyramidal neuron. **(A)** The synaptic conductance (g_{syn}) required to achieve a somatic EPSP of 0.2 mV throughout the dendritic tree (blue), or a local depolarization to -30 mV (red). **(B)** Plots of the g_{syn} that achieved either a somatic EPSP of 0.2 mV (blue) or a local depolarization to -30 mV (red) first. **(C)** The percentage of synaptic locations that achieved a somatic EPSP of 0.2 mV first (blue) or a local depolarization to -30 mV first (red) in pSR, dSR, and SLM.

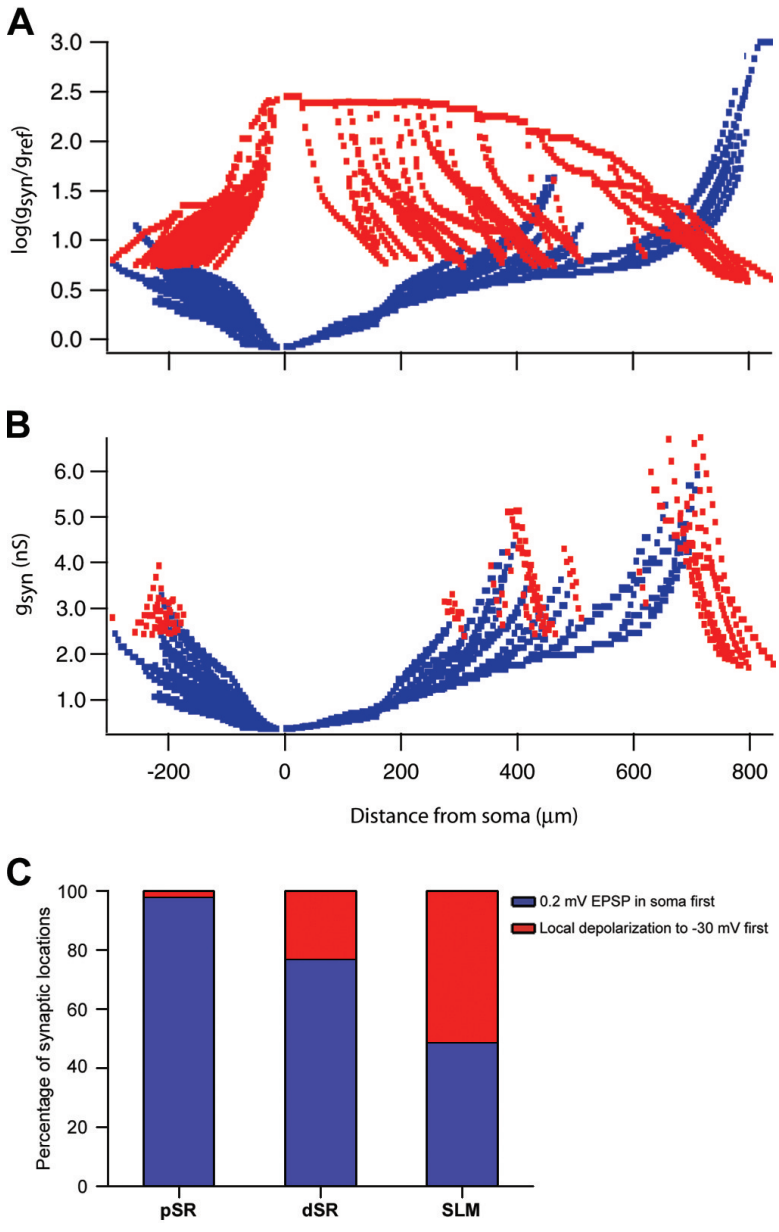
A
3.0
2.5
2.0
1.5
1.0
0.5
0.0
log(gsyn/gref)
B
6.0
5.0
4.0
3.0
2.0
1.0
gsyn (nS)
-200
0
200
400
600
800
Distance from soma (µm)
C
100
80
60
40
20
0
Percentage of synaptic locations
pSR
dSR
SLM
0.2 mV EPSP in soma first
Local depolarization to -30 mV first

Figure 2.11.

Figure 2.12. Simulation of somatic EPSPs generated by nonperforated and perforated synapses at different dendritic locations in a second model of a CA1 pyramidal neuron after adding a hyperpolarization-activated conductance

(A) g_{syn} for synapses located in stratum oriens (SO), pSR, middle stratum radiatum (mSR), dSR, and SLM in our simulation. All g_{syn} values are relative to the reference conductance (g_{ref} ; 0.46 nS) necessary for a nonperforated synapse located in pSR to generate a 0.2 mV somatic EPSP (see text for details) and are based on the AMPAR immunoreactivity of synapses in our study. **(B)** Color-coded display of the somatic EPSP generated by synaptic conductances (g_{syn}) located throughout the apical dendrite for a fixed g_{syn} characteristic of nonperforated synapses (left), or by a variable g_{syn} scaled according to the results for perforated synapses in our immunogold electron microscopy experiment (right).

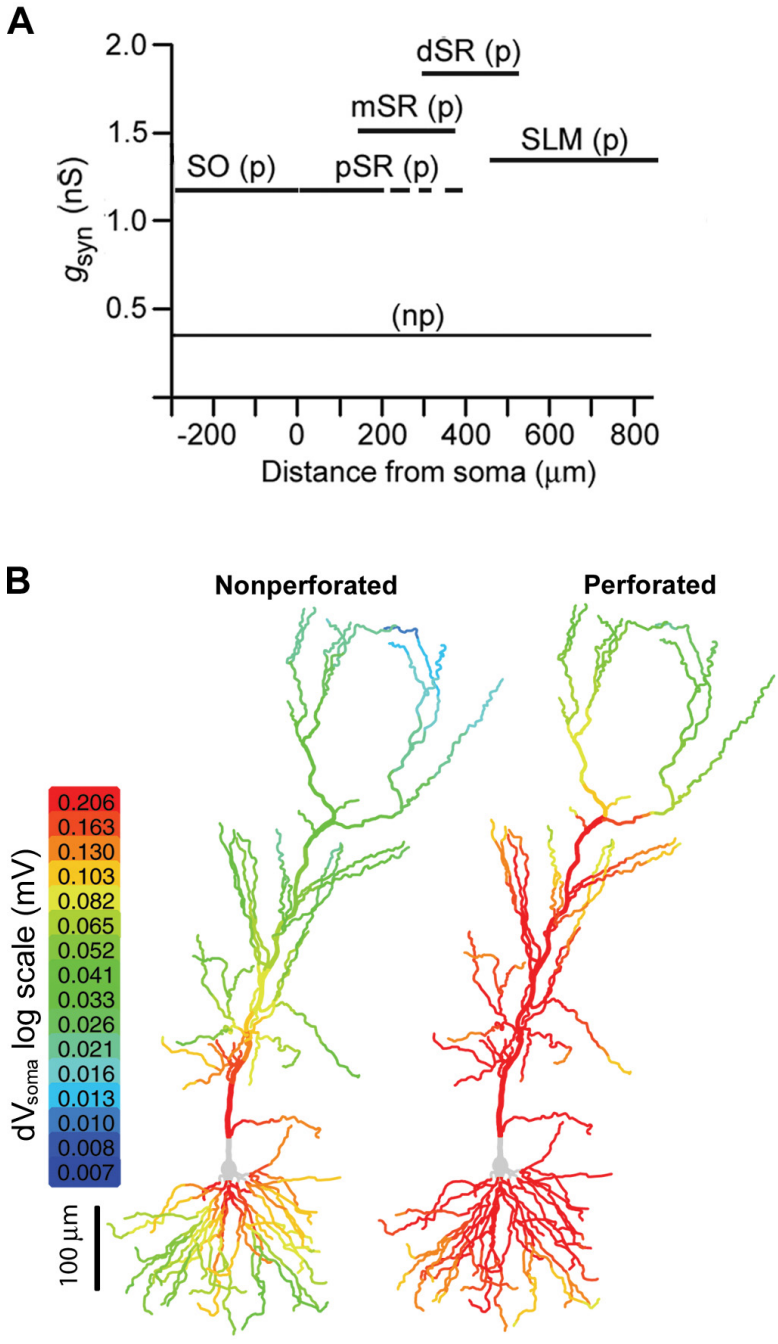
A
2.0
1.5
1.0
0.5
g_{syn} (nS)
dSR (p)
mSR (p)
SLM (p)
SO (p)
pSR (p)
(np)
-200
0
200
400
600
800
Distance from soma (µm)
B
Nonperforated
Perforated
dV_{soma} log scale (mV)
0.206
0.163
0.130
0.103
0.082
0.065
0.052
0.041
0.033
0.026
0.021
0.016
0.013
0.010
0.008
0.007
100 µm

Figure 2.12.

Figure 2.13. Modeling of the synaptic conductance required to achieve a normalized somatic EPSP or a large local depolarization in a second model of a CA1 pyramidal neuron after adding a hyperpolarization-activated conductance

(A) The synaptic conductance (g_{syn}) required to achieve a somatic EPSP of 0.2 mV throughout the dendritic tree (blue), or a local depolarization to -30 mV (red). **(B)** Plots of the g_{syn} that achieved either a somatic EPSP of 0.2 mV (blue) or a local depolarization to -30 mV (red) first. **(C)** The percentage of synaptic locations that achieved a somatic EPSP of 0.2 mV first (blue) or a local depolarization to -30 mV first (red) in pSR, dSR, and SLM.

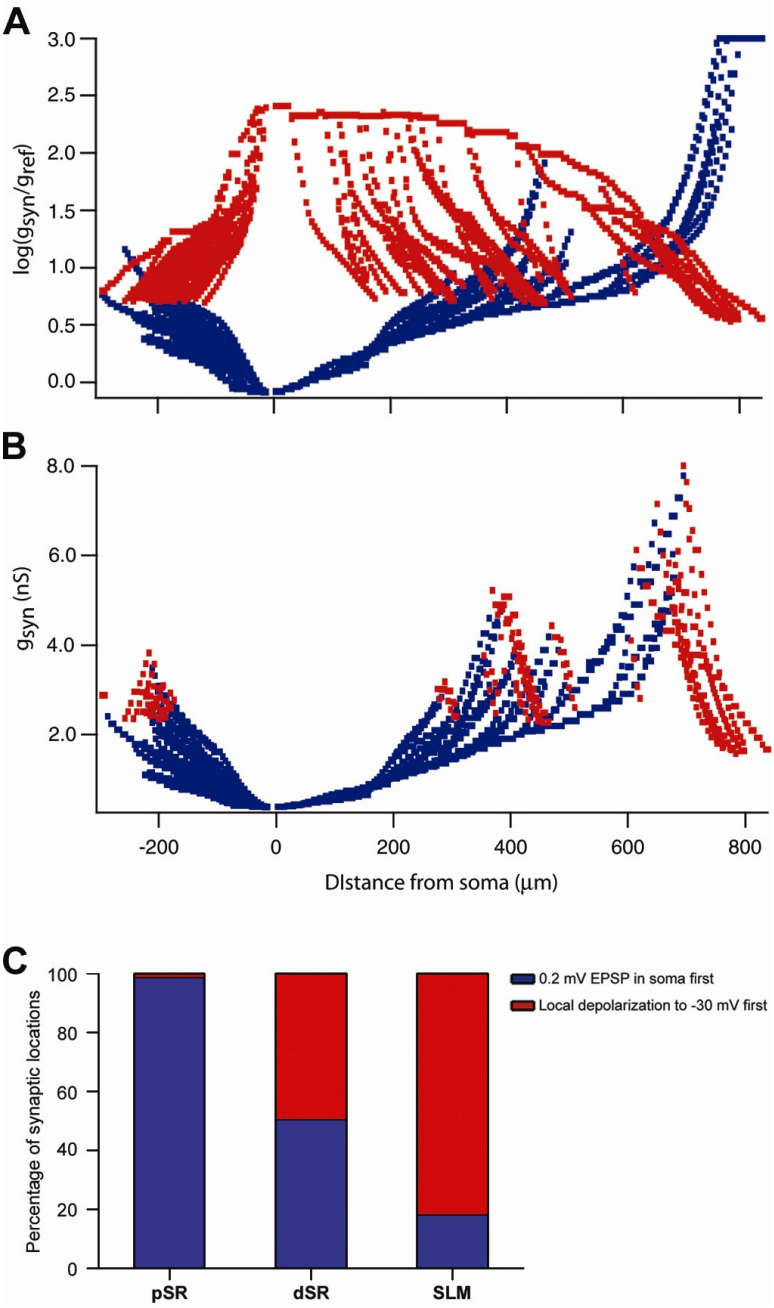
A
3.0
2.5
2.0
1.5
1.0
0.5
0.0
log(gsyn/gref)
B
8.0
6.0
4.0
2.0
gsyn (nS)
-200
0
200
400
600
800
DIstance from soma (µm)
C
100
80
60
40
20
0
Percentage of synaptic locations
0.2 mV EPSP in soma first
Local depolarization to -30 mV first
pSR
dSR
SLM

Figure 2.13.

Figure 2.14. Modeling of the synaptic conductance required to achieve a normalized somatic EPSP or a large local depolarization in a third model of a CA1 pyramidal neuron with a voltage-gated Na^+ conductance, a delayed-rectifier K^+ conductance, and two A-type K^+ conductances

(A) The synaptic conductance (g_{syn}) required to achieve a somatic EPSP of 0.2 mV throughout the dendritic tree (blue), or a local depolarization to -30 mV (red). **(B)** Plots of the g_{syn} that achieved either a somatic EPSP of 0.2 mV (blue) or a local depolarization to -30 mV (red) first. **(C)** The percentage of synaptic locations that achieved a somatic EPSP of 0.2 mV first (blue) or a local depolarization to -30 mV first (red) in pSR, dSR, and SLM.

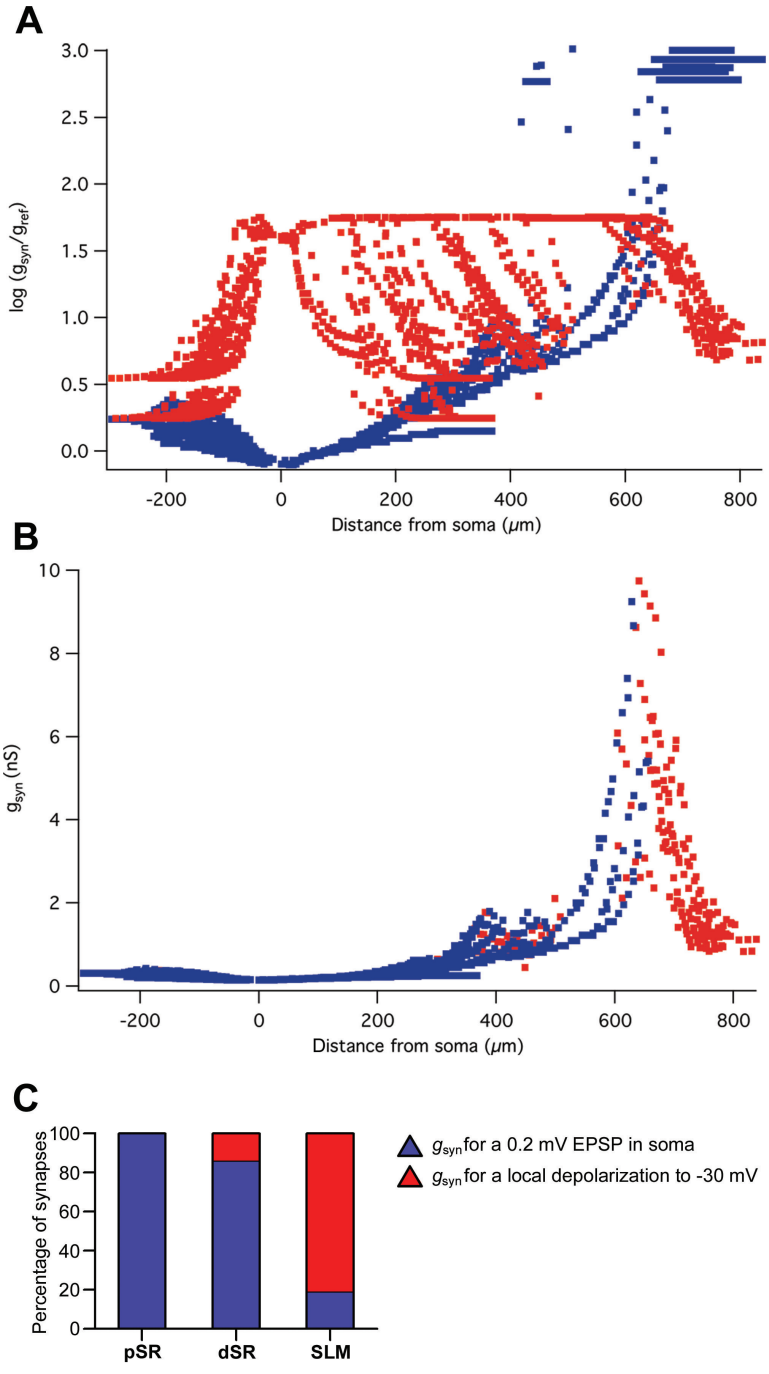
A
3.0
2.5
2.0
1.5
1.0
0.5
0.0
log (g_{syn}/g_{ref})
-200
0
200
400
600
800
Distance from soma (μm)
B
10
8
6
4
2
0
g_{syn} (nS)
-200
0
200
400
600
800
Distance from soma (μm)
C
Percentage of synapses
100
80
60
40
20
0
pSR
dSR
SLM
g_{syn} for a 0.2 mV EPSP in soma
g_{syn} for a local depolarization to -30 mV

Figure 2.14.

Figure 2.15. Modeling of the synaptic conductance required to achieve a normalized somatic EPSP or a large local depolarization in a model of a CA1 pyramidal neuron with various passive and active conductances (Poirazi et al., 2003)

(A) The synaptic conductance (g_{syn}) required to achieve a somatic EPSP of 0.2 mV throughout the dendritic tree (blue), or a local depolarization to -30 mV (red). **(B)** Plots of the g_{syn} that achieved either a somatic EPSP of 0.2 mV (blue) or a local depolarization to -30 mV (red) first. **(C)** The percentage of synaptic locations that achieved a somatic EPSP of 0.2 mV first (blue) or a local depolarization to -30 mV first (red) in pSR, dSR, and SLM.

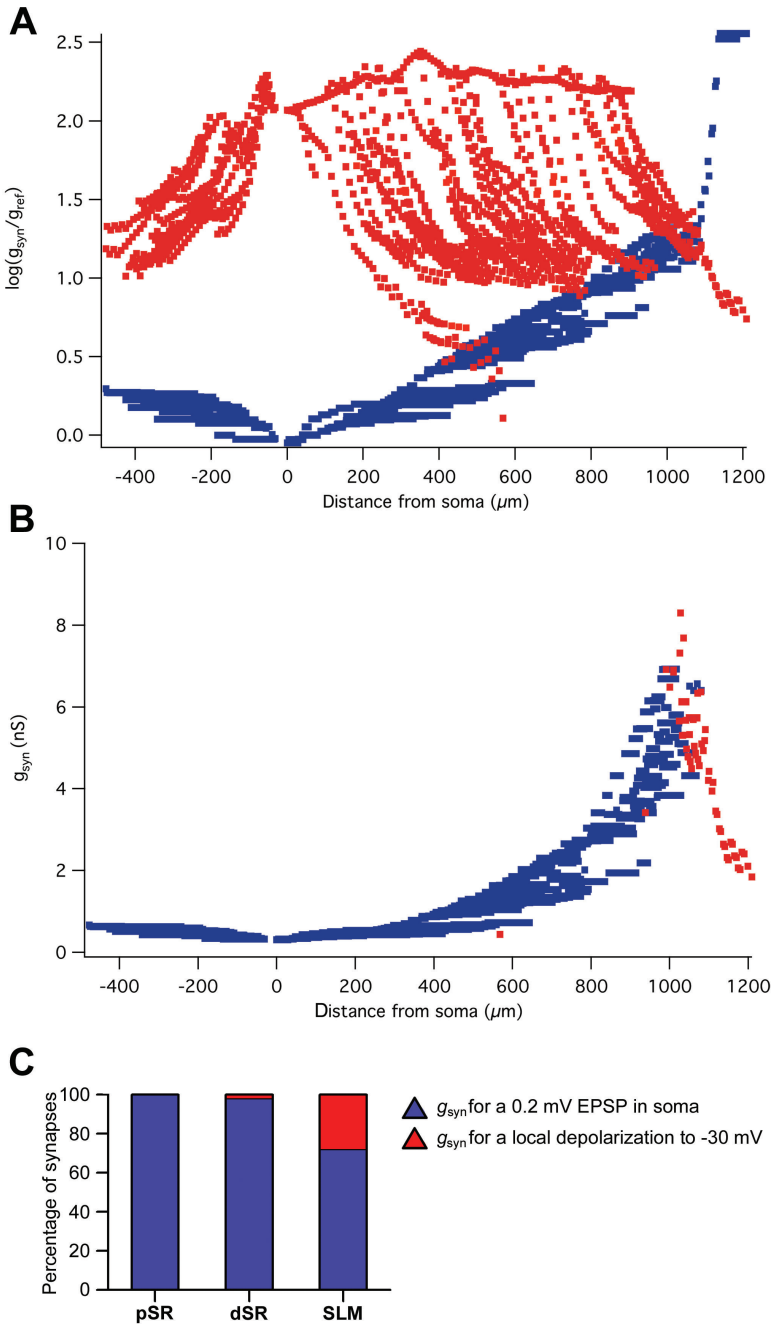
A
2.5
2.0
1.5
1.0
0.5
0.0
log(g_syn/g_ref)
-400
-200
0
200
400
600
800
1000
1200
Distance from soma (μm)
B
10
8
6
4
2
0
g_syn (nS)
-400
-200
0
200
400
600
800
1000
1200
Distance from soma (μm)
C
100
80
60
40
20
0
Percentage of synapses
pSR
dSR
SLM
g_syn for a 0.2 mV EPSP in soma
g_syn for a local depolarization to -30 mV

Figure 2.15.

Antibody	Immunosignal	Dendritic region	Synaptic subtype	PSD area (nm^2 x 10^3)	SEM	n	Pooled coefficient of variation (SD/mean)	Individual CV (rat1, rat2, rat3)
AMPAR	Negative	pSR	NP	25.4	0.60	242	0.37	0.34, 0.41, 0.36
AMPAR	Negative	dSR	NP	23.7	0.61	208	0.37	0.37, 0.38, 0.32
AMPAR	Negative	SLM	NP	25.4	0.89	119	0.38	0.35, 0.38, 0.36
AMPAR	Positive	pSR	NP	33.1	0.67	517	0.46	0.52, 0.42, 0.52
AMPAR	Positive	dSR	NP	31.5	0.66	514	0.47	0.50, 0.42, 0.43
AMPAR	Positive	SLM	NP	36.0	1.1	275	0.54	0.51, 0.62, 0.48
AMPAR	Positive	pSR	P	68.8	2.3	105	0.34	0.35, 0.35, 0.32
AMPAR	Positive	dSR	P	81.4	2.3	190	0.39	0.37, 0.38, 0.42
AMPAR	Positive	SLM	P	112.4	4.4	136	0.46	0.38, 0.45, 0.50
					Total	2,306		

Antibody	Immunosignal	Dendritic region	Synaptic subtype	PSD area (nm^2 x 10^3)	SEM	n	Pooled coefficient of variation (SD/mean)	Individual CV (rat1, rat2, rat3)
NMDAR	Positive	pSR	NP	29.4	0.49	619	0.41	0.43, 0.39, 0.38
NMDAR	Positive	dSR	NP	28.6	0.46	759	0.45	0.43, 0.45, 0.45
NMDAR	Positive	SLM	NP	28.0	0.58	647	0.53	0.50, 0.49, 0.58
NMDAR	Positive	pSR	P	69.8	2.5	93	0.35	0.38, 0.27, 0.38
NMDAR	Positive	dSR	P	87.3	3.0	137	0.41	0.35, 0.28, 0.45
NMDAR	Positive	SLM	P	99.8	3.4	126	0.39	0.38, 0.40, 0.38
					Total	2,381		

Table 2.2. PSD area measurements in pSR, dSR, and SLM

CHAPTER 3

Synapses are distributed to optimize the contribution of apical dendritic branches in hippocampal pyramidal neurons

Submitted for publication.

By: Yael Katz, Vilas Menon, Daniel A. Nicholson, William L. Kath, and Nelson Spruston.

Author contributions: I conducted the computational analysis of dendritic spike initiation generating the hypothesis that synapse strength decreases along dendrites from branch point to terminal end, and performed the electron microscopy experiment to test it. Dan Nicholson taught me how to perform electron microscopy, Vilas Menon assisted with sectioning tissue, and Krutika Lakhoo, Betsy Piekarz, and Annie Liu assisted with analyzing micrographs. I performed the simulation study assessing the functional implications of our experimental finding. Bill Kath and Nelson Spruston guided the research and Yuri Geinisman provided funding. I wrote the initial version of the paper, and the version that appears here benefited from extensive editing by Nelson Spruston.

3.1. Abstract

Neurons integrate input from synapses contacting different parts of the dendritic tree, but cable theory predicts that distal synapses will have less impact on spike initiation than more proximal synapses, which are located closer to the spike-initiation zone in the axon. Theoretically, this distal disadvantage may be overcome by increasing the conductance of distal synapses or by activating voltage-gated conductances to produce dendritic spikes. Experimental evidence supports the coexistence of both mechanisms in CA1 pyramidal neurons of the hippocampus, but normalization of synaptic efficacy by these two mechanisms leads to competing predictions about the strength of synapses along individual dendritic branches. Normalization of somatic EPSPs suggests that synapses should be stronger at more distal locations, in order to compensate for the greater loss of synaptic charge. Normalization of dendritic spike initiation suggests that synapses should be weaker at more distal locations, in order to compensate for the larger local EPSPs associated with smaller-diameter terminal dendrites. Here we used electron microscopy and immunogold labeling of AMPA receptors to examine synapse size and strength on apical oblique branches of CA1 pyramidal neurons. We find that synapses near the terminal ends of these branches are smaller and less numerous than synapses close to the branch point off the primary apical dendrite. Using computational modeling, we found that the experimentally observed distribution of synapses has two important functional implications: First, dendritic spikes are less likely to be initiated by a small number of excitatory synapses on the terminal portion of a dendrite. Second, somatic EPSPs mediated by groups of synapses are larger because the largest synapses are closer to the soma. Thus, our results suggest that synapses are distributed along individual dendritic branches to

optimize the contribution of each dendritic branch to the somatic membrane potential, rather than to normalize the contribution of each individual synapse.

3.2. Results and Discussion

Hippocampal CA1 pyramidal neurons typically have a long primary apical dendrite with many thin dendritic oblique side branches extending from it, as well as a distinct basal dendritic tree. Both basal and apical dendrites receive inputs from the CA3 region of the hippocampus, which can influence neuronal output in two ways: the first is if an EPSP depolarizes the axon directly, and the second is if the input triggers a dendritic spike, which can propagate forward under certain conditions (Gasparini et al., 2004; Jarsky et al., 2005).

Both of these influences are affected by neuronal morphology. EPSPs generated by synaptic inputs far away from the action-potential-initiation zone attenuate greatly due to the combination of high resistance and leakiness of the dendritic tree (Golding et al., 2005; Rall, 1959). In the absence of compensatory mechanisms, these distal inputs would be less efficacious than inputs that enter the neuron closer to its output site. In addition, dendritic spikes are more easily generated when synapses are located on the terminal portion of a branch than when they are located on part of the dendrite closer to the branch point with the parent dendrite. This is attributable to the characteristically small diameters of distal segments, as well as the effect of a sealed end, giving distal segments higher input impedance than more proximal dendritic segments, which tend to have larger diameters and are closer to the load of the primary apical dendrite and the soma. Small currents flowing at synapses on high-impedance distal segments lead to relatively large

voltage deflections compared to synaptic currents at lower impedance segments near the branch points(Spruston, 2008).

Experiments in CA1 pyramidal neurons suggest that inputs to the apical dendrites compensate for the effect of voltage attenuation by scaling up the strengths of synapses with distance from the axon (Magee & Cook, 2000; Nicholson et al., 2006). However, it is unknown if a mechanism exists to normalize the size of somatic EPSPs from synapses along the length of individual apical oblique branches. Using a computational model of a CA1 pyramidal neuron with excitable dendrites (Methods) to explore such "somatic EPSP normalization", we found that synaptic conductance would have to be increased approximately two fold along the lengths of oblique branches in order to normalize the size of EPSPs in the soma (Figure 3.1a, c). One consequence of such a scaling rule is that the local voltage resulting from activation of synapses at more distal positions on the branch would be larger than for more proximal synapses, both because synaptic conductance is larger (due to conductance scaling) and because input impedance is higher (due to the smaller dendritic diameter and the sealed end). A result of this bias is that dendritic spikes would likely be triggered more readily by distal than by proximal synapses.

Figure 3.1. Contrasting models of somatic EPSP and dendritic spike normalization. **a,** Top: Conductance required to produce a 0.2 mV somatic EPSP at all locations on an apical oblique dendrite of a reconstructed CA1 pyramidal neuron (223 μm from the soma; 195 μm in length; marked by the arrow in c). This branch is the focus of all simulations, unless otherwise noted. Bottom: Schematic showing the predicted gradient of synaptic strength if synapses were scaled to normalize somatic EPSP amplitude. **b,** Top: Conductance required to produce a dendritic spike at all locations on the apical oblique branch shown in a. Bottom: Schematic showing the predicted gradient in synaptic strength if synapses were scaled to normalize the probability of initiating a dendritic spike at all locations. **c,** Left: Conductance required to produce a 0.2 mV somatic EPSP at all locations on the apical dendritic tree of a reconstructed CA1 pyramidal neuron. Middle: Bar graph showing the gradient in synaptic conductance along each apical oblique dendrite on the neuron (excluding the tuft) for the somatic (gray bars) and dendritic (white bars) normalization cases. For each branch, the conductance at the terminal end of the branch divided by the conductance at the branch point is plotted on a log scale. Right: Conductance required to produce a dendritic spike at all apical dendritic locations on the reconstructed CA1 pyramidal neuron.

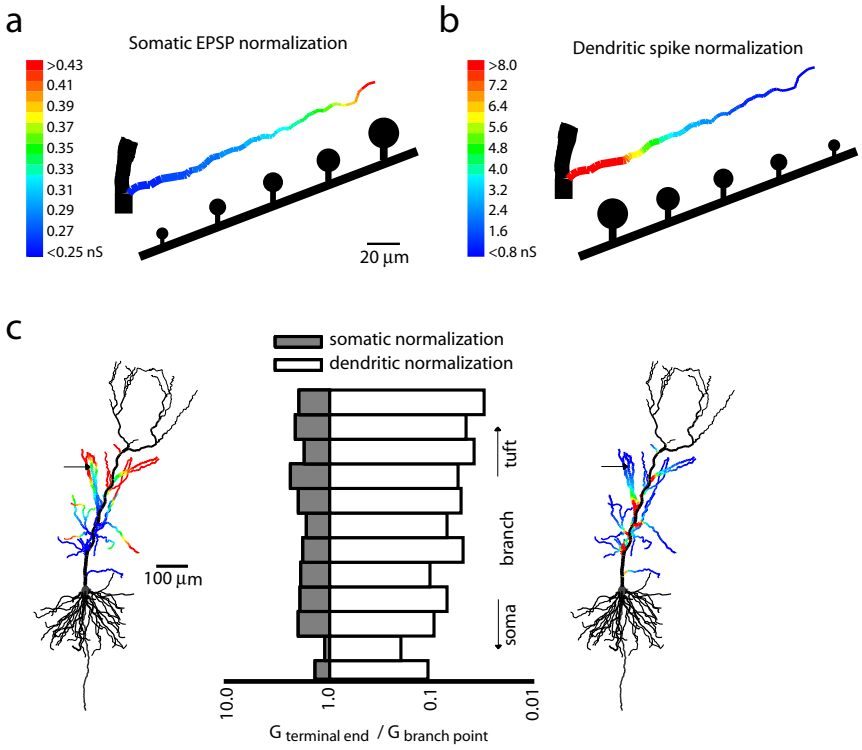
a
Somatic EPSP normalization
>0.43
0.41
0.39
0.37
0.35
0.33
0.31
0.29
0.27
<0.25 nS
20 µm
b
Dendritic spike normalization
>8.0
7.2
6.4
5.6
4.8
4.0
3.2
2.4
1.6
<0.8 nS
c
somatic normalization
dendritic normalization
100 µm
tuft
branch
soma
10.0
1.0
0.1
0.01
G terminal end / G branch point

Figure 3.1.

An alternative to this model is that synaptic strength is scaled along the length of individual dendritic branches to normalize the local dendritic EPSP and its contribution to dendritic spiking. Using the model to implement such a "dendritic spike normalization" rule resulted in scaling of synaptic conductances by 5-34 fold (mean 18 fold) in the opposite direction, with the strongest synapses located closest to the branch point from the primary apical dendrite, where input impedance is lowest (Figure 3.1b,c). Thus, the somatic and dendritic normalization models lead to competing predictions about the distribution of synapse strength along individual apical oblique branches.

To investigate this, we used serial-section electron microscopy (EM) to analyze synapse size along individual dendritic branches. Biotinylated dextran amine (BDA) was injected into rat hippocampi to achieve sparse labeling of CA1 neurons. We then used light microscopy to select isolated neurons with clearly labeled spiny dendrites. Using serial EM (Figure 3.2a,b), we reconstructed three apical oblique dendrites in their entirety and made within-dendrite comparisons of the synapses on their dendritic segments near the branch point and near the terminal end (Figure 3.2c, top). Additionally, we also performed between-dendrite comparisons between proximal dendritic segments, identified by the branch point with the primary apical dendrite, and distal dendrites, identified by the termination of the dendritic branch (Figure 3.2c, bottom). Analysis was restricted to dendritic segments at least 10 μm long and spines that were completely contained within the serial sections. A total of over 3,000 sections were analyzed. In all cases, spines were completely filled and traceable to their parent dendrite and in many cases post-synaptic densities (PSDs) were clearly visible (spine n = 433 proximal and n = 189 distal; PSD n = 195 proximal and n = 78 distal; Figure 3.2a, b).

Figure 3.2. Spines near and far from the primary apical dendrite. **a,** Serial-section view of a segment of dendrite with spines and synapses. **b,** Three-dimensional reconstruction of the segment shown in a. Spines are shown in purple and PSDs are in blue. **c,** Three-dimensional reconstructions of segments of the same (bottom) dendrite and different (top) dendrites. **d,** Scatter plot showing spine densities in dendritic segments near branch points and near terminal ends. Circles represent dendritic segments, and lines show the means. **e,** Histogram showing the relative and cumulative frequencies of spine volumes in dendritic segments near branch points and near terminal ends.

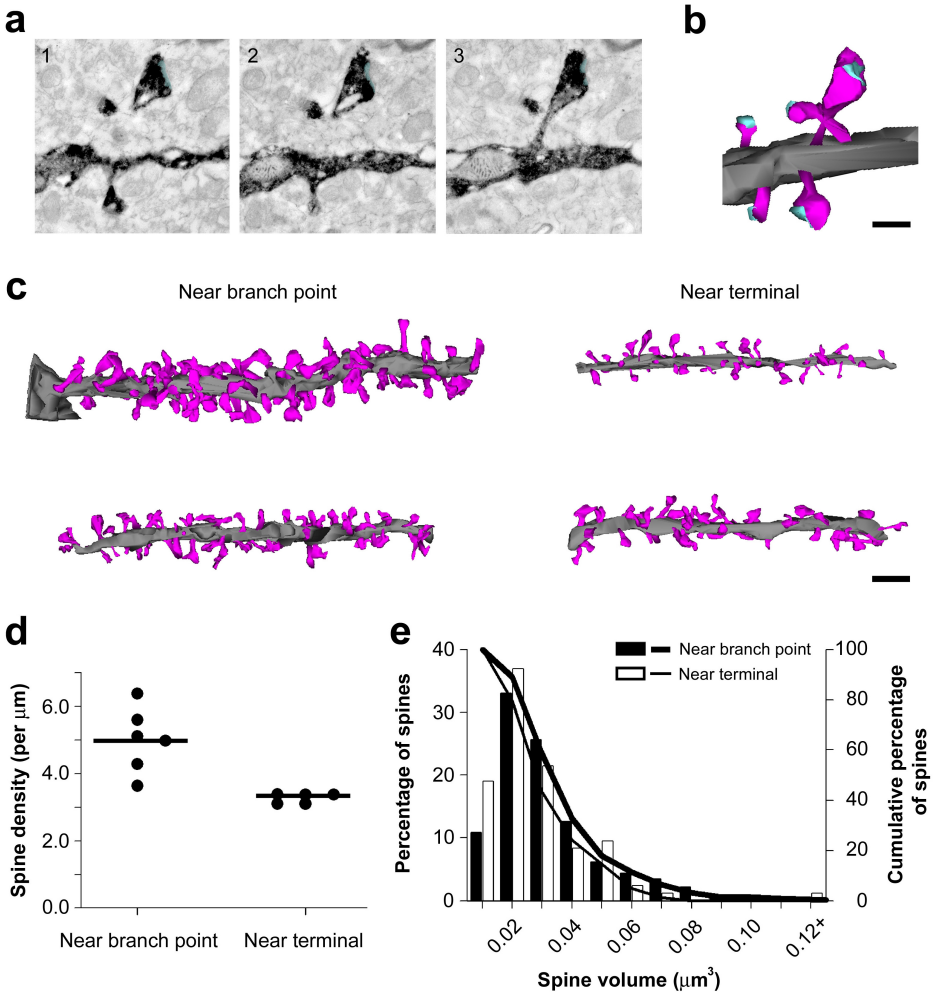
a
1
2
3
b
c
Near branch point
Near terminal
d
Spine density (per µm)
6.0
4.0
2.0
0.0
Near branch point
Near terminal
e
Near branch point
Near terminal
Percentage of spines
40
30
20
10
0
100
80
60
40
20
0
Cumulative percentage of spines
0.02
0.04
0.06
0.08
0.10
0.12+
Spine volume (µm³)

Figure 3.2.

We found two major differences between spines on segments of dendrites near branch points and those near terminal ends. First, spine density was approximately 50% greater in dendritic segments located near the branch points off of the primary apical dendrite than in the segments closer to their terminal ends (t-test, $p < 0.003$) (Figure 3.2d). Second, the distribution of spine volumes was moderately skewed toward larger spines in dendritic segments near branch points ($\chi^2 = 20.4$; $p < 0.05$; Figure 3.2e).

We compared synapses on dendritic segments near branch points to those on segments near terminal ends and found a variety of synapse shapes at all dendritic locations (Figure 3.3a). However, the distribution of postsynaptic density (PSD) areas was heavily skewed toward larger PSDs for segments near branch points relative to segments near terminal ends ($\chi^2 = 354.9$; $p < 0.00001$; Figure 3.3b). This trend was present in the overall analysis (Figure 3.3b); mean PSD area 0.057 μm^2 near the branch origin and 0.030 μm^2 near the branch terminal), as well in each within-dendrite comparison (Figure 3.4).

Figure 3.3. Synapses near and far from the primary apical dendrite. **a,** Reconstructions of several spines and synapses from our data. **b,** Histogram showing the relative and cumulative frequencies of PSD areas in dendritic segments near branch points and near terminal ends. **c,** Serial sections showing immuno-gold labeling of AMPA receptors. **d,** Three-dimensional reconstruction of objects shown in c. Spines are in purple, synapses are in blue, and gold particles are in black. **e,** Correlation of particle number with spine volume. **f,** Correlation of particle number with synapse area.

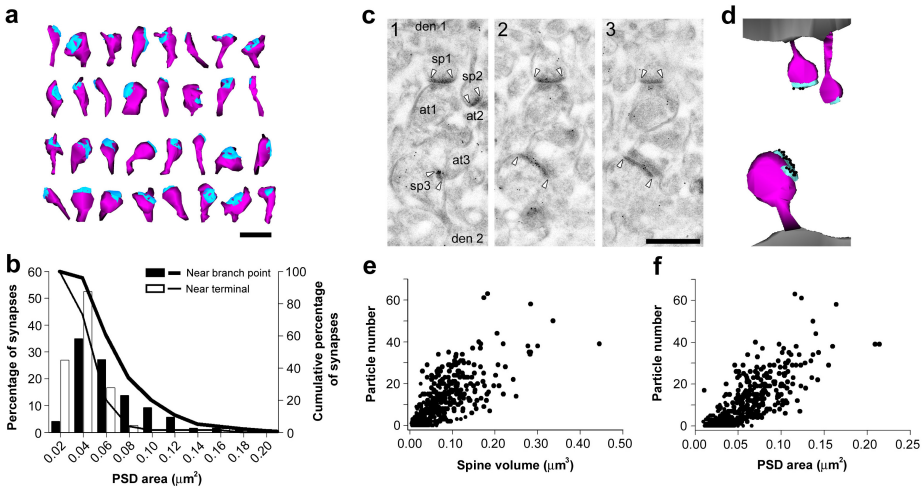
a
b
Near branch point
Near terminal
Percentage of synapses
Cumulative percentage of synapses
PSD area (μm²)
c
1
den 1
sp1
sp2
at1
at2
at3
sp3
den 2
2
3
d
e
Particle number
Spine volume (μm³)
f
Particle number
PSD area (μm²)

Figure 3.3.

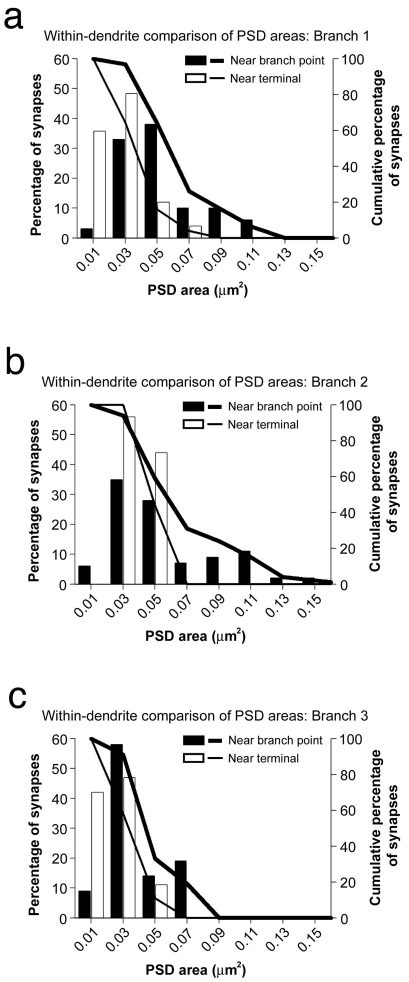

Figure 3.4.

Figure 3.4. Within-dendrite comparisons of synapses near and far from the primary apical dendrite. a, Histograms showing the relative and cumulative frequencies of PSD areas in dendritic segments near the branch point and near the terminal ends of a single branch. **b,c** Same as above for a second and third branch.

To quantify the relationship between spine volume or PSD area and synaptic strength, we performed immunogold labeling of AMPA receptors (Figure 3.3c). We could not combine immuno-EM with our BDA labeling experiment because the presence of the label obscures the gold particles. Therefore, we analyzed synapses (n=342) from area CA1 stratum radiatum of the hippocampus, each of which could be traced back to their spine necks. We found both spine volume ($R^2 = 0.7216$, $p < 0.001$; Figure 3.3d) and PSD area ($R^2 = 0.7567$, $p < 0.001$; Figure 3.3e) to be strongly correlated with the number of gold particles, indicating that these measures are good proxies for synaptic strength. Therefore, the approximately two-fold reduction of PSD size at the branch terminal relative to the branch origin suggests that synapses are about half as strong near the branch terminal than near the branch origin. Thus, synapse size is scaled in the direction of the "dendritic normalization" model, but likely not strongly enough to completely normalize dendritic spike initiation along the length of the branch. Non-uniform distribution of various conductances could provide further normalization.

To investigate the functional implications of these location-dependent differences in synapse density and strength, we used a variant of our computational model that incorporated the experimental results. Synaptic density and strength were varied along the length of each apical oblique branch according to the experimentally identified gradient (dendritic normalization) or in the reverse gradient (somatic normalization). Simulations were performed by activating synapses proportional to the observed distribution or the reverse distribution. We determined the number of synapses required to initiate a dendritic spike as a function of location by randomly selecting synapses along the branch. Typically, activation of several synapses led to initiation of a dendritic spike (60-80 mV at the

initiation site), but the spike attenuated severely by the time it reached the primary apical dendrite and attenuated further between this location and the soma (Figure 3.5a). The results of such simulations varied because synapse locations (and hence sizes) were chosen randomly. Thus simulations were repeated many times (see Methods). Performing this analysis on each of the apical oblique branches indicated that more excitatory synapses were needed to activate a dendritic spike in the dendritic normalization model (Figure 3.5b,c). Importantly, a small group of synapses was less likely to trigger a dendritic spike in this model (the experimentally observed case). The probability of initiating a spike with five or fewer inputs was 26% in the somatic normalization model, but just 2% in the dendritic normalization model.

When synaptic activation was restricted to the proximal, middle, or distal third of the branch, activation of a dendritic spike in the dendritic normalization model required fewer proximal synapses and more distal synapses compared to the somatic normalization model (proximal synapses 30 compared to 53; distal synapses 6.5 compared to 3.6; Figures 3.6-3.8, a-c). Thus, the experimentally observed synapse distribution reduces, but does not eliminate, the tendency for increasingly distal synapses to be more effective at eliciting dendritic spikes in the model. As a result, when synapses were simulated throughout the branch, more than 95% of the dendritic spikes were initiated in the most distal 10% of the dendritic branch – an effect that was not significantly different in the two models of synapse distribution (97% for somatic normalization and 96% for dendritic normalization). Qualitatively similar results were found in branches at different distances from the soma (Figure 3.5, 3.6-3.8). However, the number of synapses required for a dendritic spike

varied because more distal branches had a higher density of A-type potassium channels (Hoffman et al., 1997) and they also tended to have smaller diameters.

Figure 3.5. Location dependence of branch efficacy. a, Sample voltage traces from a simulation where synapses are randomly activated from all locations on the branch shown in figure 1 until a dendritic spike occurred. Synapses were distributed along the branch with decreasing density and strength, as observed experimentally. Voltage is indicated at the terminal end (black trace), center of the branch (red trace), branch origin (green trace), and soma (blue trace). **b,** Average somatic dV resulting from a dendritic spike in each apical dendritic branch (excluding the tuft) for the somatic (left) and dendritic (right) normalization models. **c,** Bar graph showing the average number of synapses required for a dendritic spike in each apical dendritic branch for the somatic (black bars) and dendritic (yellow bars) normalization models. **d,** Bar graph showing the average somatic dV resulting from a dendritic spike in each apical dendritic branch for the somatic (black bars) and dendritic (blue bars) normalization models. The somatic dV is divided into the EPSP component (black and dark blue bars), obtained from activation of one synapse less than the threshold number for a spike, and the dendritic spike component (grey and light blue bars), which is the total dV minus the EPSP component. **e,** Bar graph showing the dendritic spike component of the somatic dV for each branch in the somatic (grey bars) and dendritic (light blue bars) normalization models.

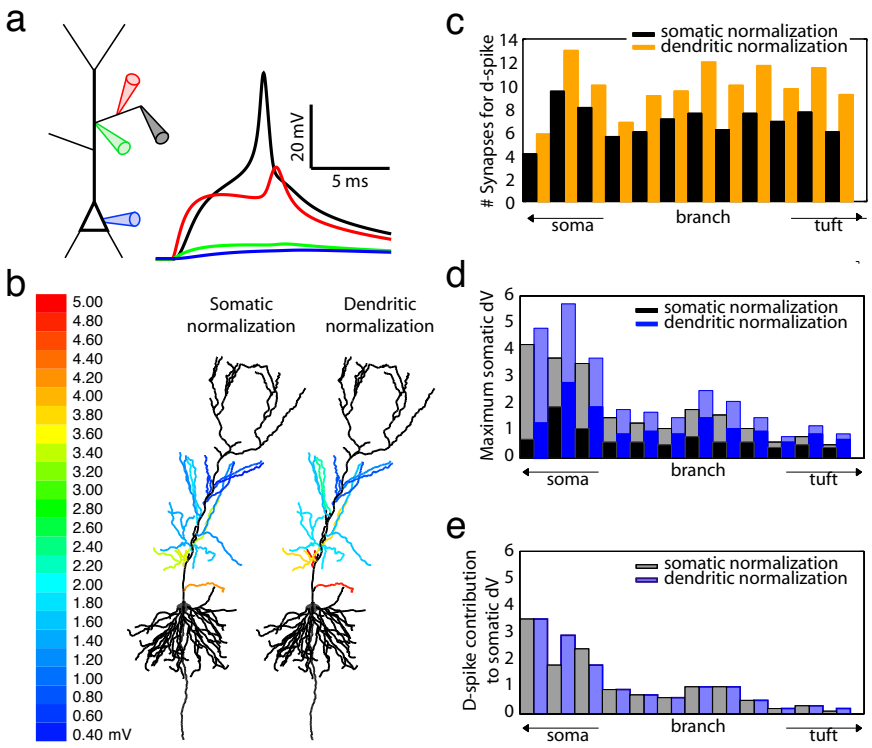
a
20 mV
5 ms
b
5.00
4.80
4.60
4.40
4.20
4.00
3.80
3.60
3.40
3.20
3.00
2.80
2.60
2.40
2.20
2.00
1.80
1.60
1.40
1.20
1.00
0.80
0.60
0.40 mV
Somatic normalization
Dendritic normalization
c
somatic normalization
dendritic normalization
Synapses for d-spike
soma
branch
tuft
d
somatic normalization
dendritic normalization
Maximum somatic dV
soma
branch
tuft
e
somatic normalization
dendritic normalization
D-spike contribution to somatic dV
soma
branch
tuft

Figure 3.5.

Figure 3.6. Functional consequences of spine and synapse distributions. **a,** Left: Reconstructed CA1 pyramidal neuron with the oblique dendrite that is the subject of simulation shown in red (origin 223 μm from the soma). Middle: Synapses were distributed along the dendrite with decreasing density and strength, as observed experimentally and randomly selected from the middle third of the branch and activated one at a time to illustrate the dendrite's input-output functions. Shown is the maximum voltage change as a function of the number of synapses at the site of spike initiation on the dendrite (red), at the branch origin from the primary apical dendrite (green), and at the soma (blue). Right: Branch origin and somatic peak voltage plots on an expanded scale. **b,** Schematics of the two cases depicted in Figure 3.1. **c-e,** Synapses were randomly activated until a dendritic spike occurred. Each point represents one simulation. Left: synapses are distributed with increasing density and strength, Middle: synapses are distributed with decreasing density and strength, Right: example voltage traces from the simulations or probability distributions for the two cases. **c,** Synapses are selected from the first third, middle third, and distal third of the branch in separate simulations (clustered input). 500 trials per simulation; horizontal lines indicate the averages. **d-e,** Synapses are selected from all locations on the branch (distributed input). 1500 trials; lines show the average. **d,** Number of synapses required to initiate a dendritic spike as a function of the centre of mass of the inputs with clustered input. **e,** Maximum voltage change for distributed input locally (red), at the branch point with the primary apical dendrite (green), and at the soma (blue). Note the progressively expanded scales from top to bottom.

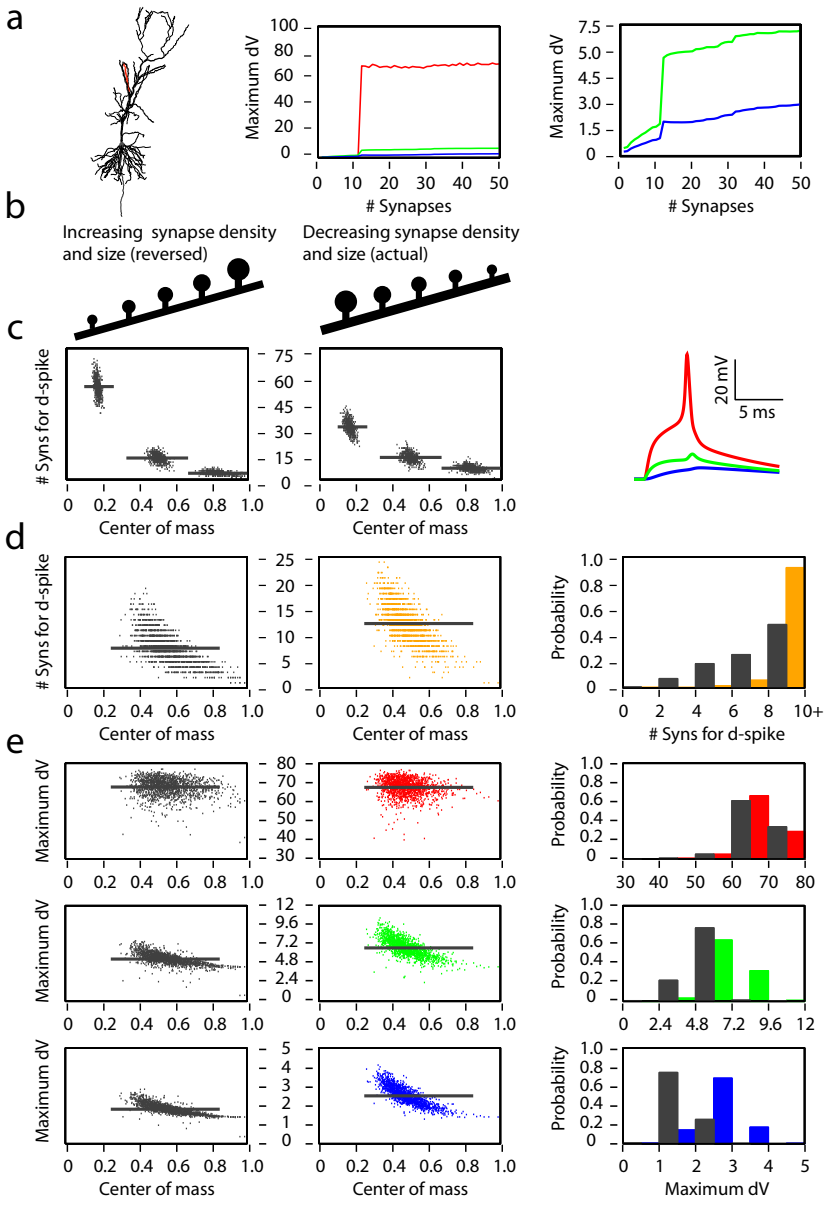
a
b
c
d
e
Maximum dV
Synapses
Increasing synapse density
and size (reversed)
Decreasing synapse density
and size (actual)
Syns for d-spike
Center of mass
20 mV
5 ms
Probability
Syns for d-spike
Maximum dV

Figure 3.6.

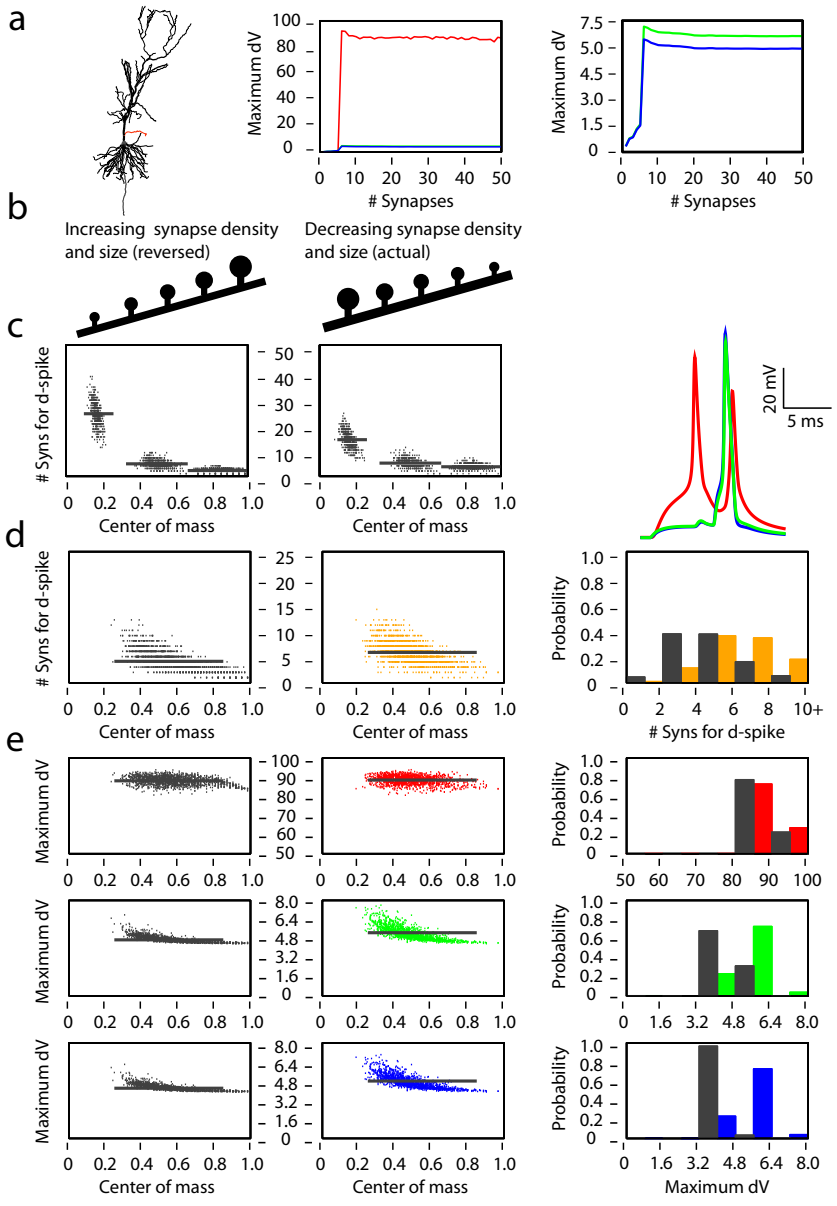

Figure 3.7.

Figure 3.7. Functional consequences of spine and synapse distributions for a proximal branch. Same as Figure 3.4, but for a proximal branch (origin 27 μm from the soma).

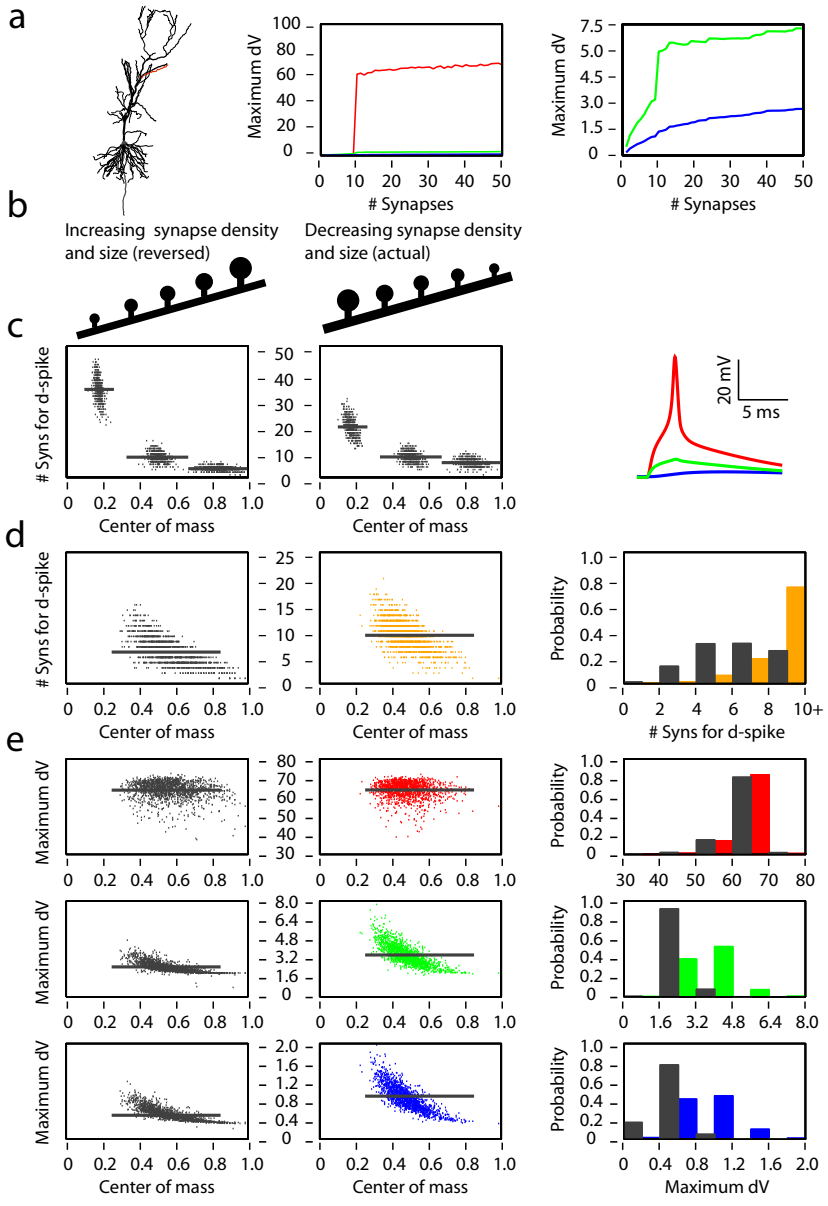

Figure 3.8.

Figure 3.8. Functional consequences of spine and synapse distributions for a distal branch. Same as Figure 3.5, but for a distal branch (origin 339 μm from the soma).

Despite the tendency for relatively distal spike initiation in both models, the mean voltage at the primary apical dendrite and in the soma was consistently larger for the dendritic normalization model (Figure 3.5d). When the minimum number of synapses necessary to trigger a dendritic spike were simulated, the resulting somatic depolarization was largest for the dendritic normalization model. Similarly, activating the number of synapses just below threshold for a dendritic spike resulted in a larger somatic EPSP in the dendritic normalization model. Subtracting the subthreshold EPSP from the above-threshold response provides a reasonable estimate of the somatic depolarization contributed by the dendritic spike (Figure 3.5e). Consistent with previous experimental results (Losonczy & Magee, 2006), this contribution was no more than a few millivolts for the most proximal branches and less than a millivolt for more distal branches. Theoretically, increases in the size or width of the dendritic spike could compensate for this distance-dependent contribution of the dendritic spike.

The contribution of the dendritic spike to the somatic membrane potential was not different for the somatic and dendritic normalization models (Figure 3.5e). Thus, the reason for the larger voltage response in the dendritic normalization model is the distribution of stronger synapses on the most proximal portions of the branch. The enhanced response of the dendritic normalization model was not attributable to the larger number of synapses required to produce a dendritic spike, as responses were larger even when fixed numbers of synapses were simulated (Table 3.1).

Peak somatic depolarization in response to fixed numbers of synapses in the somatic and dendritic normalization models

	Dendritic Normalization	**Somatic Normalization**
5 synapses	1.13 mV	1.01 mV
10 synapses	1.94 mV	1.52 mV
15 synapses	2.55 mV	1.83 mV
20 synapses	3.04 mV	2.07 mV

Table 3.1. Peak somatic depolarizations in somatic and dendritic normalization models.

Functionally, the dendritic spike has two important consequences for synaptic integration. First, it limits the amount of depolarization produced by a single dendritic branch. Activation of sufficient excitation to drive a dendritic spike produces a large depolarization of the branch and an increase in the somatic membrane potential. Activation of more than this threshold number of excitatory synapses produces no additional peak depolarization in the branch and only limited additional depolarization in the primary apical dendrite and the soma (Figure 3.6-3.8a). The second consequence of the spike is that it increases the peak somatic depolarization in the soma, thus increasing the likelihood of action potential initiation. Consistent with previous experimental observations (Golding & Spruston, 1998; Stuart et al., 1997a), in the model the action potential was initiated in the axon and propagated back into the soma and dendrites, even when a dendritic spike occurred in the oblique branch receiving the synaptic input (Figure 3.9a).

Our findings, that spine density, spine volume, and synapse size are greater near the primary apical dendrite, indicate that synaptic inputs are larger and more synchronous on these near-branch-point, low input impedance dendritic locations than they would be if synapses were organized to achieve normalization of somatic EPSPs. Dendritic spike initiation requires temporally synchronous inputs (Gasparini et al., 2004) and the increased spine density on locations near branch points makes it more likely that those regions will receive synchronous inputs. Larger spines and larger synapses lead to larger local inputs because they tend to have more AMPA receptors (and NMDA receptors (Nicholson et al., 2006)), as shown by our immuno-EM results. Our simulations suggest that the distributions of synapse density and strength we observed enhances the contribution of a dendritic branch to the output of the neuron by correlating synapse size

to input impedance, thus preventing dendritic spiking in response to small numbers of synapses, but increasing the impact of synaptic activation on the primary apical dendrite and the soma. Our model lacks any further complexity, such as ion channel gradients along individual oblique branches(Gasparini et al., 2007), which may further augment the integrative properties of oblique dendrites if present.

Although the synaptic organization we observed suggests that the contribution of individual inputs to the output of a branch is less dependent on location than in the somatic normalization model, our model also predicts that the ability of individual dendritic branches to influence neuronal output depends on branch location. It may be that distal dendrites differentially express different types of excitable ion channels, such as calcium channels, which lead to spikes with kinetic properties that enable them to propagate more effectively. Furthermore, distal branches further enhance their somatic influence due to the larger number of powerful synapses they contain (Figure 3.9b) (Magee & Cook, 2000; Nicholson et al., 2006).

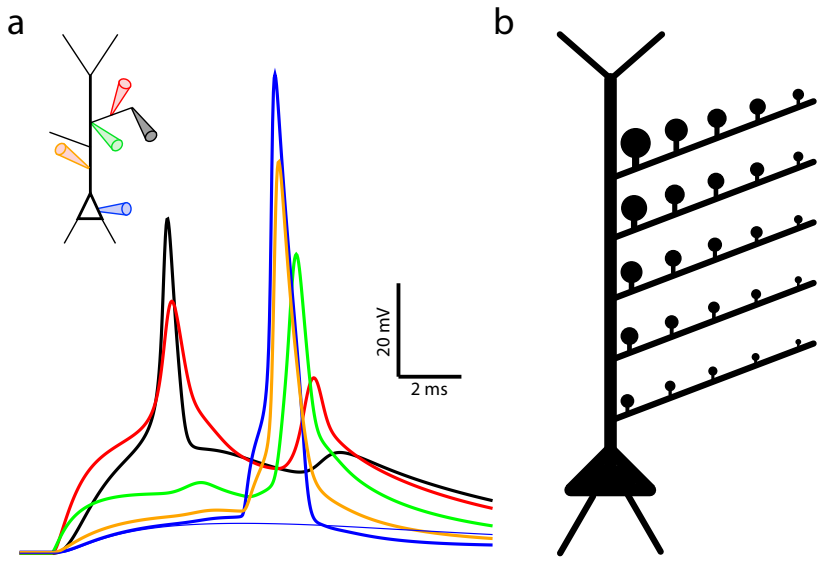

Figure 3.9.

Figure 3.9. Summary. **a**, 8 synapses are activated on the oblique dendrite (just above threshold for a dendritic spike) and an additional 40 average synapses are activated on the primary apical dendrite. Shown are sample voltage traces recorded at the terminal end of the branch (black), centre of the branch (red), branch point (green), location on the primary apical dendrite between the soma and branch point (yellow), and soma (blue) in the dendritic normalization model. The thin blue trace shows the somatic voltage for activation of 7 synapses on the branch (just below threshold for the dendritic spike) and 40 synapses on the primary apical dendrite. **b,** Schematic of the proposed synapse distribution for CA1 apical dendritic tree based upon previous(Nicholson et al., 2006) and current results.

How could such a synaptic organization be established? CA1 pyramidal neurons are equipped with numerous homeostatic mechanisms that could establish these gradients of synaptic strength(Turrigiano & Nelson, 2004). However, dendrites also grow outward from their tips(Cline & Haas, 2008), and nascent spines and synapses tend to be small(Fiala et al., 1998; Holtmaat et al., 2005). Because dendrites, even in adult animals, are dynamic (Turrigiano & Nelson, 2004), the processes of neuronal growth and maturation could contribute to the gradients of decreasing synaptic strength seen along individual dendritic branches.

Dendritic spikes are functionally important because they can contribute to axonal action potentials (Gasparini et al., 2004; Golding & Spruston, 1998; Losonczy & Magee, 2006) or propagate forward when combined with other inputs (Jarsky et al., 2005). They produce action potential output that is precise and temporally invariant (Losonczy & Magee, 2006), and in vivo may occur during sharp-wave states and facilitate feature extraction (Gasparini & Magee, 2006). In addition, some forms of synaptic plasticity are critically dependent on spikes initiated in dendrites (Golding et al., 2002; Holthoff et al., 2004; Remy & Spruston, 2007) and branch-specific plasticity in dendritic excitability has recently been shown to occur (Losonczy et al., 2008). The dendritic normalization of synaptic strength increases the likelihood than any given synapse can contribute to dendritic spikes, and thus participate in these important aspects of neuronal function.

An emerging view is that individual dendritic branches are independent computational subunits in which inputs are locally integrated before being globally summated in the axon (Polsky et al., 2004) and that the ability to perform multi-layer computations is what gives neurons their computational power (Spruston & Kath, 2004). Our findings

support this view and point to the primacy of dendritic spikes within dendritic branches as a fundamental unit of synaptic integration in pyramidal neurons.

3.3. Methods

3.3.1. Computational modeling.

The CA1 pyramidal neuron morphology used in all simulations was reconstructed from a stained neuron in a rat hippocampal slice as described previously (Golding et al., 2005). All simulations were performed using the NEURON simulation environment (Hines & Carnevale, 1997).

The model contained membrane capacitance and resistance as well as the active conductances, sodium (Na), delayed rectifier potassium (K_{DR}), and A-type potassium (K_A). Passive properties were constrained by electrophysiological recording of voltage attenuation from the soma to dendrite in the reconstructed neuron (Golding et al., 2005), and the active conductances Na and K_{DR} were uniformly distributed. K_A in the primary apical dendrite was distributed based on experimental data (Hoffman et al., 1997), and K_A in oblique dendrites was uniformly distributed using the value at the point of connection with the primary apical dendrite.

Fast excitatory synaptic conductances were modeled as a difference of exponentials with a rise time constant of 0.2 ms, decay time constant 5.0 ms, and reversal potential of 0 mV. For the simulation in figure 1b, the bisection method was used to determine convergence to a somatic depolarization of 0.2 mV with a tolerance of 0.01 mV. Dendritic spikes were defined as a voltage exceeding a threshold of –35 mV.

For the simulations in figure 4, synapses were randomly drawn from a linear distribution starting from 5 synapses/μm at the branch point and ending at 3.3 synapses/μm at the terminal end for the dendritic spike normalization case (right). For the somatic EPSP normalization case, the distribution was reversed. Synaptic weights were determined as follows: We randomly drew from the probability distributions in figure 3b to determine the PSD area as a function of the location of the synapse. For the dendritic spike normalization simulations, if the selected synapse was on the proximal third of the branch we drew from the distribution for dendritic segments near branch points, and if it was on the distal third of the branch we drew from the distribution for dendritic segments near terminal ends. If the synapse was on the middle of the branch, we drew from an average of the two distributions. For the somatic EPSP normalization simulations, we drew from the reverse distributions. Once we determined the PSD area, we chose the corresponding particle number from figure 3e. The synaptic weight was the particle number times 0.02 nS, which led to values for unitary synaptic conductance between 0.05 and 0.8 nS

3.3.2. Electron Microscopy.

Biotinylated dextran amine (BDA-3000, Invitrogen; 10% dissolved in 0.12M phosphate buffered saline; PBS) was injected into the subiculum (from bregma: AP = -2.5, ML = +1.5; DV = -4.1) of adult rats using either pressure injection (0.05 μl/min for 5 min) or iontophoresis (5 μA, alternating at 10 sec on/off for 6 min). After five days, rats were perfused with a fixative containing 3.5% paraformaldehyde, 0.1% glutaraldehyde, and 15% (v/v) picric acid in PBS. Brains were removed, hemisectioned, postfixed in fixative, rinsed in PBS, and then cut into 60 um thick slices using a vibratome.

Individual slices were then rinsed in PBS, cryoprotected in ascending concentrations of sucrose and glycerol in PBS, freeze-thawed over liquid nitrogen 3 times, treated with 1% sodium borohydride in PBS, incubated in 0.3% hydrogen peroxide, and then rinsed. Slices were then rinsed in blocking solution (0.5% BSA, 1% nonfat dry milk, and 5% normal goat serum), and incubated in avidin-biotinylated horseradish peroxidase (HRP) using the Vectastain ABC Elite Kit (Vector Laboratories, PK-6100 Standard, 1:300) for 36 hours at 4° C. Slices were then rinsed thoroughly and the BDA-HRP complex was visualized using diamino benzidine as chromogen (Sigma, SK-4100) under gentle agitation for 10-120 min. Slices containing isolated individually labeled CA1 pyramidal neurons were then rinsed, treated with 0.67% osmium tetroxide and 1% uranyl acetate, dehydrated in graded ethanols, infiltrated with Araldite (Araldite 502), and cured in a drying oven at 60° C for 48 hours for conventional serial section electron microscopy.

Slices were trimmed to isolate the labeled dendrites of CA1 neurons, cut into 68 nm thin serial sections (100-500 serial sections) using an ultramicrotome (UCT, Leica), and mounted onto gold-gilded nickel slotted grids. Grids were counter-stained with 3% aqueous uranyl acetate and Reynold's lead citrate, and then mounted in an electron microscope (JEOL 100CX) to photograph serial sections containing dendritic segments within CA1 stratum radiatum in their entirety. Terminal segments of dendrites were considered to be those dendritic segments that could be followed through >50 serial sections, and then disappear in subsequent serial sections. Branch-point dendritic segments were readily identifiable due to their bifurcation from the primary apical dendrite. Intermediate dendritic segments (i.e., dendritic segments connecting a branch off the primary apical dendrite with a daughter terminal dendritic segment) were excluded from analyses.

Electron micrograph negatives were scanned using a PowerLook 2100XL scanner, organized into image stacks for each dendritic segment, and then analyzed and reconstructed using ImageJ (Rasband, 1997-2007) and Reconstruct (Fiala, 2005), respectively.

3.3.3. Post-embedding immunogold electron microscopy.

AMPA-type receptor immunoreactivity was assessed as previously described (Nicholson et al., 2006). Synapses in CA1 stratum radiatum were included in the analysis only if their host spine could be followed to its spine neck (n = 342). Because of the low-electron density of freeze-substituted tissue, it was impossible, except in fortuitous cases, to follow spines to their parent dendrite. Importantly, however, our measurements are within those reported previously for synapses in CA1 stratum radiatum (Harris et al., 1992; Nusser et al., 1998b).

CHAPTER 4

Dendritic integration of excitatory and inhibitory inputs in a CA1 pyramidal neuron model

4.1. Abstract

Proper function of the hippocampus depends critically on the balance between excitation and inhibition. How dendritic integration depends on the relative magnitude, location, and timing of excitatory and inhibitory inputs, however, is not well understood. Here we used experimentally constrained computational models to investigate the effect of feed-forward inhibition on synaptic integration in CA1 pyramidal neurons. We examined both shunting (mediated by $GABA_A$ synapses) and hyperpolarizing (mediated by $GABA_B$ synapses) inhibition. We found that when excitation and inhibition spatially overlap, the probability of both dendritic spike initiation and propagation was reduced, but inhibition was more effective at limiting spike propagation than initiation because spikes initiated easily on thin apical dendrites and often failed through branch points. Shunting inhibition was effective when it coincided with the excitation or slightly preceded it, whereas hyperpolarizing inhibition was more powerful and could precede the inhibition by over 15 milliseconds. Distal shunting inhibition was unable to stop spikes initiated in the more proximal apical dendrites from propagating forward toward the soma or spreading backward toward the tuft, but distal hyperpolarizing inhibition was effective at preventing the spread of these spikes and was most effective when it preceded the excitation by over 5 milliseconds. Finally, dendritic spikes initiated in the tuft could be gated by inhibition. A large amount of shunting inhibition was required to stop these spikes and this was most effective when it followed the excitation by 2-3 milliseconds; by comparison, a moderate amount hyperpolarizing inhibition could achieve gating. These findings are useful to guide experiments to explore the interaction between excitation and inhibition as well as serve as a foundation for further modeling studies.

4.2. Introduction

CA1 pyramidal neurons integrate information from an estimated 30,000 excitatory and 1,700 inhibitory synapses spread over 12,000 microns of dendritic cable (Megias et al., 2001). Action potential firing in these cells is mediated by the spatio-temporal dynamics of the interactions between these inputs (Pouille & Scanziani, 2001, 2004). Understanding these dynamics is crucial both for understanding information processing in the hippocampus under normal conditions and for understanding conditions like epilepsy that occur when the balance between excitation and inhibition is altered (Dudek & Staley, 2007).

Both of the two major inputs to CA1, the perforant-path projection from entorhinal cortex and the Schaffer collaterals from hippocampal region CA3, activate feed-forward inhibition (Amaral and Witter, 1989) (Figure 4.1): they excite CA1 pyramidal neurons directly, but at the same time activate interneurons that then inhibit these cells. These two inputs innervate distinct regions of the pyramidal-neuron dendritic tree, so they are positioned to differentially modulate synaptic integration (Miles et al., 1996). For example, the perforant-path input selectively targets the tufts of pyramidal neurons, so feed-forward inhibition activated by the perforant path could limit dendritic-spike initiation. The Schaffer-collaterals arrive on the more proximal apical dendrites (as well as the basal dendrites), triggering inhibition that may affect dendritic-spike propagation. Little is known about the spatio-temporal requirements for inhibition to influence dendritic spike initiation and propagation. Additionally, CA1 pyramidal neurons receive perisomatic inhibition, which can globally restrict sodium spiking (Miles et al., 1996; Pouille & Scanziani, 2001) and feedback inhibition, which can slow firing frequency (Pouille & Scanziani, 2004), further enriching their dynamics.

Figure 4.1. Schematic of excitatory and inhibitory inputs to CA1 apical dendrites. Perforant-path inputs from entorhinal cortex supply excitation to the tufts of CA1 pyramidal neurons and Schaffer collaterals from hippocampal region CA3 excite their upper apical dendrites. CA1 pyramidal neurons also receive spatially segregated inhibition. Green and red dots represent excitatory and inhibitory synapses, respectively.

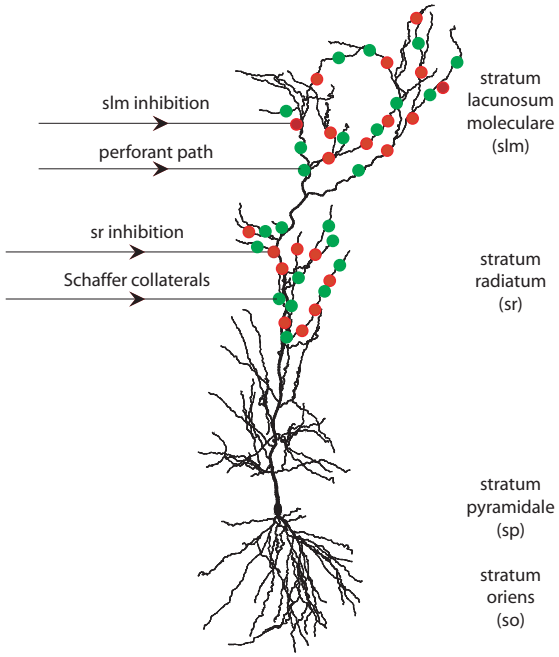
slm inhibition
perforant path
sr inhibition
Schaffer collaterals
stratum lacunosum moleculare (slm)
stratum radiatum (sr)
stratum pyramidale (sp)
stratum oriens (so)

Figure 4.1.

Two populations of CA1 pyramidal neurons can be distinguished, depending on the extent to which backpropagating action potentials invade their apical dendritic trees (Golding et al., 2001). In models of strongly backpropagating cells, dendritic spikes propagate reliably to the soma, while in models of weakly backpropagating cells, dendritic spikes initiated in the distal dendrites often fail to trigger axonal output due to voltage attenuation through the dendrites. Experiments in hippocampal slices showed that if these distally generated dendritic spikes are coincident with subthreshold depolarization entering more proximally, however, forward propagation can be rescued and action-potential output can be generated (Jarsky et al., 2005). In the strongly excitable cell, we hypothesized that inhibition could limit dendritic spike propagation.

Inhibitory synapses contain two types of receptors that deliver two different types of inhibition (Farrant & Nusser, 2005). $GABA_A$ receptors are coupled to chloride channels, which have a reversal potential close to rest, so they shunt current when an EPSP coincides with the IPSC. $GABA_B$ receptors are coupled to potassium channels, which have a reversal potential below rest. Activation of these receptors hyperpolarizes the cell, and this inhibition is effective for the entire time course of the IPSP.

In this study, we focus on feed-forward inhibition and examine four cases: perforant-path inhibition and excitation, perforant path inhibition and Schaffer-collateral excitation, Schaffer collateral inhibition and excitation, and Schaffer-collateral inhibition and perforant-path excitation and vary the magnitude, timing, and reversal potential of the inhibitory input relative to the excitatory one. We identify qualitative parameters that

characterize how these inputs interact, which are useful to guide experiments and further modeling studies on the interaction between excitation and inhibition in pyramidal neurons.

4.3. Methods

The CA1 pyramidal neuron morphology used in all simulations was obtained by reconstructing a stained neuron in a rat hippocampal slice as described previously (Golding et al., 2001).

The model contained passive membrane properties, a sodium conductance that increased slightly along the somatodendritic axis to make the cell strongly excitable (Golding et al., 2001), a uniformly distributed delayed rectifier potassium conductance, and an A-type potassium conductance with a gradient that increased along the first 300 um of apical dendrite to 4 times the somatic value (Hoffman et al., 1997). This resulted in a slight gradient in resting membrane potentials along the somato-dendritic axis. All parameters were as described previously (Golding et al., 2001).

Fast excitatory synaptic conductances were modeled as a difference of exponentials with a rise time constant of 0.2 ms, a decay time constant of 2.0 ms, and a reversal potential of 0 mV. Inhibitory synaptic conductances modeled as a difference of exponentials with a rise time constant of 1.0 ms, a decay time constant of 18.0 ms, and a reversal potential of -70 mV ($GABA_A$ "shunting inhibition") or -90 mV ($GABA_B$ "hyperpolarizing inhibition") (Hille, 2001). Although $GABA_B$ is normally slower than $GABA_A$, their kinetics were kept the same in order to facilitate comparison of differences between shunting and hyperpolarizing inhibition.

The unitary synaptic conductance was taken to be 180 pS for excitatory synapses and 540 pS for inhibitory synapses. The 180 pS value was chosen because a synapse of that conductance located 50 μm from the soma led to a somatic EPSP of 0.2 mV (Magee & Cook, 2000). The 540 pS value was chosen because inhibitory synapses are larger and more powerful than their excitatory counterparts (Megias et al., 2001).

Synapses were distributed throughout the neuron based on (Megias et al., 2001) as described in (Jarsky et al., 2005). In our simulations, only synapses in the upper apical dendrites (900 μm total dendritic length) and apical tuft (2008 μm total dendritic length) were stimulated. Our model contained 3168 excitatory and 99 inhibitory synapses in the upper apical dendrites and 1928 excitatory and 341 inhibitory synapses in the apical tuft.

A dendritic spike in a particular region of the cell was said to have occurred when the average voltage in that region exceeded a threshold of -30 mV. The probability of a spike was determined by averaging over 1000 trials.

All simulations were done in the NEURON simulation environment (Hines & Carnevale, 1997) using a 64 processor Beowulf cluster.

4.4. Results

To investigate how inhibition affects synaptic integration in CA1 pyramidal neuron models, we first simulated a fixed number of excitatory synapses randomly chosen from either the upper apical dendrites or apical tuft of the model neuron. This number was chosen so that 85% of trials resulted in an axonal action potential. Our model was strongly excitable, so dendritic spikes initiated in the tuft often triggered axonal action potentials on their own. We then simulated inhibitory inputs of different magnitudes by randomly

activating different percentages of either $GABA_A$ synapses (reversal potential -70 mV) or $GABA_B$ synapses (reversal potential -90 mV) (Figure 4.2) in the tuft or upper apical dendrites and varying the onset of inhibition relative to excitation. We measured the voltage everywhere in the cell and repeated the simulations for 1000 trials.

Figure 4.2. Shunting and hyperpolarizing inhibition. A. Right: Depolarizing IPSPs recorded in the tuft (top), upper apical dendrites (middle), and soma (bottom) when 16% of $GABA_A$ synapses (reversal potential -70 mV) in the apical tuft were activated.
Left: Minimum voltage at all dendritic locations in response to this input plotted on a color scale.
B. Right: IPSPs recorded in the tuft (top), upper apical dendrites (middle), and soma (bottom) when 16% of $GABA_B$ synapses (reversal potential -90 mV) in the apical tuft were activated.
Left: Minimum voltage at all dendritic locations in response to this input plotted on a color scale.

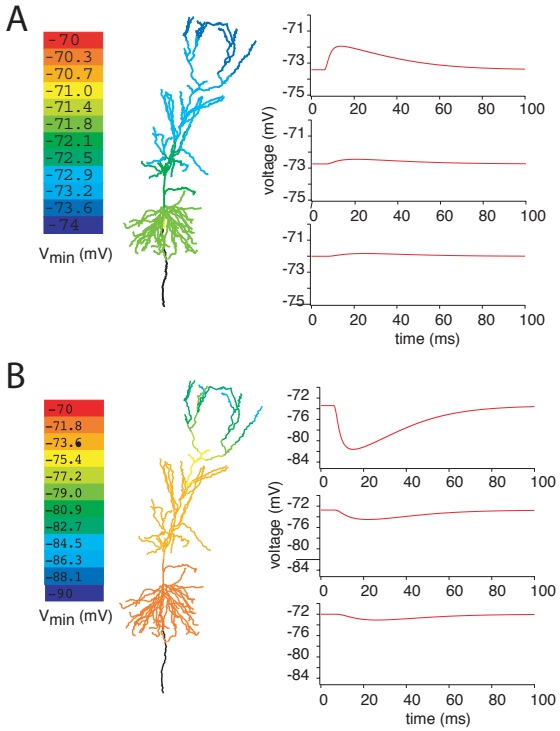
A
-70
-70.3
-70.7
-71.0
-71.4
-71.8
-72.1
-72.5
-72.9
-73.2
-73.6
-74
Vmin (mV)
voltage (mV)
time (ms)
B
-70
-71.8
-73.6
-75.4
-77.2
-79.0
-80.9
-82.7
-84.5
-86.3
-88.1
-90
Vmin (mV)
voltage (mV)
time (ms)

Figure 4.2.

CASE 1: Perforant-path excitation plus perforant-path inhibition

When the excitatory input to the tuft was fixed, such that 85% of trials resulted in an axonal action potential and 8% of $GABA_A$ inhibitory synapses in the tuft were activated, three scenarios were observed (Figure 4.3, middle): dendritic spikes were initiated in the tuft and propagated forward successfully, they failed to be initiated in the tuft, or they were initiated in the tuft but failed to propagate forward. Surprisingly, when excitation and inhibition spatially overlapped, dendritic spike propagation was affected more so than initiation; spikes were initiated in close to 90% of trials, but propagated forward only about 40% of the time (Figure 4.3, right). This is because spikes were easily initiated on small dendritic side branches, but they often failed through the branch points with the main apical dendrite. Once a spike invaded the main apical dendrite, it always reached the axon. Stronger inhibitory inputs (i.e. a greater percentage of synapses activated) were more effective at limiting both the initiation and propagation of dendritic spikes.

Hyperpolarizing inhibition was more effective than shunting inhibition at preventing both the initiation and propagation of dendritic spikes (Figure 4.3), compare thin and thick lines). With 8% of synapses activated, spikes were only initiated in approximately 10% of trials, and never propagated forward.

Figure 4.3. Perforant-path excitation and perforant-path inhibition. Left: Schematic of simulation protocol. Excitatory synapses in the tuft were randomly activated so that axonal action potentials occurred on 85% of trials. Different numbers of inhibitory synapses in the tuft were activated at varying times relative to the excitation.

Center: 8% of $GABA_A$ inhibitory synapses (reversal potential -70 mV) in the tuft were activated at the same time as the excitatory input. Voltage traces show an example of successful spike propagation (top), failed spike initiation (middle), and successful spike initiation but failed propagation (bottom). Voltage is measured in the tuft (black traces), upper apical dendrites (red traces), and at the soma (blue traces).

Right: 4% (red lines), 8% (green lines), and 12% (blue lines) of inhibitory synapses were activated at different times relative to the excitatory input. For each time, the probability of action potential generation averaged over 1000 trials in the tuft (top), upper apical dendrites (middle), and soma (bottom) was plotted. At time 0, the excitatory and inhibitory inputs were coincident, at negative times the inhibition preceded the excitation, and at positive times the inhibition followed the excitation. Thin lines represent shunting inhibition and thick lines represent hyperpolarizing inhibition. The black lines (control) are the excitatory input alone.

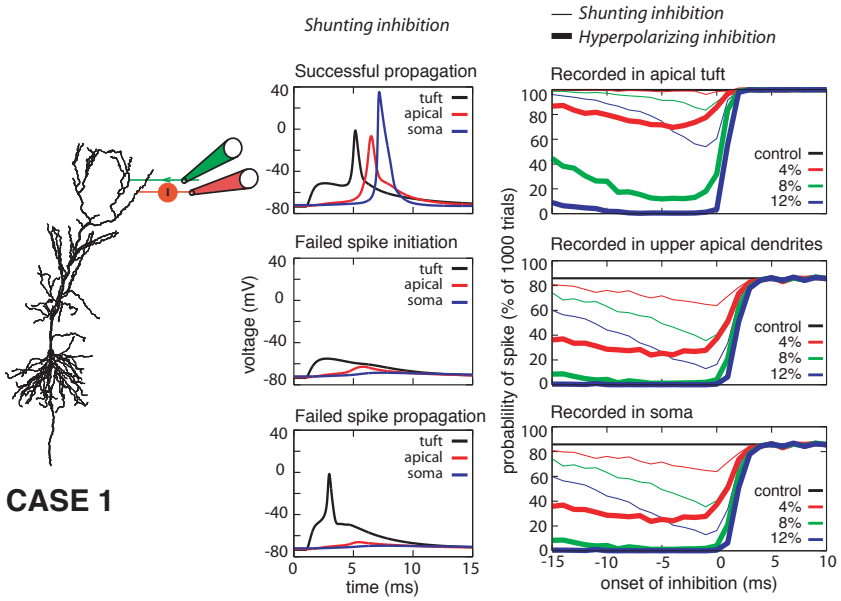
Shunting inhibition
Shunting inhibition
Hyperpolarizing inhibition
Successful propagation
Failed spike initiation
Failed spike propagation
tuft
apical
soma
voltage (mV)
time (ms)
CASE 1
Recorded in apical tuft
Recorded in upper apical dendrites
Recorded in soma
control
4%
8%
12%
probability of spike (% of 1000 trials)
onset of inhibition (ms)

Figure 4.3.

Shunting inhibition was most effective when it was coincident with the excitation or slightly preceded it (Figure 4.3). The effectiveness of shunting inhibition fell off approximately linearly with the amount of time it preceded the excitation and was not effective when it arrived more than one or two milliseconds after the excitation. Hyperpolarizing inhibition was effective when it preceded the excitation by the time course of the IPSP - up to about 50 ms, but similar to shunting inhibition was not effective when it followed the excitation by more than one or two milliseconds.

CASE 2: Schaffer-collateral excitation + perforant-path inhibition

If a spike was initiated in the apical dendrites via the Schaffer-collaterals, shunting inhibition to the tuft could not stop it from propagating forward (Figure 4.4). Hyperpolarizing inhibition was effective at stopping these spikes. Activating 9% of inhibitory synapses completely stopped the spike from backpropagating into the tuft and reduced the probability of forward propagation to about 40%. Hyperpolarizing inhibition was most effective at preventing axonal action potentials when it preceded the inhibition by at least 5 milliseconds.

Figure 4.4. Scaffer-collateral excitation and perforant-path inhibition. Left: Schematic of simulation protocol. Excitatory synapses in th upper apical dendrites were randomly activated so that axonal action potentials occurred on 85% of trials. Different numbers of inhibitory synapses in the tuft were activated at varying times relative to the excitation. Center: 6% of $GABA_A$ inhibitory synapses (reversal potential -70 mV) in the upper apical dendrites were activated at the same time as the excitatory input. Voltage traces show an example of successful spike propagation. Voltage is measured in the tuft (black traces), upper apical dendrites (red traces), and at the soma (blue traces).
Right: 3% (red lines), 6% (green lines), and 9% (blue lines) of inhibitory synapses were activated at different times relative to the excitatory input. For each time, the probability of action potential generation averaged over 1000 trials in the tuft (top), upper apical dendrites (middle), and soma (bottom) was plotted. At time 0, the excitatory and inhibitory inputs were coincident, at negative times the inhibition preceded the excitation, and at positive times the inhibition followed the excitation. Thin lines represent shunting inhibition and thick lines represent hyperpolarizing inhibition. The black lines (control) are the excitatory inputs alone.

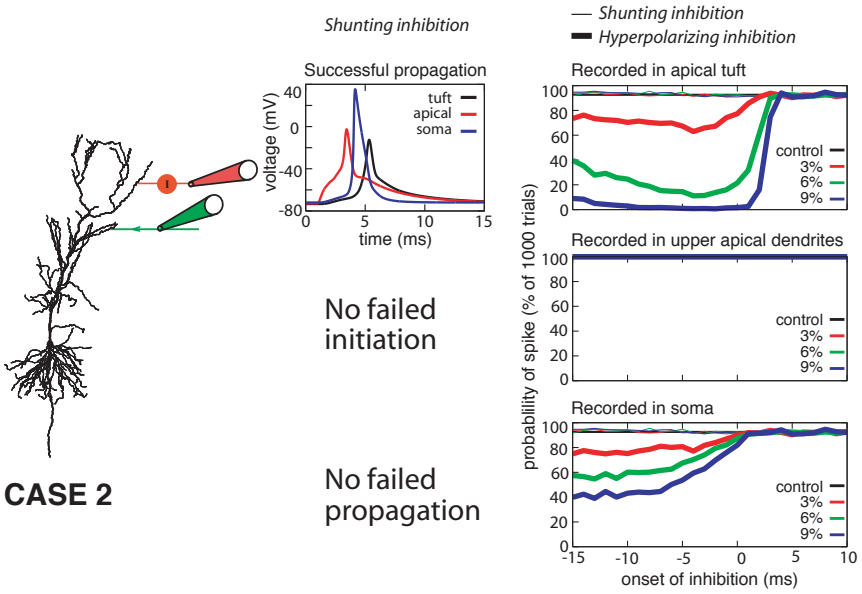
Shunting inhibition
Successful propagation
tuft
apical
soma
voltage (mV)
time (ms)
No failed initiation
No failed propagation
CASE 2
Shunting inhibition
Hyperpolarizing inhibition
Recorded in apical tuft
Recorded in upper apical dendrites
Recorded in soma
control
3%
6%
9%
probability of spike (% of 1000 trials)
onset of inhibition (ms)

Figure 4.4.

CASE 3: Schaffer-collateral excitation + Schaffer collateral inhibition

Similar to case 1, excitation and inhibition both targeting the mid- apical dendrites affected dendritic spike propagation more than initiation, but here larger amplitudes of inhibition were required to limit the spikes than when the inputs were at the tuft (Figure 4.5). 23% of $GABA_A$ synapses in the upper apical dendrites compared to 8% of synapses in the apical tuft were needed to reduce the probability of axonal action potential generation to approximately 40%. Shunting inhibition in the upper apical dendrites could not stop spikes from being generated in the apical side-branches, but sometimes these spikes failed to invade the main apical dendrite and backpropagate to the tuft or forward propagate to the axon. Hyperpolarizing inhibition in the upper apical dendrites was capable of preventing dendritic spike initiation.

Figure 4.5. Schaffer-collateral excitation and Schaffer-collateral inhibition. Left: Schematic of simulation protocol. Excitatory synapses in the upper apical dendrites were randomly activated so that axonal action potentials occurred on 85% of trials. Different numbers of inhibitory synapses in the upper apical dendrites were activated at varying times relative to the excitation.

Center: 23% of $GABA_A$ inhibitory synapses (reversal potential -70 mV) in the upper apical dendrites were activated at the same time as the excitatory input. Voltage traces show an example of successful spike propagation (top) and successful spike initiation but failed propagation (bottom). Voltage is measured in the tuft (black traces), main apical dendrite (red traces), upper oblique apical dendrite (green traces), and at the soma (blue traces).

Right: 8% (red lines), 23% (green lines), and 34% (blue lines) of inhibitory synapses were activated at different times relative to the excitatory input. For each time, the probability of action potential generation averaged over 1000 trials in the tuft (top), upper apical dendrites (middle), and soma (bottom) was plotted. At time 0, the excitatory and inhibitory inputs were coincident, at negative times the inhibition preceded the excitation, and at positive times the inhibition followed the excitation. Thin lines represent shunting inhibition and thick lines represent hyperpolarizing inhibition. The black lines (control) are the excitatory input alone.

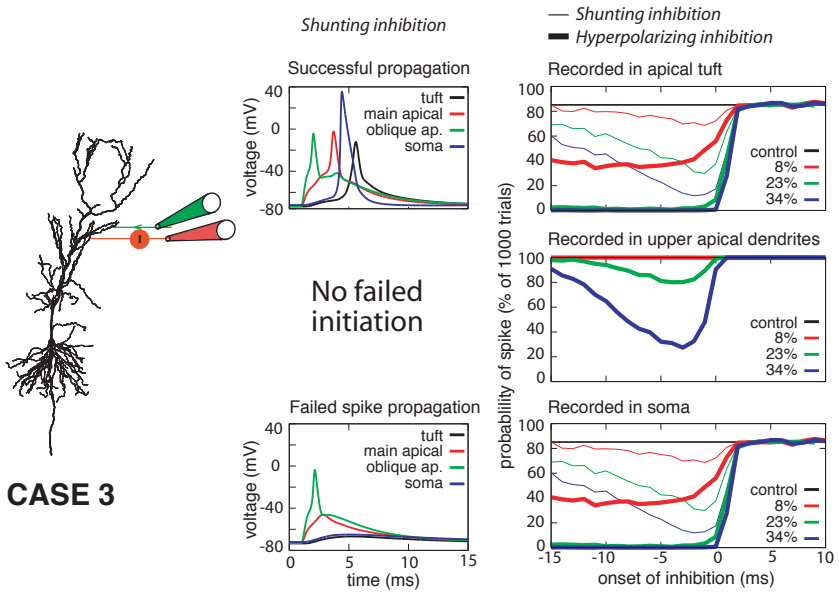
Shunting inhibition
Successful propagation
tuft
main apical
oblique ap.
soma
voltage (mV)
40
0
-40
-80
No failed initiation
Failed spike propagation
time (ms)
0
5
10
15
CASE 3
— Shunting inhibition
Hyperpolarizing inhibition
Recorded in apical tuft
Recorded in upper apical dendrites
Recorded in soma
probability of spike (% of 1000 trials)
100
80
60
40
20
0
control
8%
23%
34%
-15
-10
-5
0
5
10
onset of inhibition (ms)

Figure 4.5.

CASE 4: Perforant-path excitation + Schaffer-collateral inhibition

In many CA1 pyramidal neurons, dendritic spikes initiated in the tuft do not reach the axon on their own, but their propagation can be gated by subthreshold Schaffer-collateral excitation (Jarsky et al., 2005). In strongly excitable CA1 pyramidal neurons, dendritic spikes initiated in the tuft may propagate forward on their own, as they do in our model. We investigated whether Schaffer-collateral inhibition could gate these dendritic spikes and found that neither shunting nor hyperpolarizing Schaffer-collateral inhibition could prevent dendritic spikes from being initiated in the tuft (Figure 4.6). Distally generated dendritic spikes could be gated by shunting inhibition, but very large inputs were required. Activation of 64% of inhibitory synapses on the upper apical dendrites was needed to achieve an approximately 15% reduction in action potential firing. Interestingly, this inhibition was most effective when it arrived 2-3 milliseconds after the excitation, the time it takes for the dendritic spike initiated in the tuft to propagate to the upper apical dendrites. Schaffer-collateral hyperpolarizing inhibition was more effective at gating tuft spikes: an approximately 45% reduction in axonal action potentials was achieved with just 12% of synapses activated.

Figure 4.6. Perforant-path excitation and Schaffer-collateral inhibition. Left: Schematic of simulation protocol. Excitatory synapses in the tuft were randomly activated so that axonal action potentials occurred on 85% of trials. Different numbers of inhibitory synapses in the upper apical dendrites were activated at varying times relative to the excitation. Center: 64% of $GABA_A$ inhibitory synapses (reversal potential -70 mV) in the upper apical dendrites were activated at the same time as the excitatory input. Voltage traces show an example of successful spike propagation (top) and successful spike initiation but failed propagation (bottom). Voltage is measured in the tuft (black traces), main apical dendrite (red traces), upper apical oblique dendrite (green traces), and at the soma (blue traces).

Right: 4% (red lines), 8% (green lines), 12% (blue lines), and 64% (gold lines) of inhibitory synapses were activated at different times relative to the excitatory input. For each time, the probability of action potential generation averaged over 1000 trials in the tuft (top), upper apical dendrites (middle), and soma (bottom) was plotted. At time 0, the excitatory and inhibitory inputs were coincident, at negative times the inhibition preceded the excitation, and at positive times the inhibition followed the excitation. Thin lines represent shunting inhibition and thick lines represent hyperpolarizing inhibition. The black lines (control) are the excitatory input alone.

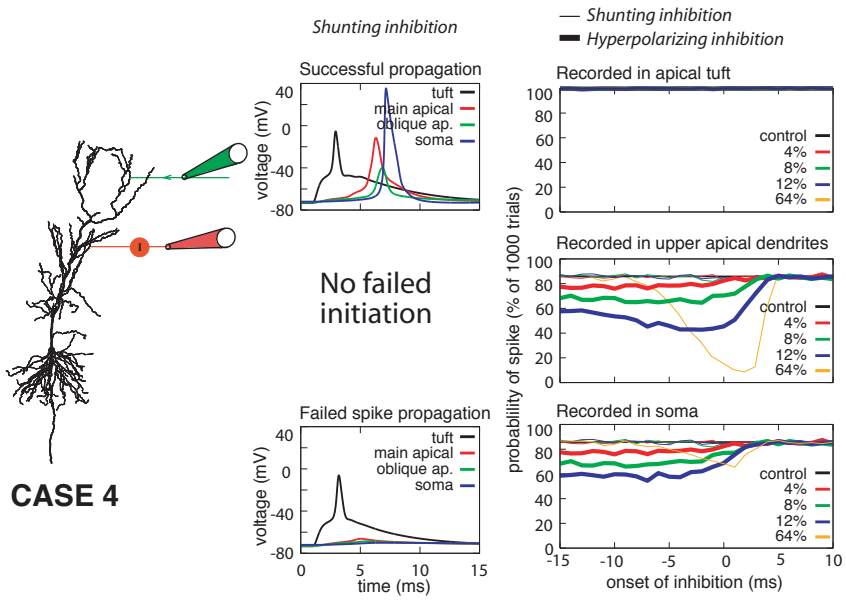
Shunting inhibition
Successful propagation
tuft
main apical
oblique ap.
soma
voltage (mV)
No failed initiation
Failed spike propagation
time (ms)
CASE 4
Shunting inhibition
Hyperpolarizing inhibition
Recorded in apical tuft
Recorded in upper apical dendrites
Recorded in soma
control
4%
8%
12%
64%
probability of spike (% of 1000 trials)
onset of inhibition (ms)

Figure 4.6.

4.5. Discussion

Our simulations show that synaptic integration in different dendritic domains of CA1 pyramidal neurons can be differentially regulated by inhibition. Feed-forward inhibition can modulate both the initiation and propagation of dendritic spikes, depending upon the magnitude, location, and timing of the inhibitory inputs relative to the excitatory drive as well as the type of inhibition. Since voltage attenuation in pyramidal neuron dendrites reduces distal EPSPs to negligible levels in the soma, dendritic spikes are likely to be an important communication mode for distal inputs. Thus understanding how dendritic spike initiation and propagation is affected by inhibition is important for understanding information processing in many areas of the cell. Additionally, synaptic plasticity can depend on spikes generated in dendrites (Golding et al., 2002) or on backpropagating action potentials (Magee & Johnston, 1997), so understanding dendritic inhibition is important for understanding these forms of plasticity as well.

Feed-forward inhibition acts at subthreshold levels of excitation and was shown to limit the time window for the summation of inputs in hippocampal slices (Pouille & Scanziani, 2001), so it may serve to control dendritic spike initiation. IPSPs evoked by synaptic stimulation of perforant-path axons reduced the amplitude of action potentials backpropagating from the more proximal apical dendrites, so inhibition may convert actively backpropagating spikes into passively spreading potentials at different points in the dendrites (Tsubokawa & Ross, 1996).

In CA3 pyramidal cells, IPSPs evoked by synaptic stimulation of the apical dendrites could suppress dendritic calcium spikes (Miles et al., 1996). In this study we looked at how feed-forward inhibition activated by the perforant path and Schaffer-collaterals affected

fast excitatory inputs typically mediated by AMPA receptors and sodium channels. It would be interesting to expand this study to include calcium spikes, which are broader and have a slower time course. Furthermore, the way inhibition affects synaptic integration in pyramidal neurons is likely to depend on the properties of pyramidal neurons themselves. Here, we looked at strongly excitable cells in which dendritic spikes propagate effectively through the dendritic arbor and the effects of dendritic inhibition on pyramidal neurons with weakly excitable dendrites may be different. In vivo, dendritic excitability can be modulated by behavioral state, and when combined with inhibition, could result in an array of combinatorial possibilities.

In vivo, inhibition targeting different somato-dendritic domains is mediated by a diversity of interneurons, each with their own unique properties (McBain & Fisahn, 2001; Somogyi & Klausberger, 2005). There have been many efforts to classify interneurons based on anatomical, physiological, and neurochemical criteria, and progress is being made on elucidating the domain-specific innervation of hippocampal interneuron types. All this is difficult to unravel experimentally, so models can be useful in dissecting how interneurons with different functional properties might differentially regulate pyramidal neuron activity. For example, fast-spiking interneurons respond to inputs in a narrow frequency band, so the strength of feed-forward inhibition could be controlled by the frequency of the perforant-path or Schaffer-collateral input.

In vivo, interneurons also contribute to the generation of extracellular rhythmic activity and can regulate pyramidal neuron spiking during these rhythms (Buzsaki et al., 1992; Mann & Paulsen, 2007). Complex input patterns, the interaction of IPSPs with

membrane potential oscillations, perisomatic and feedback inhibition that pyramidal neurons experience in vivo, as well as realistic interneuron morphologies are other important dimensions that can be addressed in simulations.

Further insight into how inhibition targeting different dendritic locations might serve different functions can be gleaned by looking at inhibitory synapses. The strength of GABA synapses is not scaled along the somato-dendritic axis like excitatory synapses are (Andrasfalvy & Mody, 2006), so their properties may be adjusted for local regulation of synaptic integration as opposed to for their effect at the soma. In most of the dendritic tree, GABA synapses form directly on the dendritic shafts, but in the apical tuft they sometimes form on spines, which may have functional implications (Megias et al., 2001). In addition, since inhibition by $GABA_A$ synapses is mediated by chloride channels that have a reversal potential near rest, local adjustments in the chloride reversal potential can change the properties of the inhibition. If the reversal potential of chloride is depolarized, like it is at some points during development (Ganguly et al., 2001) or in the axon initial segment in the adult (Szabadics et al., 2006), then interneurons may provide depolarization rather than inhibition.

In conclusion, relatively little is known about the effects of domain-specific inhibition on synaptic integration in pyramidal neurons. Our results identify important parameters that may be useful to guide experiments on dendritic inhibition in pyramidal neurons as well as serve as a building block for future modeling studies. These studies will enhance our understanding of microcircuit dynamics in the hippocampus under normal conditions and provide insight into pathologies such as epilepsy that result from alterations in the interactions between excitation and inhibition.

CHAPTER 5

Coincidence Detection of Place and Temporal Context in a Network Model of Spiking Hippocampal Neurons

Published in PLoS Comput Biol 3, e234 (2007).

By: Yael Katz, William L. Kath, Nelson Spruston, and Michael E. Hasselmo.

Author contributions: I performed initial work on this project as part of the Methods in Computational Neuroscience course at the Marine Biological Laboratory in Woods Hole, MA in August 2005. I wrote most of the code for the simulations during an internship with Mike Hasselmo in his laboratory at Boston University during the Spring of 2006. I extensively revised the simulations and generated the figures back at Northwestern during the Summer of 2006. I wrote the paper with editing by all authors. Bill Kath, Nelson Spruston, and Michael Hasselmo guided all stages of the research.

5.1. Abstract

Recent advances in single-neuron biophysics have enhanced our understanding of information processing on the cellular level, but how the detailed properties of individual neurons give rise to large-scale behavior remains unclear. Here we present a model of the hippocampal network based upon observed biophysical properties of hippocampal and entorhinal cortical neurons. We assembled our model to simulate spatial alternation, a task that requires memory of the previous path through the environment for correct selection of the current pathway to a reward site. The convergence of inputs from entorhinal cortex and hippocampal region CA3 onto CA1 pyramidal cells make them potentially important for integrating information about place and temporal context on the network level. Our model shows how place and temporal context information might be combined in CA1 pyramidal neurons to give rise to splitter cells (Wood et al., 2000), cells which fire selectively based on a combination of place and temporal context. The model leads to a number of experimentally testable predictions that may lead to a better understanding of the biophysical basis of information processing in the hippocampus.

5.2. Nontechnical Summary

Understanding how behavior is connected to cellular and network processes is one of the most important challenges in neuroscience, and computational modeling allows one to directly test hypotheses regarding the interactions between these scales. We present a model of the hippocampal network, an area of the brain important for spatial navigation and episodic memory, memory of "what, when, and where." We show how the model, which consists of neurons and connections based on biophysical properties known from experiments, can guide a virtual rat through the spatial alternation task by storing a memory of the previous path through an environment. Our model shows how neurons that fire selectively based on both the current location and past trajectory of the animal (dubbed "splitter cells") might emerge from a newly discovered biophysical interaction in these cells. Our model is not intended to be comprehensive, but rather to contain just enough detail to achieve performance of the behavioral task. Goals of this approach are to present a scenario by which the gap between biophysics and behavior can be bridged and to provide a framework for the formulation of experimentally testable hypotheses.

5.3. Introduction

The hippocampal network needs to integrate information about place and temporal context to enable an animal to navigate its environment based on previous experience (Hasselmo & Eichenbaum, 2005; Leutgeb et al., 2005; O'Keefe & Burgess, 2005; Shapiro et al., 2006; Wood et al., 2000). Since the discovery of place cells, cells which fire selectively when a rat is in a particular location (O'Keefe & Dostrovsky, 1971), it was clear that the hippocampus encodes information about space. More recently, experiments have pointed to additional components of spatial representation in the rat hippocampus. In a spatial alternation task on a T-maze, some CA1 cells fire when the rat is in a particular location on the stem of the maze, but only after either a left or a right-turn trial (Wood et al., 2000). A majority of cells respond on the basis of recent history, though some depend on future action (Ferbinteanu & Shapiro, 2003). These cells, sometimes referred to as "splitter cells" or "episodic cells" (Ferbinteanu & Shapiro, 2003; Frank et al., 2000; Markus et al., 1995; Wood et al., 2000), are thought to be neural correlates of temporal context. The term "context" can be operationally defined in many other ways (Hasselmo & Eichenbaum, 2005), including more temporally diffuse effects defining an extended period of behavior or a specific goal (Doboli & Minai, 2007; Otto & Poon, 2006), or non-temporal effects such as overall environment or presence of specific cue stimuli (Leutgeb et al., 2005). In this paper, we consistently use the phrase "temporal context" to refer specifically to the history corresponding to one lap on the alternating T-maze.

A previous model (Hasselmo & Eichenbaum, 2005) analyzed how splitter cells might emerge in the hippocampus during spatial alternation using the effect of temporal context

and based on other behavioral and physiological data available on the hippocampal formation. That model reproduced the splitter-cell phenomenon, but the result depended upon a multiplicative interaction between the two major inputs to CA1 pyramidal neurons: the perforant-path input from layer III of entorhinal cortex and the Schaffer-collateral input from CA3. At the time the model was made, the idea that a nonlinear interaction between these two inputs was required to produce CA1 output was an assumption, lacking a biophysical basis.

Recently, however, it was discovered that inputs from layer III pyramidal cells of entorhinal cortex (ECIII), which selectively target the distal dendrites of CA1 pyramidal cells, interact nonlinearly with inputs from CA3 pyramidal neurons (CA3), which arrive more proximally (Jarsky et al., 2005). Distal inputs alone typically generate dendritic spikes, but these spikes fail to propagate to the action potential initiation zone in the axon. If a subthreshold depolarization of the proximal dendrites arrives in the same time window as distal dendritic spikes, however, the more proximal input can facilitate propagation of the dendritic spike, resulting in generation of an axonal action potential. This biophysical interaction can be regarded as "gating" of the dendritic spike by the CA3 input. This suggests that CA1 pyramidal cells can act as coincidence detectors.

The previous model (Hasselmo & Eichenbaum, 2005) could not immediately be employed to examine whether gating in CA1 pyramidal neurons might provide the necessary multiplicative interaction at the network level because it uses firing rates as opposed to individual spiking units. Therefore in this study we constructed such a spiking model, using reduced models of CA1 pyramidal neurons that exhibit gating, and show how this

model can produce activity for guiding the trajectory of a rat in the simulated spatial alternation task.

Our model incorporates several biophysical considerations into a successful algorithm for simulating the spatial alternation task. In our model, gating in CA1 dendrites gives rise to splitter cells, and the output of CA1 neurons is used to guide the rat's trajectory through the maze. Thus we show directly how concerted behavior could emerge from the detailed cellular properties of hippocampal and entorhinal neurons. Our model also points to requirements for a neural representation of temporal context and suggests how the sources of place and temporal context representations could be identified experimentally.

5.4. Results

Three regions of the hippocampus were simulated: ECIII, CA3, and CA1. The network consists of representations of ECIII, CA3, and CA1 cells and their excitatory synaptic interconnections.

5.4.1. ECIII and CA3 neurons

ECIII and CA3 neurons were modeled as single nodes (equipotential compartments) using the equations proposed by Izhikevich for quadratic integrate and fire neurons with adaptive recovery and voltage reset (Izhikevich, 2003). Single nodes were sufficient to represent ECIII and CA3 pyramidal neurons because we were not concerned with dendritic processing in those cells. The Izhikevich scheme was chosen because it is simple, computationally efficient, and capable of reproducing a wide range of neuronal behaviors.

5.4.2. CA1 neurons

Multiple nodes were required to represent CA1 neurons in order to simulate gating, which is a result of the geometry of their dendritic trees. We used a conductance-based model for the CA1 cells to make connection with our previous multi-compartmental models that exhibited gating (Jarsky et al., 2005). CA1 neurons were each composed of four CA1 nodes, corresponding to the distal apical tuft, apical dendrites, soma, and basal dendrites of a CA1 pyramidal cell. These nodes were electrically coupled together in a manner corresponding to pyramidal neuron geometry (Fig. 5.1). The areas of the nodes are approximately scaled to the areas of the regions they represent in the multi-compartmental model of a reconstructed CA1 pyramidal neuron (Golding et al., 2001). In the multi-compartmental model, channel densities were adjusted to match experimental data, so in our reduced model, we use similar densities (see Methods for model equations). The response of our reduced model CA1 neuron to a somatic current injection (Fig. 5.1A) illustrates that it has weakly excitable dendrites with the backpropagating action potential failing to invade the distal dendrites, as in the full morphological models and in experiments (Golding et al., 2001).

Figure 5.1. Elements of the nework model. **(a)** ECIII and CA3 neurons are represented by single ECIII and CA3 nodes. Reduced model of a CA1 pyramidal neuron consists of 4 CA1 nodes electrically coupled together, representing the apical tuft, more proximal apical dendrites, soma, and basal dendrites. Shown are voltage responses of single, uncoupled ECIII, CA3, and CA1 neurons to 2 ms current injections of 200 pA, 200 pA, and 375 pA respectively. The backpropagating action potential into the apical dendritic compartments of our CA1 pyramidal cell model shows that it has weakly excitable dendrites. **(b)** ECIII and CA3 cells receive external current inputs during the simulations. An ECIII cell provides input to the distal dendritic compartment of a CA1 cell and a CA3 cell innervates its proximal dendritic compartment. Synaptic potentials are modeled as alpha functions, and if an EPSP exceeds a threshold of -30 mV, an action potential is generated in the postsynaptic cell.

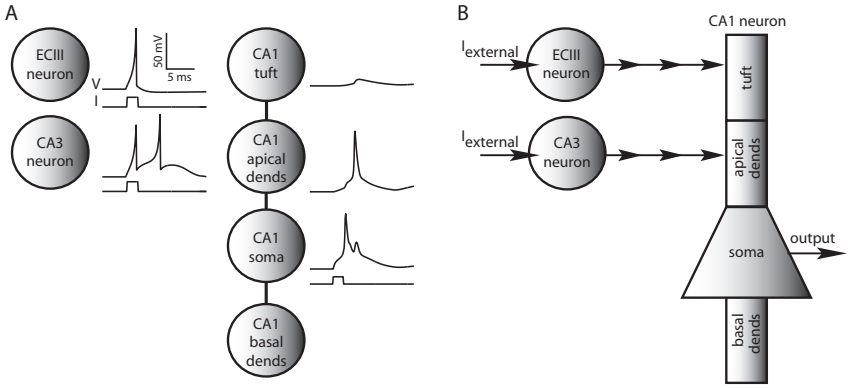
A
ECIII neuron
CA3 neuron
V
I
50 mV
5 ms
CA1 tuft
CA1 apical dends
CA1 soma
CA1 basal dends
B
CA1 neuron
I external
ECIII neuron
I external
CA3 neuron
tuft
apical dends
soma
output
basal dends

Figure 5.1.

5.4.3. The virtual environment

The virtual rat is confined to move through a T-maze with return arms (Fig. 5.2). It begins at the base of the stem, and at every time step updates its position by an amount Δx. Although the rat moves with small steps, the maze is also divided into larger positions, marked in the figure. The first time through the maze, the rat is forced to take an alternating trajectory marked by the arrows. On all subsequent runs, the rat chooses where to go by following the spiking patterns of its CA1 neurons, as discussed below.

The objective of the spatial alternation task is for the rat to earn rewards, which the experimenter alternatively places in the top right and left corners of the maze. In the model the rewards are not explicitly simulated, but a trial is considered correct if the rat runs to the reward zone that would have contained the reward in the actual task (Fig. 5.2). On each trial, the rat runs from the base of the stem to the position marked "choice point" where it must decide which way to turn. A correct choice requires the rat to remember which way it turned on the previous trial, so it can head towards the opposite reward zone.

Many areas of the hippocampal formation are known to contain place cells, but where the place representation originates in the brain is not fully understood. Similarly, while the hippocampus is known to represent temporal context, the origin of this representation has not been identified. Therefore, we test two model variants: In the first, we assume that primary place information is represented in ECIII and temporal context is represented in CA3. In the second, we assume the reverse, that primary place information is represented in CA3 and temporal context in ECIII.

Figure 5.2. The virtual environment. The virtual rat is confined to move through a T-maze with return arms. Although it moves in small steps, the maze is divided into larger positions, numbered 1-5 for positions on the stem, 6-12 for positions on the right and 6'-12' for corresponding positions on the left. The rat begins in position 1 at the base of the stem, moving up the stem to the choice point at the top of the stem. Virtual reward zones are in the right and left corners of the maze. The arrows denote a correct trajectory with the rat alternating between right and left turns at the choice point.

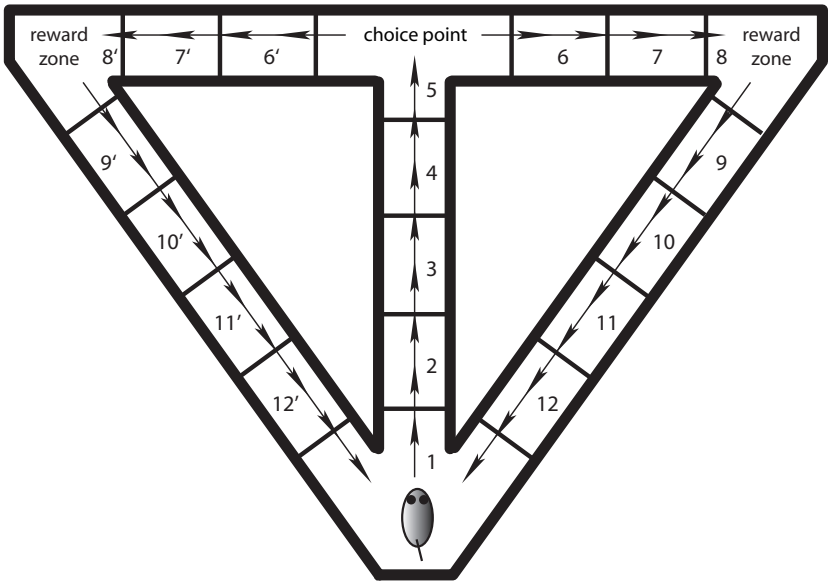
reward zone
8′
7′
6′
choice point
6
7
8
reward zone
5
4
3
2
1
9′
10′
11′
12′
9
10
11
12

Figure 5.2.

5.4.4. Forward association

Each position in the environment is represented by one primary place cell, which receives an external current input every time the rat enters a particular position. The primary place cells are either ECIII cells or CA3 cells, depending on which region is assumed to contain the raw representation of place in the particular simulation.

We assume that at the start of the simulation the rat has already learned the spatial alternation task, so the appropriate network connectivity has been established. Every primary place cell is synaptically connected only to those primary place cells representing the positions that the rat can enter from its current position. Thus cell 1 is connected to cell 2, cell 2 to cell 3, and so forth (Fig. 5.3A); this is termed forward association. When the rat is at the choice point, it can turn either right or left; cell 5, therefore, is connected both to cell 6 and 6'.

In the real brain, excitatory inputs do not typically propagate through entire networks because of the requirement for inputs from many cells to drive spiking and the abundance of inhibitory inputs (Hubel & Wiesel, 1963a,b; Wilson & Cowan, 1972). In our model, we limit the spread of activity through the network of primary place cells by decreasing the factor w in the transfer function between cells (see Methods) by 60% for each successive connection. For the first connection, w is at a maximum value (w_{max}), which is sufficient to always induce spiking in cells directly connected to the primary place cell receiving input. In order to prevent inputs from exciting the entire network, we decrease w with distance from the input site. Reducing w by 40% for every connection does not allow for sufficient membrane depolarization to bring the third cell in the chain to firing threshold. For example, if cell 1 receives an input, the connection from cell 1 to cell 2 has a weight of

w_{max}, the connection from cell 2 to cell 3 has a weight of 60% of w_{max}, which is sufficient to cause cell 3 to fire, and the connection from cell 3 to cell 4 has a weight of 60% of 60% of w_{max}, which is not sufficient to bring cell 4 to threshold. Every time the rat enters a new position, the w factors are adjusted so that the forward connections follow this pattern (Fig. 5.3A). This mechanism is not intended to directly model any biological process. Rather, it is a simple phenomenological way of limiting the forward spread of activity through the network without explicitly including more complex effects such as inhibition and stochastic firing of neurons.

Figure 5.3. The network of primary place cells. **(a)** *first column:* When the rat enters position 1, primary place cell (PPC) 1 receives an external input. Synaptic weights are decreased so that the input propagates forward to PPC3, but the response in PPC4 is below spike threshold. *second column:* When the rat enters position 2, all synaptic weights are reset. PPCs 1 and 2 receive external inputs which elicit spiking in PPCs 3 and 4, but not PPC5. When the rat enters positions 3 and 4, external inputs are delivered and synaptic weights are adjusted in a similar manner *(remaining columns).* **(b)** Time series plots for the primary place cells representing positions 1, 2, 3, and 4 on the maze. For each cell, the bottom trace is the input current and the top trace is the voltage response. PPC x gets external input at positions x, x+1, and x+2 and forward association input from positions x-1 and x-2. Therefore, a primary place cell spikes at most in 5 positions.

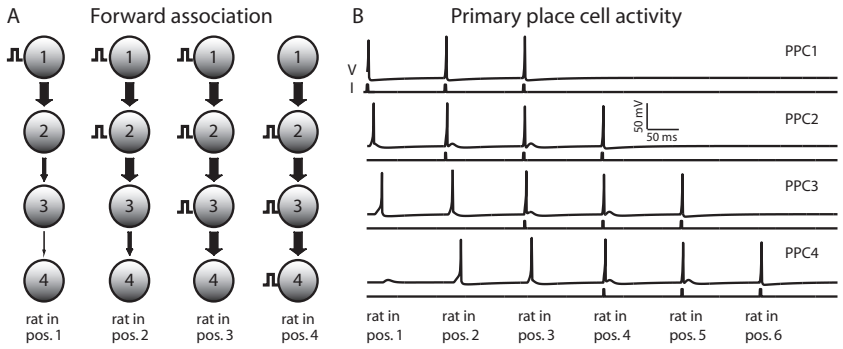
A
Forward association
B
Primary place cell activity
1
2
3
4
rat in pos. 1
rat in pos. 2
rat in pos. 3
rat in pos. 4
V
I
50 mV
50 ms
PPC1
PPC2
PPC3
PPC4
rat in pos. 1
rat in pos. 2
rat in pos. 3
rat in pos. 4
rat in pos. 5
rat in pos. 6

Figure 5.3.

When the rat enters a new position, the primary place cell representing that position receives an external current input representing place information. The primary place cell representing that position continues to get external input when the rat moves to the next two locations, so each cell has a place field that spans three positions. Combining this system with forward association results in place fields that are larger than the spatial elements in our model (Maurer et al., 2006). The size of the model place fields is reasonably consistent with the size of experimentally observed place fields (McNaughton et al., 1983). This scheme also mimics the fact that in-vivo, place cells fire on several theta cycles once they are activated (Skaggs et al., 1996).

Thus, when the rat is in the start position at the base of the stem, primary place cell 1 (PPC1) receives an external input. PPC1 then fires and forward association results in firing of PPC2 and PPC3 and an EPSP in PPC4 (Fig. 5.3B). When the rat moves up the stem into position 2, PPCs 1 and 2 receive external input, and the spike in cell 2 propagates through PPC4. When the rat gets to the choice point at the top of the stem, PPC5 gets external input that spreads both to the right to PPCs 6 and 7 and to the left to PPCs 6' and 7' (Fig. 5.4). If the rat turns to the right and enters position 6, PPCs 6' and 7' on the left will remain firing because PPC5 at the choice point continues to receive input. Once the rat reaches position 8, the right reward zone, the forward association from the choice point to PPCs 6' and 7' stops and only cells in front of the rat fire. Since the firing of the choice point cell spreads symmetrically to both the right and the left arms of the maze, the rat must use temporal context information to choose the correct trajectory.

Figure 5.4. Forward association from the choice point. *left:* Time series plots for the primary place cells representing the choice point and the three positions to the right and left of the choice point. For each cell, the bottom trace is the input current (200 pA) and the top trace is the voltage response. Activity spreads symmetrically from the choice point cell to the cells representing the right and left arms of the maze. *right:* Place fields for the cells depicted on the left. The dots represent spikes, showing where the animal was located when the cell fired.

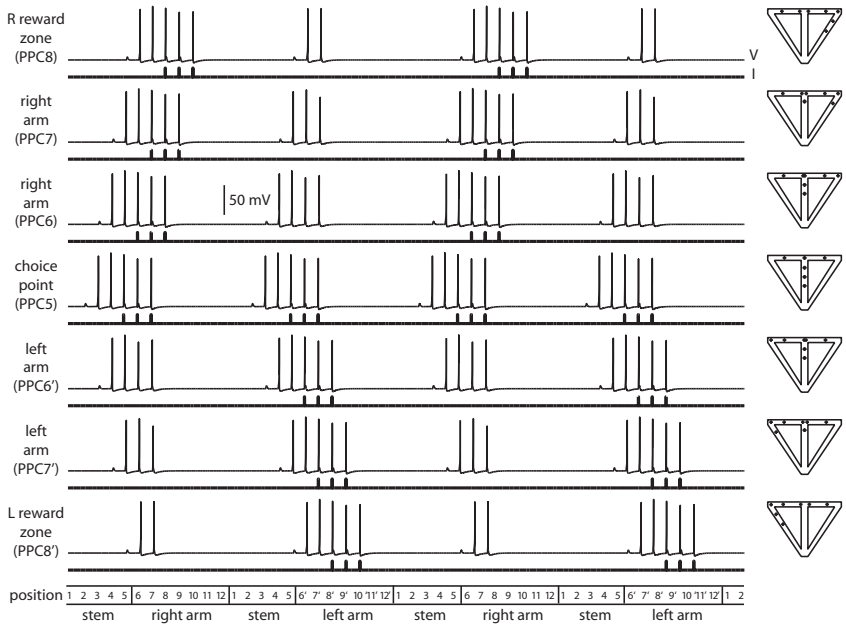
R reward zone (PPC8)
right arm (PPC7)
right arm (PPC6)
choice point (PPC5)
left arm (PPC6')
left arm (PPC7')
L reward zone (PPC8')
50 mV
V
I
position
1 2 3 4 5 6 7 8 9 10 11 12 1 2 3 4 5 6' 7' 8' 9' 10 11' 12' 1 2 3 4 5 6 7 8 9 10 11 12 1 2 3 4 5 6' 7' 8' 9' 10 11' 12' 1 2
stem
right arm
stem
left arm
stem
right arm
stem
left arm

Figure 5.4.

5.4.5. Temporal context

Our model utilizes two temporal context cells with very broad place fields to encode temporal context; one represents the stem and the left half of the environment and the other represents the stem and the right half (Fig. 5.5A). In our model a temporal context cell (TTC) is a place cell whose firing outlasts the external input, but is not sustained forever. Such sustained neuronal firing is the fundamental requirement for a representation of temporal context. There are several mechanisms available both on the single-cell and network levels that could give rise to it, and in our model we choose a recurrent network for simplicity. The first time a TCC fires, it activates a large network that feeds back onto itself, and as it fires successive spikes, the percentage of the network that it succeeds in recruiting decreases (Fig. 5.5B). Specifically, the recurrent network for each TCC contains 22 neurons and for every 40 spikes fired the number of network cells activated is decreased by 1. This has the effect of keeping a TCC firing for a limited amount of time after input to it has ceased.

As the rat enters each position on the stem of the maze, both temporal context cells receive an external input that is too weak to induce firing in either cell (Fig. 5.5C). If it makes a right turn, the input to the right TCC increases, causing it to fire, but the input to the left TCC ceases. When the rat re-enters the stem after the right turn, both TCCs receive weak input again, but this is sufficient to keep the right TCC firing, but not to initiate firing of the left TCC. Furthermore, the right TCC continues to fire for several positions after the rat has made a left turn even though input to it has ceased. Thus when the rat turns left after a preceding right turn run, the right TCC is still spiking and the left temporal context cell has not yet begun to fire. As the rat continues to move through

the left arm of the maze, the right TCC shuts off and the left one begins to fire. This lateral selectivity of the right and the left TCCs is used by the virtual rat to determine which way to turn.

Figure 5.5. The network of temporal context cells. **(a)** At first, the left and right temporal context cells (TCCs) are each connected to large recurrent networks of 22 cells each. **(b)** When the rat enters the right arm of the maze, the right TCC receives strong external input (200 pA) causing it to fire. With successive spiking, the right TCC can recruit a smaller and smaller portion of its network. The TCC continues to fire without external input only as long as it can recruit a recurrent network of sufficient strength. **(c)** *left:* Time series plots for the right and left temporal context cells. Bottom traces are the input current, and top traces are the voltage response. Note that the magnitude of the input current increases (from 100 to 200 pA) as the rat moves from the stem into the arms of the maze. *right:* Context place fields for the cells on the left. Note that the context place fields are extremely broad.

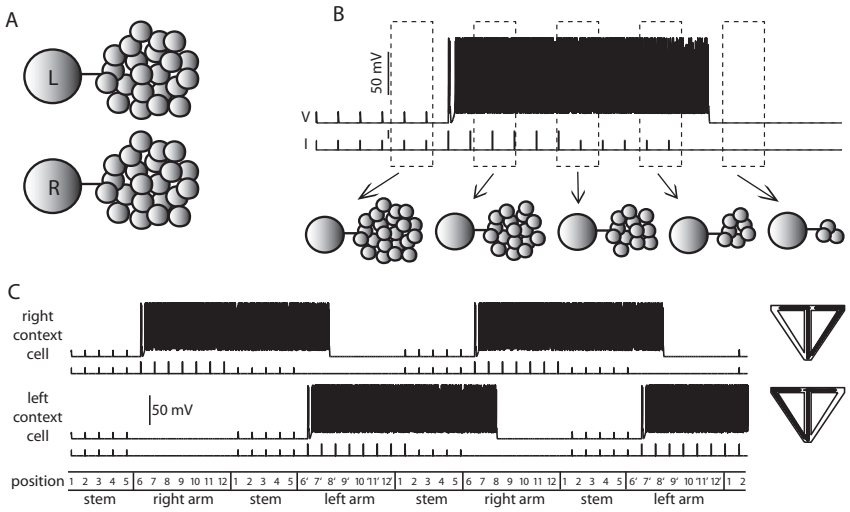
A
L
R
B
50 mV
V
I
C
right
context
cell
left
context
cell
50 mV
position
1 2 3 4 5 6 7 8 9 10 11 12 1 2 3 4 5 6' 7' 8' 9' 10 11' 12' 1 2 3 4 5 6 7 8 9 10 11 12 1 2 3 4 5 6' 7' 8' 9' 10 11' 12' 1 2
stem
right arm
stem
left arm
stem
right arm
stem
left arm

Figure 5.5.

5.4.6. Computation by CA1 neurons

Each position in the maze is also represented by two CA1 neurons. The model CA1 neurons have just four compartments, but are capable of reproducing the gating phenomenon (Jarsky et al., 2005). In our model, input from ECIII enters the distal dendritic compartments of the CA1 cells, mimicking the perforant-path input that selectively innervates the apical tufts of CA1 pyramidal neurons, and input from CA3 enters their more proximal dendritic compartments, mimicking the Schaffer-collateral input. On their own, the ECIII inputs generate dendritic spikes in the CA1 tuft, which fail to propagate forward to the soma. The CA3 inputs on their own generate EPSPs in the proximal apical dendritic compartment of the CA1 neurons, but are insufficient to induce spiking. When the ECIII and CA3 inputs are coincident, however, propagation of the dendritic spike is rescued, resulting in somatic action potentials.

If we assume the ECIII cells are primary place cells and the CA3 cells represent temporal context, the CA1 neurons fire dendritic spikes in their most distal nodes and experience sustained depolarization of their more proximal ones, but fire somatic spikes only when both the place cells and the temporal context cells are active. This case corresponds to gating, since the spike is initiated in the apical tuft and propagates forward to the soma on account of the extra depolarization entering the more proximal region (Fig. 5.6A).

If we assume that the place cells occur in CA3 and temporal context cells in ECIII, the output of the CA1 neuron is the same as in the previous case since we require both the ECIII and CA3 inputs for spiking (Fig. 5.6B). In our reduced model, the persistent input to the CA1 apical tuft compartment due to the ECIII temporal context cell serves

to depolarize the apical tuft for long periods of time. This depolarization sums with the depolarization entering more proximally, bringing the apical dendritic compartment past action potential threshold. With a different choice of parameters in our model, the action potential could have been initiated in the soma instead of the proximal apical dendrites, but in either case, the action potential readily spreads throughout the rest of the cell. The facilitated spike propagation in the dendrites (compare Figs. 5.1 and 5.6) results from the synaptic depolarization associated with activation of the Schaffer collateral input.

Figure 5.6. Gating in the reduced model of a CA1 pyramidal neuron. **(a)** Shown are the cells representing position 2 of the maze. Here, the ECIII cell encodes place information and the CA3 cell represents temporal context. The CA1 cell only fires somatic spikes when the ECIII and CA3 inputs are coincident. As the rat enters the stem from the right arm, the subthreshold responses in the proximal apical dendrites and soma correspond to dendritic spikes that fail as they propagate forward. The gray inset shows the first set of CA1 spikes on an expanded time scale. **(b)** Same as above except the ECIII cell represents temporal context and the CA3 cell encodes raw place information. Although the somatic action potential profiles in A and B are roughly identical, in this case the spike is initiated in the proximal apical dendritic compartment and propagates forward to the soma and backwards to the apical tuft as can be seen in the gray inset.

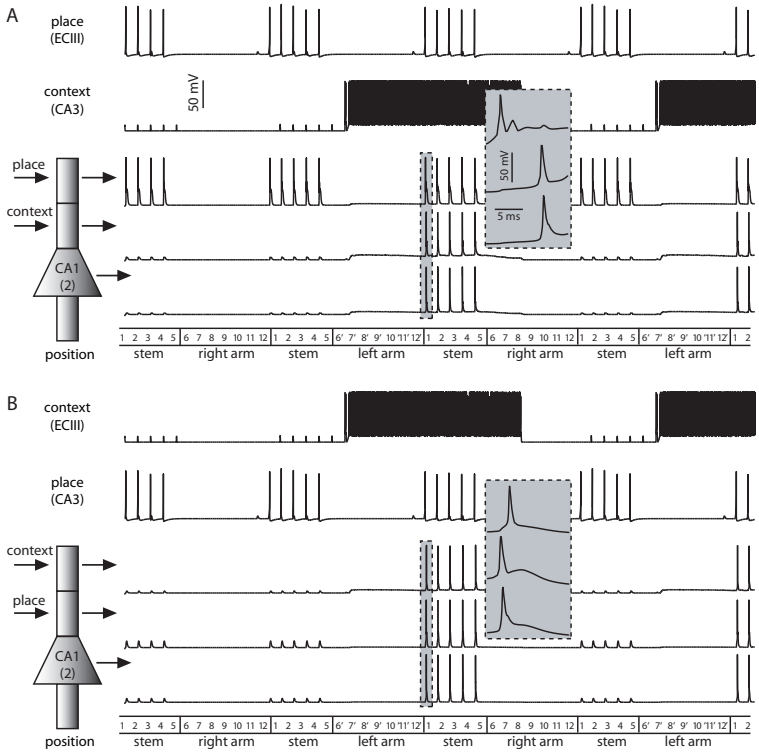
A
place
(ECIII)
context
(CA3)
50 mV
50 mV
5 ms
place
context
CA1
(2)
position
1 2 3 4 5 6 7 8 9 10 11 12 1 2 3 4 5 6' 7' 8' 9' 10 '11' 12' 1 2 3 4 5 6 7 8 9 10 11 12 1 2 3 4 5 6' 7' 8' 9' 10 '11' 12' 1 2
stem
right arm
stem
left arm
stem
right arm
stem
left arm
B
context
(ECIII)
place
(CA3)
context
place
CA1
(2)
position
1 2 3 4 5 6 7 8 9 10 11 12 1 2 3 4 5 6' 7' 8' 9' 10 '11' 12' 1 2 3 4 5 6 7 8 9 10 11 12 1 2 3 4 5 6' 7' 8' 9' 10 '11' 12' 1 2
stem
right arm
stem
left arm
stem
right arm
stem
left arm

Figure 5.6.

5.4.7. CA1 output guides the trajectory of the rat

In our model, the rat uses the output of its hippocampus to select actions at all locations in the maze. Action selection in spatial memory tasks is a complex process involving interactions of the hippocampus with the prefrontal cortex and other regions, which receive hippocampal output as their input. Instead of trying to simulate these dynamics, we use a simple rule by which action selection is determined from the output of the hippocampus directly: the rat always moves to a position corresponding to a spiking CA1 neuron with the stipulations that it can only move to an adjacent position and it cannot move backwards.

In order for a single rule to govern the movement of the rat through the entire task, the wiring of the network was set up as follows. The two CA1 cells representing each position in the maze receive input from the primary place cell representing that position and from both temporal context cells (Fig. 5.7). Although both TCCs project to every CA1 cell, we presume that some learning process has taken place to strengthen some connections and weaken others. Thus, for positions on the stem of the maze, one CA1 cell receives strong input from the right TCC and weak input from the left one and the other receives strong input from the left TCC and weak input from the right one. CA1 cells for the right return arm of the maze (positions 8-12) receive strong input from the right TCC and CA1 cells for the left return arm of the maze (positions 8'-12') receive strong input from the left TCC. For the two positions adjacent to the choice point on either side, the situation is reversed: CA1 cells 6 and 7 on the right side of the maze receive strong input from the left TCC and CA1 cells 6' and 7' on the left side of the maze receive strong input from the right TCC (Fig. 5.7). This enables the rat to move simply by following the spiking

of its CA1 neurons. For example, if the rat is at the choice point and it has previously completed a right turn run, CA1 cell 6' will be spiking but cell 6 will not. Based on this information, the rat will enter position 6' and move towards the reward zone on the left side of the maze (Fig. 5.8). Thus, with biophysically realistic elements wired together in this manner, a simple rule is sufficient to simulate the spatial alternation task.

Figure 5.7. Network wiring diagram. Circles represent ECIII cells, triangles represent CA1 cells, and squares represent CA3 cells, and lines indicate connections. The solid lines show robust connections that came about as a result of a presumed learning process, while the dashed lines suggest weak connections that have not been strengthened due to learning. Cells representing positions in the stem of the maze are connected as depicted for position 3: one CA1 cell for position 3 is connected to primary place cell 3 and the right temporal context cell, while the other CA1 cell representing position 3 is connected to PPC3 and the left temporal context cell. Cells representing positions in the arms of the maze (except for positions on either side of the choice point, see below) are connected in the same way as the cells for position 11'. Both CA1 cells representing position 11' are connected to PPC11' and the to the temporal context cell representing the ipsilateral side of the maze, in this case the left TCC. The exception to this is positions 6, 7, 6', and 7', which are wired as follows: both CA1 cells representing each position are connected to primary place cell representing that position and to the temporal context cell representing the *opposite* side of the maze from which the position is located.

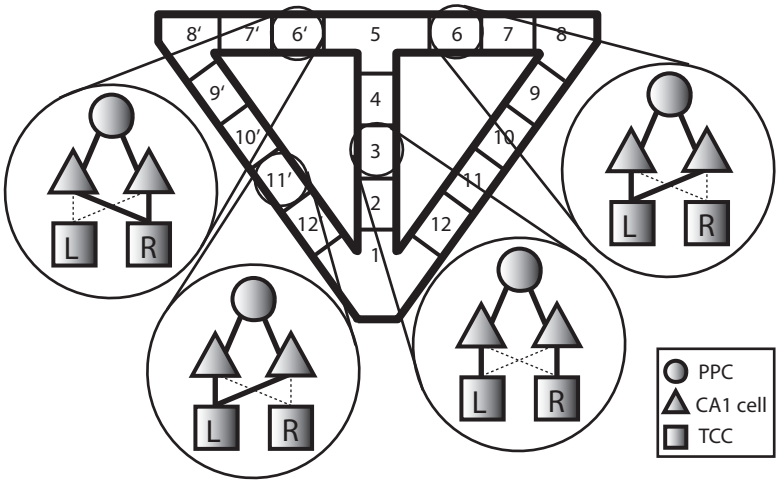

Figure 5.7.

Figure 5.8. The CA1 network. *left:* Time series data for the somata of CA1 neurons representing the choice point and the three positions to the right and left of the choice point. Here primary place cells are taken to be ECIII cells and temporal context cells to be CA3 cells, but when the representations are switched, the time series is essentially unchanged. Note that this figure includes the first time the rat goes through the maze, so it contains the initial transient where the final dynamics of all the neurons have not yet been established. *right:* Place fields for the somata of the cells on the left.

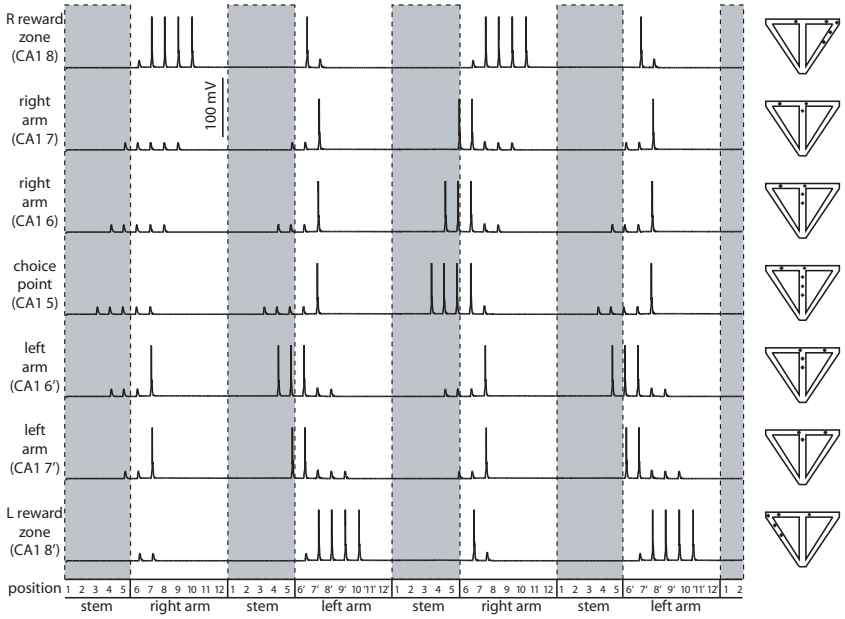
R reward zone (CA1 8)
right arm (CA1 7)
100 mV
right arm (CA1 6)
choice point (CA1 5)
left arm (CA1 6')
left arm (CA1 7')
L reward zone (CA1 8')
position
1 2 3 4 5 6 7 8 9 10 11 12 1 2 3 4 5 6' 7' 8' 9' 10' 11' 12' 1 2 3 4 5 6 7 8 9 10 11 12 1 2 3 4 5 6' 7' 8' 9' 10' 11' 12' 1 2
stem
right arm
stem
left arm
stem
right arm
stem
left arm

Figure 5.8.

5.4.8. Simulation of splitter cells

The interaction of place and temporal context inputs to cells representing locations in the stem effectively results in splitter cell responses. Figure 5.9 illustrates the output of CA1 neurons representing all positions in the maze. When the virtual rat enters the stem from the right arm, the network shows clear firing activity in one set of neurons representing the stem (1R, 2R, 3R, 4R, 5R), but not in the other set of neurons representing the stem (lack of activity in 1L, 2L, 3L, 4L, 5L). In contrast, when the virtual rat enters the stem from the left arm, the network shows firing activity in a different set of neurons representing the stem (1L, 2L, 3L, 4L, 5L), and does not show firing activity in the previously active set of neurons representing the stem. This demonstrates that the cellular gating phenomenon used by the model CA1 cells provides the necessary mechanism for selective firing based on prior temporal context.

In summary, we have shown how a differential representation of temporal context in the hippocampus might be constructed from the biophysics of hippocampal and entorhinal pyramidal neurons. The CA1 cells in the stem of the maze are place cells, but they also fire selectively based on temporal context. One population of CA1 cells in the stem fires only after left-turn trials, and the other fires only after right-turn trials (Fig. 5.9). This is a direct consequence of a nonlinear interaction between the ECIII and CA3 inputs, causing the CA1 cells only to fire if they get coincident input from these two pathways. Because one population of CA1 cells in the stem is connected to the right temporal context cell and the other to the left temporal context cell, the CA1 cells in the stem become splitter cells.

Figure 5.9. The CA1 network. Raster plot showing spiking patterns for the entire CA1 network (including the initial transient). Cell number is plotted against position, and a vertical bar indicates a somatic spike when the rat is in a particular position. Cells in the stem are splitter cells: CA1 cells 1-5 R and 1-5 L fire only after right and left turn trials respectively. The lines show how the rat can use the output of its CA1 cells to determine correct trajectories through the maze.

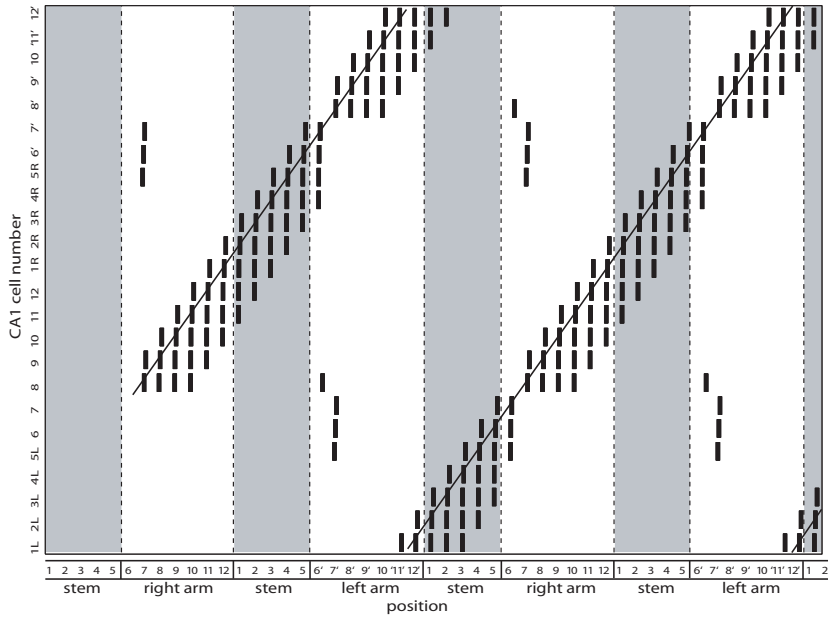
CA1 cell number
1L 2L 3L 4L 5L 6 7 8 9 10 11 12 1R 2R 3R 4R 5R 6' 7' 8' 9' 10' 11' 12'
1 2 3 4 5 6 7 8 9 10 11 12 1 2 3 4 5 6' 7' 8' 9' 10' 11' 12' 1 2 3 4 5 6 7 8 9 10 11 12 1 2 3 4 5 6' 7' 8' 9' 10' 11' 12' 1 2
stem
right arm
stem
left arm
stem
right arm
stem
left arm
position

Figure 5.9.

5.5. Discussion

5.5.1. Representations of context in the rat hippocampus

Although studies in humans suggest that the role of the hippocampus in episodic memory requires context for where and when an event occurs (Eichenbaum & Cohen, 2001), the idea that the representation of space in the rat hippocampus includes a contextual component remains somewhat controversial. Early evidence for a hippocampal representation of context comes from the observation that some place cells are active only when a rat is traveling in a particular direction in tasks such as the radial maze or linear track, but not when the rat is running on an open field (McNaughton et al., 1983; O'Keefe & Recce, 1993). Place cells also remap their firing locations when a rat searches for food in a directed manner as opposed to foraging randomly (Markus et al., 1995). These data indicate that the hippocampus not only encodes locations, but the representation changes depending on the behavioral context.

Additional evidence for a contextual component of spatial representation in the hippocampus comes from the discovery of splitter cells, CA1 place cells that fire only after a left- or a right-turn trial in a spatial alternation task (Ferbinteanu & Shapiro, 2003; Frank et al., 2000; Wood et al., 2000). Splitter cells were not observed in spatial alternation on a Y-maze (Lenck-Santini et al., 2001); later experiments, however, showed that a reward presented at the base of the stem prevents the splitter cell phenomenon, and splitter cells are observed if a reward is not presented at the start of the overlapping segment (Bower et al., 2005).

Behavioral data show that hippocampal lesions impair a rat's performance of spatial alternation when a delay is imposed between right and left-turn trials, but do not impair its performance of the task when it alternates through the maze continuously (Frank et al., 2000; Lee et al., 2006; Lenck-Santini et al., 2001; Wood et al., 2000). Recent recording experiments show that context-dependent hippocampal activity occurs in both the delayed and continuous versions of the spatial alternation task, although, paradoxically, in the delayed version it occurs during the delay period and not on the stem of the maze (Ainge et al., 2007). Thus, although the hippocampus is not required for continuous spatial alternation, it generates splitter-cell activity during the task. The differences in hippocampal activity during the delayed and continuous versions of spatial alternation indicate that the hippocampus is a dynamic system that may adapt to the demands of different tasks (Ainge et al., 2007).

Another study shows that neurons recorded in the same spatial location but in recording chambers with different shapes have firing rates differing by several orders of magnitude while their place fields remain the same. Conversely, neurons recorded in recording chambers of the same shape but in different spatial locations show a change in both the rate and location of firing (Leutgeb et al., 2005), indicating that the hippocampus contains codes for both spatial position relative to local cues and the context of the overall location of the local cues in the environment.

Although it now seems clear that the hippocampus represents context, the origin of the contextual representation in the hippocampal network is not known. In our model, a requirement for a representation of temporal context is a transient response that outlasts

the stimulus that generated it (e.g. a right turn), but is not sustained forever. In different versions of our model, we incorporated this in ECIII neurons or in CA3 networks, under the assumption that each cell type has the potential to perform that function. ECIII neurons have been shown to exhibit sustained firing that could be manipulated by varying their inputs (Egorov et al., 2002; Tahvildari et al., 2007). The representation of temporal context by a gradual reduction in sustained neural activity used here resembles previous models of temporal context (Howard & Kahana, 2002; Howard et al., 2005). A distinguishing anatomical feature of the CA3 network is that CA3 pyramidal cells are reciprocally connected to one another (Amaral & Witter, 1989), which could enable them to continue spiking long after input to them has ceased (Lee et al., 2004). Since either single neurons in ECIII or the recurrent network connectivity in CA3 could instantiate the representation of temporal context in the real hippocampus, we represented temporal context alternately in these two ways in different versions of our model. While both models were able to reproduce splitter cells in CA1, the responsible biophysical interaction was slightly different in the two models.

5.5.2. Predictions of the model

Our model predicts different behavior in CA1 cells depending on which of its afferents carry temporal context information. If temporal context enters CA1 from CA3, its function is to facilitate forward propagation of dendritic spikes triggered by the place information arriving in the distal tuft via the ECIII input (Fig. 5.7A). If temporal context enters CA1 from entorhinal cortex, it depolarizes the apical dendrites and facilitates a spike in response to the place information arriving in more proximal dendrites via the CA3 input.

In this case the action potential is initiated in the soma and backpropagates into the dendrites (Fig. 5.7B). This is because in our model, the high frequency input arriving from the temporal context cells causes a depolarization of the CA1 dendrite rather than causing dendritic spikes.

The model also makes a specific prediction that splitter cell activity in CA1 requires inputs from both ECIII and CA3. Although inputs from CA3 to CA1 have been reduced or eliminated in a few studies (Brun et al., 2002; McNaughton et al., 1989; Mizumori et al., 1989), the effects of these manipulations on splitter cells have not been determined. However, the finding that CA1 place cells are not disrupted by elimination of CA3 inputs (Brun et al., 2002) is seemingly at odds with our model, which requires both CA3 and ECIII inputs to produce firing. This result could be explained, however, by an upregulation of ECIII innervation following CA3 lesions. Rapid and reversible inactivation of ECIII or CA3 inputs would provide more stringent tests of our model.

5.5.3. Relation to previous models

There are many models of the hippocampus that attribute specific functions to individual subregions, and a few full models that attempt to integrate the functions of the different subregions (Hasselmo & Wyble, 1997; Rolls & Kesner, 2006). The model presented here is related to a previous model of neural activity during spatial alternation (Hasselmo & Eichenbaum, 2005), which effectively simulates the phenomenon of splitter cells due to a multiplicative interaction of ECIII and CA3 inputs to CA1 neurons. However, our model is fundamentally different from the previous one because in that model activity was represented in a more abstract manner, using mean firing rates in hippocampal regions,

rather than spikes in biophysically realistic neurons. In this study we recast many aspects of the previous model into a spiking model constrained by experimental data. Another difference is that the previous model used single neurons to represent locations on the stem, and obtained splitter cell responses during retrieval through the differential activation of neurons representing the left or right reward arm. In contrast to the current model, the previous model showed more splitting primarily near the choice point, and the presence of splitters at earlier points on the stem required the specification of very large place fields. The previous model also differed in that it modeled a learning-based development of the representation of space and temporal context, it incorporated theta rhythms, and it included an abstract representation of prefrontal cortex to guide behavior.

The model presented here addresses specific biophysical mechanisms important for solving problems that require the use of context. Earlier models have addressed different mechanisms for context-dependent changes in neural firing activity using more abstract threshold units (Doboli & Minai, 2003; Doboli et al., 2000). In other models, spiking network models of the hippocampus were developed to guide navigation toward different goal locations (Gorchetchnikov & Hasselmo, 2005; Koene et al., 2003). Our model complements these previous approaches by using more biophysically realistic models of neurons and relating these properties to the context-dependent properties of splitter cells.

5.5.4. Limitations of our model and opportunities for developing anatomically and biophysically realistic models of the hippocampus

Our model is a very simple representation of place and temporal context in the hippocampus, intended primarily to highlight possible biophysical mechanisms by which these properties could be represented in ECIII and CA3 and mechanisms by which coincidence of these signals could lead to spiking in CA1 pyramidal neurons. While simple models can offer insight and predictions, identifying some of the simplifying assumptions highlights the possibility of future enhancements to the model.

One simplification in the present model is the fact that we simulate only three of the many hippocampal regions likely to be important for delayed spatial alternation. Input to CA3 comes from ECII both directly and indirectly via the dentate gyrus, and information processing in these regions should be considered in future models.

Increasing the number of neurons could also enhance our model by allowing for a more continuous representation of space and a more distributed representation of temporal context. In addition, representing each location by a population of neurons would allow each cell to respond to its inputs stochastically, which would be a closer reflection of reality than our simple implementation.

Also not considered in our model are the prominent theta and gamma oscillations in the hippocampus believed to be important for spatial processing (Mehta et al., 2002; O'Keefe & Recce, 1993; Skaggs et al., 1996). Oscillations are likely to be important for the encoding of place and context information, as well as for the synaptic plasticity that may underlie the dynamic nature of their hippocampal representation.

CA1 pyramidal neuron dendrites are innervated by several types of interneurons, which are not included in our model. As inhibition is likely to profoundly influence the integration of excitatory inputs from ECIII and CA3 as well as hippocampal oscillations, biophysically realistic models of hippocampal networks should certainly include such interneurons.

In our model, we assumed that learning has already taken place to establish the network wiring. Other models have addressed the process of encoding associations between sequentially active place cells (Jensen et al., 1996; Jensen & Lisman, 1998; Koene et al., 2003). Incorporation of these mechanisms could be used to study the mechanisms by which the connectivity we used in our model (e.g. forward association and cross wiring) could be established.

Another simplification of our model is that primary place and temporal context information are represented separately in ECIII or CA3. In reality, however, there is evidence for representations of space in both CA3 (O'Keefe & Dostrovsky, 1971; O'Keefe & Nadel, 1978; Wilson & McNaughton, 1993)) and in EC (Brun et al., 2002; Hafting et al., 2005; Hargreaves et al., 2005). In addition, transverse lesions to the dorsal CA3 region of rat hippocampus revealed impairments in spatial memory retention in the Morris water-maze task (Steffenach et al., 2005), and selective CA3 lesions impair detection of novel spatial arrangements of objects (Lee et al., 2005). Both of these studies suggest that CA3 can also encode different types of context during specific behavioral tasks. A more sophisticated model would therefore utilize hybrid place-context neurons in CA3 and possibly in ECIII as well.

These limitations represent opportunities for improvements and enhancements of our model. In addition, they highlight the need for the merger of cellular and systems-level studies of the hippocampus before a complete picture will emerge regarding the dynamic and complex representation of information in the hippocampus.

5.6. Materials and Methods

The ECIII and CA3 node types use the equations due to Izhikevich for a quadratic integrate and fire neuron with adaptive recovery and the rule that after a spike, the voltage, v, is reset to the parameter c and the recovery variable, u, is incremented by the parameter d (Izhikevich, 2003).

$$\frac{dv}{dt} = 0.04v^2 + 5v + 140 - u + \frac{I}{CA}$$
$$\frac{du}{dt} = a(bv - u)$$
$$\text{if } (v \geq 30mV)\,, v \rightarrow c \text{ and } u \rightarrow u + d$$

The model requires two other parameters: a, which represents the inverse time scale of u, and b, which represents the sensitivity of u to subthreshold changes in v. In all simulations, the parameters take the values $a = 0.02\ ms^{-1}$, $b = 0.2$, $c = -65\ mV$, and $d = 4\ mV$, which result in regular spiking behavior. When a node is designated as a temporal context cell, however, the parameters are $a = 1\ ms^{-1}$, $b = 0.2$, $c = -60\ mV$, and $d = -20\ mV$, which produce a more prominent after-depolarization and increased excitability. All ECIII and CA3 cells are assumed to have an area of 1000 μm^2 and a capacitance of 1 μF/cm^2.

The CA1 node types use Hodgkin-Huxley style equations for sodium channels, delayed rectifier potassium channels, and A-type potassium channels.

$$\begin{aligned} C\frac{dv}{dt} = &- g_{Na}m(v)^3h(v)(v - E_{Na}) - g_{K_{dr}}n(v)^4(v - E_K) \\ &- g_{K_A}k(v)l(v)(v - E_K) - g_L(v - E_L) + \frac{I}{A} \end{aligned}$$

$$\begin{aligned} \frac{dm}{dt} &= \frac{m_\infty(v) - m}{\tau_m}; & \frac{dh}{dt} &= \frac{h_\infty(v) - h}{\tau_h} \\ \frac{dn}{dt} &= \frac{n_\infty(v) - n}{\tau_n}; & \frac{dk}{dt} &= \frac{k_\infty(v) - k}{\tau_k} \\ \frac{dl}{dt} &= \frac{l_\infty(v) - l}{\tau_l} \end{aligned}$$

The model parameters are as in (Migliore et al., 1999) and (Golding et al., 2001) and are listed in Tables 5.1 and 5.2.

The current, I, on the right hand side of the above equations, has three components:

$$I = I_{coupling} + I_{synaptic} + I_{external}$$

At every time step in the simulations, the voltage of every node is checked and the currents are calculated and added to the derivative.

The four nodes comprising each CA1 neuron are connected electrically. The coupling current is calculated from the voltage difference between two nodes and a coupling conductance (Table 5.3 using Ohm's law:

$$I_{coupling} = g_{coupling}\ (v_{node1} - v_{node2})$$

Nodes can also be connected with synapses. When the voltage of a node exceeds a threshold of -30 mV, it is said to have generated an event, an action potential, at time t_{event}. This creates a synaptic current that is added to the derivative of voltage:

$I_{synaptic} = weight * te^{-t/\tau}$

where t is measured from the time of the event. Synapses are modeled as alpha functions and have a time constant of 5-20 ms (Table 5.4. For computational efficiency, events that happen more than 50 ms in the past are not considered. Since the alpha function approaches zero at large t, the resulting synaptic current would be negligible. The selection of synaptic weights is discussed in the main text and they are listed in Table 5.4.

At various points in the simulation, cells receive external current inputs. These inputs are 2 ms current pulses ranging between 100 and 200 pA.

$$I_{external} = I_0 \ for \ 2 \ ms$$

Numerical integration of equations 1 and 2 is performed using the 4th order Runge-Kutta algorithm with a time step of.001 milliseconds.

All code was written in C and run on a Mac PowerPC with OS 10.4.

5.7. Parameter Tables

Sodium channel parameters — $E_{NA} = 55$ mV

Activation	Inactivation	Parameters
$m_\infty(v) = \frac{a_m}{a_m + b_m}$	$h_\infty(v) = \frac{1}{1 + e^{v - th_\infty / q_\infty}}$	th_a -30 mV
		q_a 7.2 mV
		R_a 0.4 (mVms)$^{-1}$
$\tau_m(v) = \frac{1}{(a_m + b_m)/qt}$	$\tau_h(v) = \frac{1}{(a_h + b_h)/qt}$	R_b 0.124 (mVms)$^{-1}$
		th_i -45 mV
		q_d 1.5 mV
$a_m = \frac{R_a(v - th_a)}{1 - e^{-(v - th_a)/q_a}}$	$a_h = \frac{R_d(v - th_i)}{1 - e^{-(v - th_i)/q_d}}$	q_g 1.5 mV
		R_g 0.01 (mVms)$^{-1}$
		R_d .03 (mVms)$^{-1}$
$b_m = \frac{R_b(v - th_a)}{e^{(v - th_a)/q_a} - 1}$	$b_h = \frac{R_g(v - th_i)}{e^{(v - th_i)/q_g} - 1}$	th_∞ -50 mV
		q_∞ 4 mV
$\tau_m \geq \tau_{m\min}$	$\tau_h \geq \tau_{h\min}$	$\tau_{m\min}$ 0.02 ms
		$\tau_{h\min}$ 0.5 ms
		qt = 2.1435

Delayed rectifier potassium channel parameters — $E_K = -72$ mV

Activation	parameters
$n_\infty(v) = \frac{1}{1 + a_n}$	ζ_n -3
	$vhalf_n$ 13 mV
	gm_n 0.7
$\tau_n(v) = \frac{b_n}{qt\, a_{0n}(1 - a_n)}$	a_{0n} 0.02 (ms)$^{-1}$
	$\tau_{n\min}$ 1 ms
	qt = 5.873
$a_n = e^{\frac{\zeta_n (v - vhalf_n).001*9.648*10000}{8.315(273.16 + celsius)}}$	
$b_n = e^{\frac{\zeta_n gm_n (v - vhalf_n).001*9.648*10000}{8.315(273.16 + celsius)}}$	
$\tau_n \geq \tau_{n\min}$	

A-type potassium channel parameters — $E_K = -72$ mV

Activation	Inactivation	parameters
$k_\infty(v) = \frac{1}{1 + a_k}$	$l_\infty(v) = \frac{1}{1 + a_l}$	qt = 5.873;
		ζ_k -1.8
		pw -1
$\tau_k(v) = \frac{b_k}{qt a_{0k}(1 + a_k)}$	$\tau_l(v) = \frac{0.26(v + 50.13)}{qt_l}$	tq -40 mV
		qq 5 mV
		$vhalf_k$ -1 mV
$\zeta = \zeta_k + \frac{pw}{(1 + e^{(v - tq)/qq})}$	$a_l = e^{\frac{\zeta_l (v - vhalf_l).001*9.648*10000}{8.315(273.16 + celsius)}}$	gm_k 0.39
		a_{0k} .1 (ms)$^{-1}$
		ζ_l 3
$a_k = e^{\frac{\zeta (v - vhalf_k).001*9.648*10000}{8.315(273.16 + celsius)}}$	$b_l = e^{\frac{\zeta_l + gm_l (v - vhalf_l).001*9.648*10000}{8.315(273.16 + celsius)}}$	$vhalf_l$ -56 mV
		gm_l 1
$b_k = e^{\frac{\zeta + gm_k (v - vhalf_a).001*9.648*10000}{8.315(273.16 + celsius)}}$	$\tau_l \geq \frac{\tau_{l\min}}{qt_l}$	a_{0l} 0.05 (ms)$^{-1}$
		qt_l 1
$\tau_k \geq \tau_{k\min}$		$\tau_{k\min}$ 0.1 ms
		$\tau_{l\min}$ 2 ms

Parameters of leak conductance — $E_{leak} = -65$ mV; $g_{leak} = .3$

Table 5.1. Parameters of CA1 Pyramidal Cell Models

Node	$\overline{g}_{Na}$ (S/cm^2)	$\overline{g}_{K(DR)}$ (S/cm^2)	$\overline{g}_{K(A)}$ (S/cm^2)	area (um^2)
tuft	.025	.050	.070	2000
prox. dend.	.025	.050	.050	4000
soma	.025	.050	.050	1000
basal dend.	.025	.050	.050	2500

Capacitance is 1 μF/cm^2 in every node.

Table 5.2. Further parameters of CA1 Pyramidal Cell Models

Node 1	node 2	$g_{coupling}$ (nS)
tuft	prox. dend	3.5
prox. dend	soma	12.5
soma	basal dend	12.5

Table 5.3. Parameters for Electrical Coupling between CA1 Nodes

Node 1	node 2	τ_{syn} (ms)	delay (ms)	weight (nA/ms)
For temporal context in ECIII				
ECIII	ECIII net	1.0	2	20
ECIII net	ECIII	0.01	2	20
CA3	CA3	3.6	2	5
ECIII	CA1	0.2	0	5
CA3	CA1	3.4	0	5
For temporal context in CA3				
ECIII	ECIII	3.6	2	5
CA3	CA3 net	1.0	2	20
CA3 net	CA3	0.01	2	20
ECIII	CA1	12.0	0	5
CA3	CA1	0.28	0	5

Table 5.4. Parameters of Synapse Model

CHAPTER 6

Conclusion

6.1. Dendrites: costs and benefits

Much of this work has focused on the challenges that dendrites pose to information processing in pyramidal neurons. First, their high axial resistivity and leaky membranes imposes strong filtering on postsynaptic potentials, creating a distance-dependence to the weighting of inputs and making it difficult for distal inputs to influence neuronal output (Golding et al., 2005; Rall, 1967). Second, the geometry of dendritic branching results in differences in input resistance along individual oblique branches, making it more than ten times easier to generate a dendritic spike near the terminal ends of dendrites than near branch points (Katz et al., chapter 3; (Rall, 1964). In order to compensate for these effects, synaptic conductance is scaled with distance along the dendritic tree in two dimensions. Synaptic conductance increases along the somato-dendritic axis, but only up to a point, decreasing in the most distal region of the cell (Magee & Cook, 2000; Nicholson et al., 2006). Synaptic conductance also decreases from branch point to terminal end along individual apical oblique branches (Katz et al., chapter 3). Given the putative biological cost of maintaining such nontrivial synaptic distributions, one might wonder why pyramidal neurons have dendrites in the first place. Would they not be much more efficient input-output devices if they were electrotonically compact, like many interneurons or like transistors in man-made circuits?

One answer that has been proposed is that a branching dendritic architecture is required by the stipulation that the cortex and hippocampus must be highly interconnected (Chklovskii, 2004). In order to implement a network as interconnected as the cortex in the volume it takes up, neurons must have branching dendrites, branching axons, and dendritic spines. Supporting this hypothesis is the observation that the lengths of dendrites

and axons in the cortex are the shortest possible, given the required interconnectivity (Chklovskii, 2004). It is possible that the cost of creating and maintaining a complex distribution of synaptic strengths is less than the cost of increasing cortical volume. Still, there are many possible dendritic configurations: why might pyramidal neurons have their unique architectures?

Another idea is that pyramidal neuron dendrites serve to compartmentalize the cell, allowing for multiple levels of information processing (Polsky et al., 2004). Each dendritic branch can act as an independent computational subunit, summing up the contributions of the inputs it receives. The output of each dendritic branch then propagates to the axon where a global summation takes place. In a compartmental model of a CA1 pyramidal neuron, it was shown that the neuron's firing rate in response to arbitrary distributed inputs could be predicted by a mapping of the neuronal morphology onto those of such a two-layer neural network (Polsky et al., 2004). Our finding that synapses are distributed to normalize the contribution of inputs to dendritic spikes lends support to this idea (Katz et al., chapter 3). Thus, the cost of maintaining a non-trivial distribution of synaptic weights may be outweighed by the benefit of increased computing power. It would be interesting to determine whether a neuron with dendrites has computational advantages over a two-layer network of equipotential elements.

6.2. Dendritic democracy?

One view is that synapses are scaled to normalize their contributions to neuronal output (Hausser, 2001; Magee & Cook, 2000). Our work suggests that instead synapses are scaled to normalize the contribution of inputs to the local output of their parent branch,

rather than to the global output of the cell (Katz et al., chapter 3). A consequence of this is that the impact of each branch at the soma is predicted to depend on branch location. In CA1 pyramidal neurons, the more distal apical dendrites contain stronger synapses than their more proximal counterparts, which may boost the representation of distal branches at the soma. However, synapses in the CA1 apical tuft are not conductance-scaled, nor are synapses anywhere in the apical dendritic trees of neocortical pyramidal neurons (Nicholson et al., 2006; Williams & Stuart, 2002).

Since pyramidal neurons receive layer-specific inputs, it may be that it is advantageous for information entering the apical tufts of pyramidal neurons not to trigger axonal firing on its own, whereas more proximal inputs may be more crucial to the neuron. Differences in synapse ultrastructure between the tuft and elsewhere on the apical tree support the idea that inputs are integrated differently in those two regions (Megias et al., 2001). In CA1 pyramidal neurons, the propagation of distally generated dendritic spikes can be facilitated by subthreshold inputs entering more proximally (Jarsky et al., 2005). Such coincidence detection may be a general mechanism by which distal inputs communicate with the soma in all pyramidal neurons, or it may be unique to CA1 cells.

Alternatively, other mechanisms may exist that enhance the representation of distal branches at the soma. In CA1 pyramidal neurons an increasing gradient of A-type potassium channels along the somato-dendritic axis of CA1 pyramidal neurons may serve this function (Hoffman et al., 1997), although these channels are expressed uniformly in neocortical pyramidal neurons (Bekkers, 2000). Distal inputs may also trigger calcium spikes, which are broader and slower than sodium spikes and hence propagate more effectively.

So far we have focused on apical dendrites, but pyramidal neurons also have basal dendrites, which are typically shorter than apical branches and have shorter electrotonic lengths (Ramon y Cajal, 1897). They also contact the soma directly instead of via a main apical dendrite and the integrative properties of basal dendrites may differ from apical ones. Thus the degree to which there is "dendritic democracy" (Hausser, 2001) at all dendritic locations in pyramidal neurons is unknown.

6.3. Perforated vs. nonperforated synapses: implications for synaptic plasticity

In chapter 5, we made connection between biophysical properties of CA1 pyramidal neurons and hippocampus-dependent learning and memory (Katz et al., 2007). In a model of the hippocampal network, we showed that the conditional propagation of dendritic spikes in CA1 neurons representing the stem of a T maze can make them "splitter cells", neurons which fire selectively based on a combination of place and temporal context. The information stored by splitter cells could be used by a virtual animal to choose correct paths through the maze in a simulated spatial alternation task. In our electron-microscopy studies of synaptic integration in CA1 pyramidal neurons in chapters 2 and 3, we uncovered an organization to the way synapses are distribution in the apical dendritic tree (Nicholson et al., 2006), Katz et al., chapter 3). An interesting direction would be to investigate how this synaptic organization might contribute to performance of hippocampus-dependent tasks. Furthermore, since both spines and synapses are dynamic structures, it would be interesting to investigate how spine and synapse changes

following learning interact with the baseline synaptic organization that we found in CA1 apical oblique dendrites.

Two approaches have been used thus far to investigate structural correlates of learning, each with distinct pros and cons (Nicholson & Geinisman, 2006). Electron microscopy has the ability to resolve synapses, however it is limited in that it can only provide snapshopts of synapses at a single time point after learning. Two-photon laser scanning microcopy together with molecular probes can produce time-lapse images of dendritic spines in slices and in vivo, however this technique is limited by the wavelength of light, which is too large to resolve synapses.

Two photon laser scanning microscopy has shown that both spines and synapses are dynamic structures, emerging and retracting from the parent dendrite or changing shape and size. Furthermore, subpopulations of spines remain stable over periods of months, suggesting that they may be loci of long-term memory storage (Grutzendler et al., 2002; Holtmaat et al., 2006, 2005). Electron microscopy studies have shown that the number of multiple synapse boutons (MSBs) and PSD areas increase after certain behavioral tasks (Geinisman et al., 2001, 2000) (An MSB is a presynaptic contact with two or more discrete postsynaptic elements). For example, rabbits that underwent trace eyeblink conditioning did not show a change in total synapse number in CA1 stratum radiatum. However, conditioned rabbits had 18% more MSBs relative to controls and showed an enlargement in nonperforated PSD area (Geinisman et al., 2001, 2000). Together, these approaches can be used to develop a mechanistic understanding of spine and synapse remodeling following learning (Nicholson & Geinisman, 2006). For example, in vivo studies using

light microscopy can be conducted and electron microscopy can be done only when new spines are shown to have formed.

The ultimate experiment would be to compare spine and synapse distributions obtained at different time points following learning to the ones that we characterized in naive animals (Nicholson et al., 2006), Katz et al., chapter 3). Quantitative modeling could assist in determining the functional consequences of synaptogenesis, restructuring of synaptic connectivity by addition of MSBs, and changes in synaptic strength.

6.4. Outlook

The studies conducted here focused on CA1 pyramidal neurons, but the same issues confront all neurons with extended branched morphologies. Pyramidal neurons in different species and brain structures differ significantly in their branching patterns and numbers of spines and synapses as well as with respect to ion channel expression and synaptic organization (Ramon y Cajal, 1897; Spruston, 2008). More experiments are needed to determine whether and how neurons with different structures and properties function differently. The results of such experiments can constrain more sophisticated models that are crucial to developing a more complete theory of pyramidal neuron computation. Once we have a better understanding of how individual pyramidal neurons process information, how networks of these neurons work together to give rise to higher cognitive functions can be explored.

References

Abbott, L. F. & Blum, K. I. (7788). Functional significance of long-term potentiation for sequence learning and prediction. Cereb Cortex, 6, 406–16.

Acker, C. D. & White, J. A. (2007). Roles of ia and morphology in action potential propagation in CA1 pyramidal cell dendrites. J Comput Neurosci, 23, 201–16. 0929-5313 (Print) Journal Article.

Ainge, J. A., van der Meer, M. A., Langston, R. F., & Wood, E. R. (2007). Exploring the role of context-dependent hippocampal activity in spatial alternation behavior. Hippocampus, 17. 1050-9631 (Print) Journal article.

Amaral, D. G. & Witter, M. P. (1989). The three-dimensional organization of the hippocampal formation: a review of anatomical data. Neuroscience, 31, 571–91. 0306-4522 (Print) Journal Article Review.

Amaral, D. G. & Witter, M. P. (1995). The hippocampal formation. In The Rat Nervous System, G. Paxinos, ed. (Academic Press, New York).

Andrasfalvy, B. K. & Magee, J. C. (2001). Distance-dependent increase in ampa receptor number in the dendrites of adult hippocampal ca1 pyramidal neurons. J Neurosci, 21, 9151–9159.

Andrasfalvy, B. K. & Mody, I. (2006). Differences between the scaling of miniature ipscs and epscs recorded in the dendrites of CA1 mouse pyramidal neurons. J Physiol, 576, 191–6. 0022-3751 (Print) Comparative Study Journal Article.

Bailey, C. H. & Kandel, E. R. (1993). Structural changes accompanying memory storage. Annu Rev Physiol, 55, 397–426.

Bannister, N. J. & Larkman, A. U. (1995). Dendritic morphology of CA1 pyramidal neurones from the rat hippocampus: I. branching patterns. J Comp Neurol, 360, 150–60. 0021-9967 (Print) In Vitro Journal Article Research Support, Non-U.S. Gov't.

Bekkers, J. M. (2000). Distribution and activation of voltage-gated potassium channels in cell-attached and outside-out patches from large layer 5 cortical pyramidal neurons of the rat. J Physiol, 525 Pt 3, 611–20. 0022-3751 (Print) In Vitro Journal Article Research Support, Non-U.S. Gov't.

Berger, T., Larkum, M. E., & Luscher, H. R. (2001). High i(h) channel density in the distal apical dendrite of layer v pyramidal cells increases bidirectional attenuation of epsps. J Neurophysiol, 85, 855–68. 0022-3077 (Print) In Vitro Journal Article Research Support, Non-U.S. Gov't.

Bi, G. Q. & Poo, M. M. (1998). Synaptic modifications in cultured hippocampal neurons: dependence on spike timing, synaptic strength, and postsynaptic cell type. J Neurosci, 18, 10464–72. 0270-6474 (Print) In Vitro Journal Article Research Support, Non-U.S. Gov't Research Support, U.S. Gov't, P.H.S.

Bliss, T. V. & Lomo, T. (1973). Long-lasting potentiation of synaptic transmission in the dentate area of the anaesthetized rabbit following stimulation of the perforant path. J Physiol, 232, 331–56. 0022-3751 (Print) Journal Article.

Borisyuk, A. & Rinzel, J. (2003). Understanding neuronal dynamics by geometrical dissection of minimal models. Methods and Models in Neurophysics, Volume Session LXXX: Lecture Notes of the Les Houches Summer School 2003. (Amsterdam: Elsevier).

Bourne, J. & Harris, K. M. (2007). Do thin spines learn to be mushroom spines that remember? Curr Opin Neurobiol, 17, 381–6. 0959-4388 (Print) Journal Article Research Support, N.I.H., Extramural Review.

Bower, M. R., Euston, D. R., & McNaughton, B. L. (2005). Sequential-context-dependent hippocampal activity is not necessary to learn sequences with repeated elements. J Neurosci, 25, 1313–23. 1529-2401 (Electronic) Journal Article.

Brown, B. S. & Yu, S. P. (2000). Modulation and genetic identification of the m channel. Prog Biophys Mol Biol, 73, 135–66. 0079-6107 (Print) Journal Article Review.

Brun, V. H., Otnass, M. K., Molden, S., Steffenach, H. A., Witter, M. P., Moser, M. B., & Moser, E. I. (2002). Place cells and place recognition maintained by direct entorhinal-hippocampal circuitry. Science, 296, 2243–6. 1095-9203 (Electronic) Journal Article.

Buzsaki, G., Horvath, Z., Urioste, R., Hetke, J., & Wise, K. (1992). High-frequency network oscillation in the hippocampus. Science, 256, 1025–7. 0036-8075 (Print) Journal Article Research Support, Non-U.S. Gov't Research Support, U.S. Gov't, P.H.S.

Cai, X., Liang, C. W., Muralidharan, S., Muralidharan, S., Kao, J. P. Y., Tang, C.-M., & Thompson, S. M. (2004). Unique roles of sk and kv4.2 potassium channels in dendritic integration. Neuron, 44, 351–364.

Carlin, R. K., Grab, D. J., Cohen, R. S., & Siekevitz, P. (1980). Isolation and characterization of postsynaptic densities from various brain regions: enrichment of different types of postsynaptic densities. J Cell Biol, 86, 831–845.

Chklovskii, D. B. (2004). Synaptic connectivity and neuronal morphology: two sides of the same coin. Neuron, 43, 609–17. 0896-6273 (Print) Journal Article Research Support, Non-U.S. Gov't Research Support, U.S. Gov't, P.H.S.

Christie, J. M. & Jahr, C. E. (2006). Multivesicular release at schaffer collateral-ca1 hippocampal synapses. J Neurosci, 26, 210–216.

Cline, H. & Haas, K. (2008). The regulation of dendritic arbor development and plasticity by glutamatergic synaptic input: a review of the synaptotrophic hypothesis. J Physiol, 586, 1509–17. 1469-7793 (Electronic) Journal Article Research Support, N.I.H., Extramural Research Support, Non-U.S. Gov't.

Coetzee, W. A., Amarillo, Y., Chiu, J., Chow, A., Lau, D., McCormack, T., Moreno, H., Nadal, M. S., Ozaita, A., Pountney, D., Saganich, M., Vega-Saenz de Miera, E., & Rudy, B. (1999). Molecular diversity of k+ channels. Ann N Y Acad Sci, 868, 233–85. 0077-8923 (Print) Journal Article Review.

Cohen, N. J. & Squire, L. R. (1980). Preserved learning and retention of pattern-analyzing skill in amnesia: dissociation of knowing how and knowing that. Science, 210, 207–10. 0036-8075 (Print) Journal Article Research Support, Non-U.S. Gov't Research Support, U.S. Gov't, P.H.S.

Colbert, C. M., Magee, J. C., Hoffman, D. A., & Johnston, D. (1997). Slow recovery from inactivation of na+ channels underlies the activity-dependent attenuation of dendritic action potentials in hippocampal ca1 pyramidal neurons. J Neurosci, 17, 6512–6521.

Connor, J. A. & Stevens, C. F. (1971). Voltage clamp studies of a transient outward membrane current in gastropod neural somata. J Physiol, 213, 21–30. 0022-3751 (Print) Journal Article.

Conti, R. & Lisman, J. (2003). The high variance of ampa receptor- and nmda receptor-mediated responses at single hippocampal synapses: evidence for multiquantal release. Proc Natl Acad Sci U S A, 100, 4885–4890.

Corkin, S. (1968). Acquisition of motor skill after bilateral medial temporal-lobe excision. Neuropsychologia, 6, 225264.

Corkin, S. (2002). What's new with the amnesic patient h.m.? Nat Rev Neurosci, 3, 153–60. 1471-003X (Print) Journal Article Review.

Crill, W. E. (1996). Persistent sodium current in mammalian central neurons. Annu Rev Physiol, 58, 349–62. 0066-4278 (Print) Journal Article Review.

DeFelipe, J. & Farinas, I. (1992). The pyramidal neuron of the cerebral cortex: morphological and chemical characteristics of the synaptic inputs. Prog Neurobiol, 39, 563–607. 0301-0082 (Print) Journal Article Research Support, Non-U.S. Gov't Review.

Desmond, N. L. & Weinberg, R. J. (1998). Enhanced expression of ampa receptor protein at perforated axospinous synapses. Neuroreport, 9, 857–860.

Doboli, S. & Minai, A. A. (2003). Network capacity analysis for latent attractor computation. Network, 14, 273–302. 0954-898X (Print) Journal Article Research Support, U.S. Gov't, Non-P.H.S.

Doboli, S. & Minai, A. A. (2007). Latent Attractors: A general paradigm for context-dependent neural computation. Trends in Neural Computation. (Springer Verlag).

Doboli, S., Minai, A. A., & Best, P. J. (2000). Latent attractors: a model for context-dependent place representations in the hippocampus. Neural Comput, 12, 1009–43. 0899-7667 (Print) Journal Article Research Support, U.S. Gov't, Non-P.H.S.

Dudek, F. E. & Staley, K. J. (2007). How does the balance of excitation and inhibition shift during epileptogenesis? Epilepsy Curr, 7, 86–8. 1535-7597 (Print) Journal Article.

Egorov, A. V., Hamam, B. N., Fransen, E., Hasselmo, M. E., & Alonso, A. A. (2002). Graded persistent activity in entorhinal cortex neurons. Nature, 420, 173–8. 0028-0836

(Print) Journal Article.

Ehlers, M. D. (2002). Molecular morphogens for dendritic spines. Trends Neurosci, 25, 64–67.

Eichenbaum, H. (2000). A cortical-hippocampal system for declarative memory. Nat Rev Neurosci, 1, 41–50. 1471-003X (Print) Journal Article Research Support, U.S. Gov't, P.H.S. Review.

Eichenbaum, H. & Cohen, N. J. (2001). From conditioning to conscious recollection: Memory systems of the brain. (New York: Oxford University Press).

Farrant, M. & Nusser, Z. (2005). Variations on an inhibitory theme: phasic and tonic activation of gaba(a) receptors. Nat Rev Neurosci, 6, 215–29. 1471-003X (Print) Journal Article Research Support, Non-U.S. Gov't Review.

Ferbinteanu, J. & Shapiro, M. L. (2003). Prospective and retrospective memory coding in the hippocampus. Neuron, 40, 1227–39. 0896-6273 (Print) Journal Article.

Fiala, J. C. (2005). Reconstruct: a free editor for serial section microscopy. J Microsc, 218, 52–61. 0022-2720 (Print) Journal Article Research Support, U.S. Gov't, Non-P.H.S. Research Support, U.S. Gov't, P.H.S.

Fiala, J. C., Feinberg, M., Popov, V., & Harris, K. M. (1998). Synaptogenesis via dendritic filopodia in developing hippocampal area ca1. J Neurosci, 18, 8900–11. 0270-6474 (Print) Journal Article Research Support, U.S. Gov't, Non-P.H.S. Research Support, U.S. Gov't, P.H.S.

FitzHugh, R. (1961). Impulses and physiological states in theoretical models of nerve membrane. Biophys J, 1, 445–466.

Frank, L. M., Brown, E. N., & Wilson, M. (2000). Trajectory encoding in the hippocampus and entorhinal cortex. Neuron, 27, 169–78. 0896-6273 (Print) Journal Article.

Frick, A., Magee, J., Koester, H. J., Migliore, M., & Johnston, D. (2003). Normalization of ca2+ signals by small oblique dendrites of CA1 pyramidal neurons. J Neurosci, 23, 3243–50. 1529-2401 (Electronic) In Vitro Journal Article Research Support, Non-U.S. Gov't Research Support, U.S. Gov't, P.H.S.

Ganeshina, O., Berry, R. W., Petralia, R. S., Nicholson, D. A., & Geinisman, Y. (2004a). Differences in the expression of ampa and nmda receptors between axospinous perforated and nonperforated synapses are related to the configuration and size of postsynaptic densities. J Comp Neurol, 468, 86–95. 0021-9967 (Print) Journal Article Research Support, U.S. Gov't, P.H.S.

Ganeshina, O., Berry, R. W., Petralia, R. S., Nicholson, D. A., & Geinisman, Y. (2004b). Synapses with a segmented, completely partitioned postsynaptic density express more ampa receptors than other axospinous synaptic junctions. Neuroscience, 125, 615–23. 0306-4522 (Print) Journal Article Research Support, U.S. Gov't, P.H.S.

Ganguly, K., Schinder, A. F., Wong, S. T., & Poo, M. (2001). Gaba itself promotes the developmental switch of neuronal gabaergic responses from excitation to inhibition. Cell, 105, 521–32. 0092-8674 (Print) Journal Article Research Support, U.S. Gov't, P.H.S.

Gasparini, S., Losonczy, A., Chen, X., Johnston, D., & Magee, J. C. (2007). Associative pairing enhances action potential back-propagation in radial oblique branches of ca1 pyramidal neurons. J Physiol, 580, 787–800. 0022-3751 (Print) In Vitro Journal Article Research Support, N.I.H., Extramural.

Gasparini, S. & Magee, J. C. (2006). State-dependent dendritic computation in hippocampal CA1 pyramidal neurons. J Neurosci, 26, 2088–100. 1529-2401 (Electronic) In Vitro Journal Article Research Support, N.I.H., Extramural Research Support, Non-U.S. Gov't.

Gasparini, S., Migliore, M., & Magee, J. C. (2004). On the initiation and propagation of dendritic spikes in ca1 pyramidal neurons. J Neurosci, 24, 11046–56. 1529-2401 (Electronic) In Vitro Journal Article Research Support, N.I.H., Extramural Research Support, Non-U.S. Gov't Research Support, U.S. Gov't, Non-P.H.S. Research Support, U.S. Gov't, P.H.S.

Geinisman, Y. (1993). Perforated axospinous synapses with multiple, completely partitioned transmission zones: probable structural intermediates in synaptic plasticity. Hippocampus, 3, 417–33. 1050-9631 (Print) Journal Article Research Support, U.S. Gov't, Non-P.H.S. Research Support, U.S. Gov't, P.H.S.

Geinisman, Y. (2000). Structural synaptic modifications associated with hippocampal ltp and behavioral learning. Cereb Cortex, 10, 952–62. 1047-3211 (Print) Journal Article Research Support, U.S. Gov't, P.H.S. Review.

Geinisman, Y., Berry, R. W., Disterhoft, J. F., Power, J. M., & der Zee, E. A. V. (2001). Associative learning elicits the formation of multiple-synapse boutons. J Neurosci, 21, 5568–5573.

Geinisman, Y., Disterhoft, J. F., Gundersen, H. J., McEchron, M. D., Persina, I. S., Power, J. M., van der Zee, E. A., & West, M. J. (2000). Remodeling of hippocampal synapses after hippocampus-dependent associative learning. J Comp Neurol, 417, 49–59.

Geinisman, Y., Ganeshina, O., Yoshida, R., Berry, R. W., Disterhoft, J. F., & Gallagher, M. (2004). Aging, spatial learning, and total synapse number in the rat CA1 stratum radiatum. Neurobiol Aging, 25, 407–16. 0197-4580 (Print) Journal Article Research Support, U.S. Gov't, P.H.S.

Golding, N. L., Jung, H. Y., Mickus, T., & Spruston, N. (1999). Dendritic calcium spike initiation and repolarization are controlled by distinct potassium channel subtypes in CA1 pyramidal neurons. J Neurosci, 19, 8789–98. 1529-2401 (Electronic) Journal Article Research Support, Non-U.S. Gov't Research Support, U.S. Gov't, P.H.S.

Golding, N. L., Kath, W. L., & Spruston, N. (2001). Dichotomy of action-potential backpropagation in CA1 pyramidal neuron dendrites. J Neurophysiol, 86, 2998–3010. 0022-3077 (Print) Journal Article.

Golding, N. L., Mickus, T. J., Katz, Y., Kath, W. L., & Spruston, N. (2005). Factors mediating powerful voltage attenuation along ca1 pyramidal neuron dendrites. J Physiol, 568, 69–82. 0022-3751 (Print) In Vitro Journal Article Research Support, N.I.H., Extramural Research Support, U.S. Gov't, Non-P.H.S. Research Support, U.S. Gov't, P.H.S.

Golding, N. L. & Spruston, N. (1998). Dendritic sodium spikes are variable triggers of axonal action potentials in hippocampal ca1 pyramidal neurons. Neuron, 21, 1189–200. 0896-6273 (Print) In Vitro Journal Article Research Support, Non-U.S. Gov't Research Support, U.S. Gov't, P.H.S.

Golding, N. L., Staff, N. P., & Spruston, N. (2002). Dendritic spikes as a mechanism for cooperative long-term potentiation. Nature, 418, 326–31. 0028-0836 (Print) Journal Article Research Support, Non-U.S. Gov't.

Gorchetchnikov, A. & Hasselmo, M. (2005). A biophysical implementation of a bidirectional graph search algorithm to solve multiple goal navigation tasks. Connection Science, 17, 145–164.

Greenough, W. T. & H., B. C. (1988). Anatomy of a memory: convergence of results across a diversity of tests. Trends Neurosci., 11, 142–147.

Grutzendler, J., Kasthuri, N., & Gan, W. B. (2002). Long-term dendritic spine stability in the adult cortex. Nature, 420, 812–6. 0028-0836 (Print) Journal Article Research Support, Non-U.S. Gov't Research Support, U.S. Gov't, P.H.S.

Hafting, T., Fyhn, M., Molden, S., Moser, M. B., & Moser, E. I. (2005). Microstructure of a spatial map in the entorhinal cortex. Nature, 436, 801–6. 1476-4687 (Electronic) Journal Article.

Hargreaves, E. L., Rao, G., Lee, I., & Knierim, J. J. (2005). Major dissociation between medial and lateral entorhinal input to dorsal hippocampus. Science, 308, 1792–4. 1095-9203 (Electronic) Journal Article.

Harris, K. M., Jensen, F. E., & Tsao, B. (1992). Three-dimensional structure of dendritic spines and synapses in rat hippocampus (ca1) at postnatal day 15 and adult ages: implications for the maturation of synaptic physiology and long-term potentiation. J Neurosci, 12, 2685–705. 0270-6474 (Print) Journal Article Research Support, Non-U.S. Gov't Research Support, U.S. Gov't, P.H.S.

Harris, K. M. & Kater, S. B. (1994). Dendritic spines: cellular specializations imparting both stability and flexibility to synaptic function. Annu Rev Neurosci, 17, 341–71. 0147-006X (Print) Journal Article Research Support, Non-U.S. Gov't Research Support, U.S. Gov't, P.H.S. Review.

Harris, K. M. & Stevens, J. K. (1989). Dendritic spines of ca 1 pyramidal cells in the rat hippocampus: serial electron microscopy with reference to their biophysical characteristics. J Neurosci, 9, 2982–97. 0270-6474 (Print) Comparative Study Journal Article Research Support, Non-U.S. Gov't Research Support, U.S. Gov't, P.H.S.

Harris, K. M. & Sultan, P. (1995). Variation in the number, location and size of synaptic vesicles provides an anatomical basis for the nonuniform probability of release at hippocampal ca1 synapses. Neuropharmacology, 34, 1387–1395.

Hasselmo, M. E. & Eichenbaum, H. (2005). Hippocampal mechanisms for the context-dependent retrieval of episodes. Neural Netw, 18, 1172–90. 0893-6080 (Print) Journal Article.

Hasselmo, M. E. & Schnell, E. (1994). Laminar selectivity of the cholinergic suppression of synaptic transmission in rat hippocampal region CA1: computational modeling and brain slice physiology. J Neurosci, 14, 3898–914. 0270-6474 (Print) Journal Article Research Support, Non-U.S. Gov't Research Support, U.S. Gov't, Non-P.H.S.

Hasselmo, M. E. & Wyble, B. P. (1997). Free recall and recognition in a network model of the hippocampus: simulating effects of scopolamine on human memory function. Behav Brain Res, 89, 1–34. 0166-4328 (Print) Journal Article Research Support, Non-U.S. Gov't Research Support, U.S. Gov't, Non-P.H.S. Research Support, U.S. Gov't, P.H.S. Review.

Hausser, M. (2001). Synaptic function: dendritic democracy. Curr Biol, 11, R10–2. 0960-9822 (Print) Journal Article Review.

Hausser, M., Spruston, N., & Stuart, G. J. (2000). Diversity and dynamics of dendritic signaling. Science, 290, 739–44. 0036-8075 (Print) Journal Article Research Support,

Non-U.S. Gov't Research Support, U.S. Gov't, Non-P.H.S. Research Support, U.S. Gov't, P.H.S. Review.

Hebb, D. (1949). Organization of behavior: a Neuropsychological theory. (New York: John Wiley).

Hestrin, S., Nicoll, R. A., Perkel, D. J., & Sah, P. (1990). Analysis of excitatory synaptic action in pyramidal cells using whole-cell recording from rat hippocampal slices. J Physiol, 422, 203–225.

Hille, B. (2001). Ion channels of excitable membranes. (Sunderland, MA: Sinauer Associates).

Hines, M. L. & Carnevale, N. T. (1997). The NEURON simulation environment. Neural Comput, 9, 1179–209. 0899-7667 (Print) Journal Article Research Support, Non-U.S. Gov't Research Support, U.S. Gov't, P.H.S. Review.

Hodgkin, A. L. (1948). The local electric changes associated with repetitive action in a non-medullated axon. J Physiol, 107, 165–81. 0022-3751 (Print) Journal Article.

Hodgkin, A. L. & Huxley, A. F. (1952). A quantitative description of membrane current and its application to conduction and excitation in nerve. J Physiol, 117, 500–44. 0022-3751 (Print) Journal Article.

Hoffman, D. A., Magee, J. C., Colbert, C. M., & Johnston, D. (1997). K+ channel regulation of signal propagation in dendrites of hippocampal pyramidal neurons. Nature, 387, 869–75. 0028-0836 (Print) In Vitro Journal Article Research Support, Non-U.S. Gov't Research Support, U.S. Gov't, P.H.S.

Holthoff, K., Kovalchuk, Y., Yuste, R., & Konnerth, A. (2004). Single-shock ltd by local dendritic spikes in pyramidal neurons of mouse visual cortex. J Physiol, 560, 27–36.

0022-3751 (Print) Journal Article Research Support, Non-U.S. Gov't Research Support, U.S. Gov't, P.H.S.

Holtmaat, A., Wilbrecht, L., Knott, G. W., Welker, E., & Svoboda, K. (2006). Experience-dependent and cell-type-specific spine growth in the neocortex. Nature, 441, 979–83. 1476-4687 (Electronic) Journal Article Research Support, N.I.H., Extramural Research Support, Non-U.S. Gov't.

Holtmaat, A. J., Trachtenberg, J. T., Wilbrecht, L., Shepherd, G. M., Zhang, X., Knott, G. W., & Svoboda, K. (2005). Transient and persistent dendritic spines in the neocortex in vivo. Neuron, 45, 279–91. 0896-6273 (Print) Journal Article Research Support, Non-U.S. Gov't Research Support, U.S. Gov't, P.H.S.

Howard, M. & Kahana, M. (2002). A distributed representation of temporal context. J Math Psychol, 46, 269–299.

Howard, M. W., Fotedar, M. S., Datey, A. V., & Hasselmo, M. E. (2005). The temporal context model in spatial navigation and relational learning: toward a common explanation of medial temporal lobe function across domains. Psychol Rev, 112, 75–116. 0033-295X (Print) Journal Article.

Hubel, D. H. & Wiesel, T. N. (1963a). Receptive fields of cells in striate cortex of very young, visually inexperienced kittens. J Neurophysiol, 26, 994–1002. 0022-3077 (Print) Journal Article.

Hubel, D. H. & Wiesel, T. N. (1963b). Shape and arrangement of columns in cat's striate cortex. J Physiol, 165, 559–68. 0022-3751 (Print) Journal Article.

Isaac, J. T. R., Nicoll, R. A., & Malenka, R. C. (1995). Evidence for silent synapses: Implications for the expression of ltp. Neuron, 15, 427–434.

Ishizuka, N., Cowan, W. M., & Amaral, D. G. (1995). A quantitative analysis of the dendritic organization of pyramidal cells in the rat hippocampus. J Comp Neurol, 362, 17–45.

Izhikevich, E. M. (2003). Simple model of spiking neurons. IEEE Trans Neural Netw, 14, 1569–72. 1045-9227 (Print) Comparative Study Journal Article Research Support, Non-U.S. Gov't.

Izhikevich, E. M. (2007). Dynamical systems in neuroscience: The geometry of excitability and bursting. (MIT Press).

James, W. (1890). The principles of psychology. (New York: Holt).

Jarsky, T., Roxin, A., Kath, W. L., & Spruston, N. (2005). Conditional dendritic spike propagation following distal synaptic activation of hippocampal CA1 pyramidal neurons. Nat Neurosci, 8, 1667–76. 1097-6256 (Print) Journal Article Research Support, N.I.H., Extramural Research Support, U.S. Gov't, Non-P.H.S.

Jensen, O., Idiart, M. A., & Lisman, J. E. (1996). Physiologically realistic formation of autoassociative memory in networks with theta/gamma oscillations: role of fast nmda channels. Learn Mem, 3, 243–56. 1072-0502 (Print) Journal Article.

Jensen, O. & Lisman, J. E. (1998). An oscillatory short-term memory buffer model can account for data on the sternberg task. J Neurosci, 18, 10688–99. 0270-6474 (Print) Journal Article.

Jones, D. G. & Harris, R. J. (1995). An analysis of contemporary morphological concepts of synaptic remodelling in the cns: perforated synapses revisited. Rev Neurosci, 6, 177–219.

Jung, H. Y., Mickus, T., & Spruston, N. (1997). Prolonged sodium channel inactivation contributes to dendritic action potential attenuation in hippocampal pyramidal neurons. J Neurosci, 17, 6639–6646.

Kasai, H., Matsuzaki, M., Noguchi, J., Yasumatsu, N., & Nakahara, H. (2003). Structure-stability-function relationships of dendritic spines. Trends Neurosci, 26, 360–8. 0166-2236 (Print) Journal Article Research Support, Non-U.S. Gov't Review.

Katz, Y., Kath, W. L., Spruston, N., & Hasselmo, M. E. (2007). Coincidence detection of place and temporal context in a network model of spiking hippocampal neurons. PLoS Comput Biol, 3, e234.

Kaupmann, K., Huggel, K., Heid, J., Flor, P. J., Bischoff, S., Mickel, S. J., McMaster, G., Angst, C., Bittiger, H., Froestl, W., & Bettler, B. (1997). Expression cloning of gaba(b) receptors uncovers similarity to metabotropic glutamate receptors. Nature, 386, 239–46. 0028-0836 (Print) Journal Article.

Kennedy, M. B. (2000). Signal-processing machines at the postsynaptic density. Science, 290, 750–754.

Koch, C. & Zador, A. (1993). The function of dendritic spines: devices subserving biochemical rather than electrical compartmentalization. J Neurosci, 13, 413–22. 0270-6474 (Print) Journal Article Research Support, Non-U.S. Gov't Research Support, U.S. Gov't, Non-P.H.S. Research Support, U.S. Gov't, P.H.S. Review.

Koene, R. A., Gorchetchnikov, A., Cannon, R. C., & Hasselmo, M. E. (2003). Modeling goal-directed spatial navigation in the rat based on physiological data from the hippocampal formation. Neural Netw, 16, 577–84. 0893-6080 (Print) Journal Article.

Lang, C., Barco, A., Zablow, L., Kandel, E. R., Siegelbaum, S. A., & Zakharenko, S. S. (2004). Transient expansion of synaptically connected dendritic spines upon induction of hippocampal long-term potentiation. Proc Natl Acad Sci U S A, 101, 16665–16670.

Lee, I., Griffin, A. L., Zilli, E. A., Eichenbaum, H., & Hasselmo, M. E. (2006). Gradual translocation of spatial correlates of neuronal firing in the hippocampus toward prospective reward locations. Neuron, 51, 639–50. 0896-6273 (Print) Journal Article Research Support, N.I.H., Extramural Research Support, Non-U.S. Gov't Research Support, U.S. Gov't, Non-P.H.S.

Lee, I., Hunsaker, M. R., & Kesner, R. P. (2005). The role of hippocampal subregions in detecting spatial novelty. Behav Neurosci, 119, 145–53. 0735-7044 (Print) Journal Article.

Lee, I., Rao, G., & Knierim, J. J. (2004). A double dissociation between hippocampal subfields: differential time course of CA3 and CA1 place cells for processing changed environments. Neuron, 42, 803–15. 0896-6273 (Print) Comparative Study Journal Article Research Support, Non-U.S. Gov't Research Support, U.S. Gov't, P.H.S.

Lenck-Santini, P. P., Save, E., & Poucet, B. (2001). Place-cell firing does not depend on the direction of turn in a y-maze alternation task. Eur J Neurosci, 13, 1055–8. 0953-816X (Print) Journal Article.

Lesage, F. & Lazdunski, M. (2000). Molecular and functional properties of two-pore-domain potassium channels. Am J Physiol Renal Physiol, 279, F793–801. 0363-6127 (Print) Journal Article Review.

Leutgeb, S., Leutgeb, J. K., Barnes, C. A., Moser, E. I., McNaughton, B. L., & Moser, M. B. (2005). Independent codes for spatial and episodic memory in hippocampal neuronal ensembles. Science, 309, 619–23. 1095-9203 (Electronic) Journal Article Research Support, Non-U.S. Gov't.

Li, K. W., Hornshaw, M. P., Schors, R. C. V. D., Watson, R., Tate, S., Casetta, B., Jimenez, C. R., Gouwenberg, Y., Gundelfinger, E. D., Smalla, K.-H., & Smit, A. B. (2004). Proteomics analysis of rat brain postsynaptic density. implications of the diverse protein functional groups for the integration of synaptic physiology. J Biol Chem, 279, 987–1002.

Liao, D., Hessler, N. A., & Malinow, R. (1995). Activation of postsynaptically silent synapses during pairing-induced ltp in ca1 region of hippocampal slice. Nature, 375, 400–404.

Liu, G., Choi, S., & Tsien, R. W. (1999). Variability of neurotransmitter concentration and nonsaturation of postsynaptic ampa receptors at synapses in hippocampal cultures and slices. Neuron, 22, 395–409.

Lorincz, A., Notomi, T., Tamas, G., Shigemoto, R., & Nusser, Z. (2002). Polarized and compartment-dependent distribution of hcn1 in pyramidal cell dendrites. Nat Neurosci, 5, 1185–93. 1097-6256 (Print) Journal Article Research Support, Non-U.S. Gov't.

Losonczy, A. & Magee, J. C. (2006). Integrative properties of radial oblique dendrites in hippocampal CA1 pyramidal neurons. Neuron, 50, 291–307. 0896-6273 (Print) Journal Article Research Support, N.I.H., Extramural.

Losonczy, A., Makara, J. K., & Magee, J. C. (2008). Compartmentalized dendritic plasticity and input feature storage in neurons. Nature, 452, 436–441.

Mackenzie, P. J., Kenner, G. S., Prange, O., Shayan, H., Umemiya, M., & Murphy, T. H. (1999). Ultrastructural correlates of quantal synaptic function at single cns synapses. J Neurosci, 19, RC13.

Magee, J. (2008). Dendrites. (Oxford: Oxford University Press).

Magee, J. C. (1998). Dendritic hyperpolarization-activated currents modify the integrative properties of hippocampal CA1 pyramidal neurons. J Neurosci, 18, 7613–24. 0270-6474 (Print) Journal Article Research Support, U.S. Gov't, P.H.S.

Magee, J. C. (1999). Dendritic ih normalizes temporal summation in hippocampal CA1 neurons. Nat Neurosci, 2, 848. 1097-6256 (Print) Journal article.

Magee, J. C. & Cook, E. P. (2000). Somatic epsp amplitude is independent of synapse location in hippocampal pyramidal neurons. Nat Neurosci, 3, 895–903. 1097-6256 (Print) Journal Article Research Support, Non-U.S. Gov't Research Support, U.S. Gov't, P.H.S.

Magee, J. C. & Johnston, D. (1995). Characterization of single voltage-gated na+ and ca2+ channels in apical dendrites of rat ca1 pyramidal neurons. J Physiol, 487 (Pt 1), 67–90.

Magee, J. C. & Johnston, D. (1997). A synaptically controlled, associative signal for hebbian plasticity in hippocampal neurons. Science, 275, 209–13. 0036-8075 (Print) In Vitro Journal Article Research Support, U.S. Gov't, P.H.S.

Maguire, E. A., Gadian, D. G., Johnsrude, I. S., Good, C. D., Ashburner, J., Frackowiak, R. S., & Frith, C. D. (2000). Navigation-related structural change in the hippocampi of taxi drivers. Proc Natl Acad Sci U S A, 97, 4398–403. 0027-8424 (Print) Journal Article Research Support, Non-U.S. Gov't.

Maguire, E. A., Woollett, K., & Spiers, H. J. (2006). London taxi drivers and bus drivers: a structural mri and neuropsychological analysis. Hippocampus, 16, 1091–101. 1050-9631 (Print) Comparative Study Journal Article Research Support, Non-U.S. Gov't.

Mainen, Z. F., Malinow, R., & Svoboda, K. (1999). Synaptic calcium transients in single spines indicate that nmda receptors are not saturated. Nature, 399, 151–155.

Mann, E. O. & Paulsen, O. (2007). Role of gabaergic inhibition in hippocampal network oscillations. Trends Neurosci, 30, 343–9. 0166-2236 (Print) Journal Article Research Support, Non-U.S. Gov't Review.

Markus, E. J., Qin, Y. L., Leonard, B., Skaggs, W. E., McNaughton, B. L., & Barnes, C. A. (1995). Interactions between location and task affect the spatial and directional firing of hippocampal neurons. J Neurosci, 15, 7079–94. 0270-6474 (Print) Journal Article Research Support, U.S. Gov't, Non-P.H.S. Research Support, U.S. Gov't, P.H.S.

Matsuzaki, M., Honkura, N., Ellis-Davies, G. C., & Kasai, H. (2004). Structural basis of long-term potentiation in single dendritic spines. Nature, 429, 761–6. 1476-4687 (Electronic) In Vitro Journal Article Research Support, Non-U.S. Gov't Research Support, U.S. Gov't, Non-P.H.S.

Matus, A. (2000). Actin-based plasticity in dendritic spines. Science, 290, 754–8. 0036-8075 (Print) Journal Article Review.

Maurer, A. P., Cowen, S. L., Burke, S. N., Barnes, C. A., & McNaughton, B. L. (2006). Organization of hippocampal cell assemblies based on theta phase precession. Hippocampus, 16, 785–94. 1050-9631 (Print) Journal Article Research Support, N.I.H., Extramural.

McAllister, A. K. & Stevens, C. F. (2000). Nonsaturation of ampa and nmda receptors at hippocampal synapses. Proc Natl Acad Sci U S A, 97, 6173–6178.

McBain, C. J. & Fisahn, A. (2001). Interneurons unbound. Nat Rev Neurosci, 2, 11–23. 1471-003X (Print) Journal Article Review.

McNaughton, B. L., Barnes, C. A., Meltzer, J., & Sutherland, R. J. (1989). Hippocampal granule cells are necessary for normal spatial learning but not for spatially-selective pyramidal cell discharge. Exp Brain Res, 76, 485–96. 0014-4819 (Print) Journal Article Research Support, Non-U.S. Gov't Research Support, U.S. Gov't, P.H.S.

McNaughton, B. L., Barnes, C. A., & O'Keefe, J. (1983). The contributions of position, direction, and velocity to single unit activity in the hippocampus of freely-moving rats. Exp Brain Res, 52, 41–9. 0014-4819 (Print) Journal Article.

Megias, M., Emri, Z., Freund, T. F., & Gulyas, A. I. (2001). Total number and distribution of inhibitory and excitatory synapses on hippocampal CA1 pyramidal cells. Neuroscience, 102, 527–40. 0306-4522 (Print) Journal Article Research Support, Non-U.S. Gov't Research Support, U.S. Gov't, P.H.S.

Mehta, M. R., Lee, A. K., & Wilson, M. A. (2002). Role of experience and oscillations in transforming a rate code into a temporal code. Nature, 417, 741–6. 0028-0836 (Print) Journal Article Research Support, Non-U.S. Gov't Research Support, U.S. Gov't, P.H.S.

Metz, A. E., Jarsky, T., Martina, M., & Spruston, N. (2005). R-type calcium channels contribute to afterdepolarization and bursting in hippocampal ca1 pyramidal neurons. J Neurosci, 25, 5763–5773.

Mickus, T., Jung, H., & Spruston, N. (1999). Properties of slow, cumulative sodium channel inactivation in rat hippocampal ca1 pyramidal neurons. Biophys J, 76, 846–860.

Migliore, M., Hoffman, D. A., Magee, J. C., & Johnston, D. (1999). Role of an a-type k+ conductance in the back-propagation of action potentials in the dendrites of hippocampal pyramidal neurons. J Comput Neurosci, 7, 5–15. 0929-5313 (Print) Journal Article Research Support, Non-U.S. Gov't Research Support, U.S. Gov't, P.H.S.

Miles, R., Toth, K., Gulyas, A. I., Hajos, N., & Freund, T. F. (1996). Differences between somatic and dendritic inhibition in the hippocampus. Neuron, 16, 815–23. 0896-6273 (Print) In Vitro Journal Article Research Support, Non-U.S. Gov't.

Milner, B. & Penfield, W. (1955). The effect of hippocampal lesions on recent memory. Trans Am Neurol Assoc, 1, 42–8. 0065-9479 (Print) Journal Article.

Mizumori, S. J., McNaughton, B. L., Barnes, C. A., & Fox, K. B. (1989). Preserved spatial coding in hippocampal ca1 pyramidal cells during reversible suppression of ca3c output: evidence for pattern completion in hippocampus. J Neurosci, 9, 3915–28. 0270-6474 (Print) Journal Article Research Support, U.S. Gov't, P.H.S.

Morris, C. & Lecar, H. (1981). Voltage oscillations in the barnacle giant muscle fiber. Biophys J, 35, 193–213. 0006-3495 (Print) Comparative Study Journal Article.

Morris, R. G. (2001). Episodic-like memory in animals: psychological criteria, neural mechanisms and the value of episodic-like tasks to investigate animal models of neurodegenerative disease. Philos Trans R Soc Lond B Biol Sci, 356, 1453–1465.

Narayanan, R. & Johnston, D. (2007). Long-term potentiation in rat hippocampal neurons is accompanied by spatially widespread changes in intrinsic oscillatory dynamics and

excitability. Neuron, 56, 1061–1075.

Narayanan, R. & Johnston, D. (2008). The h channel mediates location dependence and plasticity of intrinsic phase response in rat hippocampal neurons. J. Neurosci., 28, 5846–5450.

Neher, E., Sakmann, B., & Steinbach, J. H. (1978). The extracellular patch clamp: a method for resolving currents through individual open channels in biological membranes. Pflugers Arch, 375, 219–28. 0031-6768 (Print) Journal Article.

Nevian, T., Larkum, M. E., Polsky, A., & Schiller, J. (2007). Properties of basal dendrites of layer 5 pyramidal neurons: a direct patch-clamp recording study. Nat Neurosci, 10, 206–14. 1097-6256 (Print) Journal Article Research Support, N.I.H., Extramural Research Support, Non-U.S. Gov't.

Nicholson, D. A. & Geinisman, Y. (2006). Structural synaptic correlates of learning and memory. Molecular mechanisms of synaptogenesis. (U.S.: Springer).

Nicholson, D. A., Trana, R., Katz, Y., Kath, W. L., Spruston, N., & Geinisman, Y. (2006). Distance-dependent differences in synapse number and ampa receptor expression in hippocampal CA1 pyramidal neurons. Neuron, 50, 431–42. 0896-6273 (Print) Journal Article Research Support, N.I.H., Extramural Research Support, U.S. Gov't, Non-P.H.S.

Nikonenko, I., Jourdain, P., Alberi, S., Toni, N., & Muller, D. (2002). Activity-induced changes of spine morphology. Hippocampus, 12, 585–591.

Nimchinsky, E. A., Sabatini, B. L., & Svoboda, K. (2002). Structure and function of dendritic spines. Annu Rev Physiol, 64, 313–53. 0066-4278 (Print) Journal Article Research Support, Non-U.S. Gov't Review.

Noguchi, J., Matsuzaki, M., Ellis-Davies, G. C. R., & Kasai, H. (2005). Spine-neck geometry determines nmda receptor-dependent ca2+ signaling in dendrites. Neuron, 46, 609–622.

Nusser, Z. (2000). Ampa and nmda receptors: similarities and differences in their synaptic distribution. Curr Opin Neurobiol, 10, 337–341.

Nusser, Z., Cull-Candy, S., & Farrant, M. (1997). Differences in synaptic gaba(a) receptor number underlie variation in gaba mini amplitude. Neuron, 19, 697–709.

Nusser, Z., Hjos, N., Somogyi, P., & Mody, I. (1998a). Increased number of synaptic gaba(a) receptors underlies potentiation at hippocampal inhibitory synapses. Nature, 395, 172–177.

Nusser, Z., Lujan, R., Laube, G., Roberts, J. D., Molnar, E., & Somogyi, P. (1998b). Cell type and pathway dependence of synaptic ampa receptor number and variability in the hippocampus. Neuron, 21, 545–559.

O'Keefe, J. & Burgess, N. (2005). Dual phase and rate coding in hippocampal place cells: theoretical significance and relationship to entorhinal grid cells. Hippocampus, 15, 853–66. 1050-9631 (Print) Journal Article Research Support, Non-U.S. Gov't Review.

O'Keefe, J. & Dostrovsky, J. (1971). The hippocampus as a spatial map. preliminary evidence from unit activity in the freely-moving rat. Brain Res, 34, 171–5. 0006-8993 (Print) Journal Article.

O'Keefe, J. & Nadel, L. (1978). The hippocampus as a cognitive map. (Oxford University Press).

O'Keefe, J. & Recce, M. L. (1993). Phase relationship between hippocampal place units and the eeg theta rhythm. Hippocampus, 3, 317–30. 1050-9631 (Print) Journal Article.

Otmakhova, N. A., Otmakhov, N., & Lisman, J. E. (2002). Pathway-specific properties of ampa and nmda-mediated transmission in ca1 hippocampal pyramidal cells. J Neurosci, 22, 1199–1207.

Ottersen, O. P. & Landsend, A. S. (1997). Organization of glutamate receptors at the synapse. Eur J Neurosci, 9, 2219–2224.

Otto, T. & Poon, P. (2006). Dorsal hippocampal contributions to unimodal contextual conditioning. J Neurosci, 26, 6603–9. 1529-2401 (Electronic) Comparative Study Journal Article Research Support, U.S. Gov't, Non-P.H.S.

Peng, J., Kim, M. J., Cheng, D., Duong, D. M., Gygi, S. P., & Sheng, M. (2004). Semiquantitative proteomic analysis of rat forebrain postsynaptic density fractions by mass spectrometry. J Biol Chem, 279, 21003–21011.

Peters, A. & Kaiserman-Abramof, I. R. (1969). The small pyramidal neuron of the rat cerebral cortex. the synapses upon dendritic spines. Z Zellforsch Mikrosk Anat, 100, 487–506. 0340-0336 (Print) Journal Article.

Petralia, R. S., Esteban, J. A., Wang, Y. X., Partridge, J. G., Zhao, H. M., Wenthold, R. J., & Malinow, R. (1999). Selective acquisition of ampa receptors over postnatal development suggests a molecular basis for silent synapses. Nat Neurosci, 2, 31–36.

Poirazi, P., Brannon, T., & Mel, B. W. (2003). Arithmetic of subthreshold synaptic summation in a model CA1 pyramidal cell. Neuron, 37, 977–87. 0896-6273 (Print) Journal Article Research Support, Non-U.S. Gov't Research Support, U.S. Gov't, Non-P.H.S.

Polsky, A., Mel, B. W., & Schiller, J. (2004). Computational subunits in thin dendrites of pyramidal cells. Nat Neurosci, 7, 621–7. 1097-6256 (Print) Journal Article Research

Support, Non-U.S. Gov't Research Support, U.S. Gov't, Non-P.H.S. Research Support, U.S. Gov't, P.H.S.

Pouille, F. & Scanziani, M. (2001). Enforcement of temporal fidelity in pyramidal cells by somatic feed-forward inhibition. Science, 293, 1159–63. 0036-8075 (Print) In Vitro Journal Article Research Support, Non-U.S. Gov't.

Pouille, F. & Scanziani, M. (2004). Routing of spike series by dynamic circuits in the hippocampus. Nature, 429, 717–23. 1476-4687 (Electronic) In Vitro Journal Article Research Support, Non-U.S. Gov't Research Support, U.S. Gov't, P.H.S.

Racca, C., Stephenson, F. A., Streit, P., Roberts, J. D., & Somogyi, P. (2000). Nmda receptor content of synapses in stratum radiatum of the hippocampal ca1 area. J Neurosci, 20, 2512–2522.

Raghavachari, S. & Lisman, J. E. (2004). Properties of quantal transmission at ca1 synapses. J Neurophysiol, 92, 2456–2467.

Rall, W. (1959). Branching dendritic trees and motoneuron membrane resistivity. Exp Neurol, 1, 491–527. 0014-4886 (Print) Journal Article.

Rall, W. (1964). Theoretical significance of dendritic trees for neuronal input-output relations. Neural theory and modeling. (Palo Alto: Stanford University Press).

Rall, W. (1967). Distinguishing theoretical synaptic potentials computed for different soma-dendritic distributions of synaptic input. J Neurophysiol, 30, 1138–68. 0022-3077 (Print) Journal Article.

Rall, W. (1977). Core conductor theory and cable properties of neurons. In Handbook of Physiology. The Nervous System. Cellular Biology of Neurons, E. R. Kandel, J. M. Brookhart, & V. B. Mountcastle, eds. (American Physiological Society, Bethesda, MD).

Ramon y Cajal, S. (1897). Histology of the nervous system of man and vertebrates. (Oxford: Oxford University Press (Reprinted 1995)).

Rasband, W. (1997-2007). Imagej.

Remy, S. & Spruston, N. (2007). Dendritic spikes induce single-burst long-term potentiation. Proc Natl Acad Sci U S A, 104, 17192–7. 0027-8424 (Print) Journal Article Research Support, N.I.H., Extramural Research Support, Non-U.S. Gov't.

Rolls, E. T. & Kesner, R. P. (2006). A computational theory of hippocampal function, and empirical tests of the theory. Prog Neurobiol, 79, 1–48. 0301-0082 (Print) Journal Article Research Support, N.I.H., Extramural Research Support, Non-U.S. Gov't Research Support, U.S. Gov't, Non-P.H.S. Review.

Schiller, J., Major, G., Koester, H. J., & Schiller, Y. (2000). Nmda spikes in basal dendrites of cortical pyramidal neurons. Nature, 404, 285–9. 0028-0836 (Print) In Vitro Journal Article Research Support, Non-U.S. Gov't.

Schiller, J. & Schiller, Y. (2001). Nmda receptor-mediated dendritic spikes and coincident signal amplification. Curr Opin Neurobiol, 11, 343–8. 0959-4388 (Print) Journal Article Research Support, Non-U.S. Gov't Review.

Schiller, J., Schiller, Y., Stuart, G., & Sakmann, B. (1997). Calcium action potentials restricted to distal apical dendrites of rat neocortical pyramidal neurons. J Physiol, 505 (Pt 3), 605–16. 0022-3751 (Print) In Vitro Journal Article Research Support, Non-U.S. Gov't.

Scoville, W. B. (1954). The limbic lobe in man. J Neurosurg, 11, 64–6. 0022-3085 (Print) Journal Article.

Shapiro, M. L., Kennedy, P. J., & Ferbinteanu, J. (2006). Representing episodes in the mammalian brain. Curr Opin Neurobiol, 16, 701–9. 0959-4388 (Print) Journal Article.

Silberberg, G. & Markram, H. (2007). Disynaptic inhibition between neocortical pyramidal cells mediated by martinotti cells. Neuron, 53, 735–46. 0896-6273 (Print) Journal Article Research Support, Non-U.S. Gov't.

Skaggs, W. E., McNaughton, B. L., Wilson, M. A., & Barnes, C. A. (1996). Theta phase precession in hippocampal neuronal populations and the compression of temporal sequences. Hippocampus, 6, 149–72. 1050-9631 (Print) Journal Article.

Smith, M. A., Ellis-Davies, G. C. R., & Magee, J. C. (2003). Mechanism of the distance-dependent scaling of schaffer collateral synapses in rat ca1 pyramidal neurons. J Physiol, 548, 245–258.

Somogyi, P. & Klausberger, T. (2005). Defined types of cortical interneurone structure space and spike timing in the hippocampus. J Physiol, 562, 9–26. 0022-3751 (Print) Journal Article Research Support, Non-U.S. Gov't Review.

Sorra, K. E., Fiala, J. C., & Harris, K. M. (1998). Critical assessment of the involvement of perforations, spinules, and spine branching in hippocampal synapse formation. J Comp Neurol, 398, 225–40. 0021-9967 (Print) Journal Article Research Support, Non-U.S. Gov't Research Support, U.S. Gov't, Non-P.H.S. Research Support, U.S. Gov't, P.H.S.

Sorra, K. E. & Harris, K. M. (2000). Overview on the structure, composition, function, development, and plasticity of hippocampal dendritic spines. Hippocampus, 10, 501–11. 1050-9631 (Print) Journal Article Research Support, U.S. Gov't, Non-P.H.S. Research Support, U.S. Gov't, P.H.S. Review.

Spruston, N. (2008). Pyramidal neurons: dendritic structure and synaptic integration. Nat Rev Neurosci, 9, 206–21. 1471-0048 (Electronic) Journal Article Research Support, N.I.H., Extramural Review.

Spruston, N., Jonas, P., & Sakmann, B. (1995). Dendritic glutamate receptor channels in rat hippocampal ca3 and ca1 pyramidal neurons. J Physiol, 482 (Pt 2), 325–352.

Spruston, N. & Kath, W. L. (2004). Dendritic arithmetic. Nat Neurosci, 7, 567–9. 1097-6256 (Print) Comment News.

Squire, L. R. (1992). Memory and the hippocampus: a synthesis from findings with rats, monkeys, and humans. Psychol Rev, 99, 195–231. 0033-295X (Print) Journal Article Research Support, Non-U.S. Gov't Research Support, U.S. Gov't, Non-P.H.S. Research Support, U.S. Gov't, P.H.S. Review.

Steffenach, H. A., Witter, M., Moser, M. B., & Moser, E. I. (2005). Spatial memory in the rat requires the dorsolateral band of the entorhinal cortex. Neuron, 45, 301–13. 0896-6273 (Print) Journal Article.

Storm, J. F. (1987). Action potential repolarization and a fast after-hyperpolarization in rat hippocampal pyramidal cells. J Physiol, 385, 733–59. 0022-3751 (Print) In Vitro Journal Article Research Support, Non-U.S. Gov't Research Support, U.S. Gov't, Non-P.H.S. Research Support, U.S. Gov't, P.H.S. Review.

Stuart, G. & Sakmann, B. (1995). Amplification of epsps by axosomatic sodium channels in neocortical pyramidal neurons. Neuron, 15, 1065–76. 0896-6273 (Print) Journal Article Research Support, Non-U.S. Gov't.

Stuart, G., Schiller, J., & Sakmann, B. (1997a). Action potential initiation and propagation in rat neocortical pyramidal neurons. J Physiol, 505 (Pt 3), 617–32. 0022-3751

(Print) In Vitro Journal Article Research Support, Non-U.S. Gov't.

Stuart, G., Spruston, N., Sakmann, B., & Hausser, M. (1997b). Action potential initiation and backpropagation in neurons of the mammalian cns. Trends Neurosci, 20, 125–31. 0166-2236 (Print) Journal Article Research Support, Non-U.S. Gov't Review.

Stuart, G. J. & Hausser, M. (2001). Dendritic coincidence detection of epsps and action potentials. Nat Neurosci, 4, 63–71. 1097-6256 (Print) In Vitro Journal Article Research Support, Non-U.S. Gov't.

Szabadics, J., Varga, C., Molnar, G., Olah, S., Barzo, P., & Tamas, G. (2006). Excitatory effect of gabaergic axo-axonic cells in cortical microcircuits. Science, 311, 233–5. 1095-9203 (Electronic) In Vitro Journal Article Research Support, N.I.H., Extramural Research Support, Non-U.S. Gov't.

Tahvildari, B., Fransen, E., Alonso, A., & Hasselmo, M. (2007). Switching between on and off states of persistent activity lateral entorhinal layer iii neurons. Hippocampus, in press.

Takumi, Y., Ramrez-Len, V., Laake, P., Rinvik, E., & Ottersen, O. P. (1999). Different modes of expression of ampa and nmda receptors in hippocampal synapses. Nat Neurosci, 2, 618–624.

Trommald, M. & Hulleberg, G. (1997). Dimensions and density of dendritic spines from rat dentate granule cells based on reconstructions from serial electron micrographs. J Comp Neurol, 377, 15–28. 0021-9967 (Print) Journal Article Research Support, Non-U.S. Gov't.

Tsay, D. & Yuste, R. (2004). On the electrical function of dendritic spines. Trends Neurosci, 27, 77–83. 0166-2236 (Print) Comparative Study Journal Article Research

Support, Non-U.S. Gov't Research Support, U.S. Gov't, P.H.S. Review.

Tsubokawa, H. & Ross, W. N. (1996). IPSPs modulate spike backpropagation and associated [ca2+]i changes in the dendrites of hippocampal CA1 pyramidal neurons. J Neurophysiol, 76, 2896–906. 0022-3077 (Print) Journal Article Research Support, Non-U.S. Gov't Research Support, U.S. Gov't, P.H.S.

Tulving, E. (2002). Episodic memory: from mind to brain. Annu Rev Psychol, 53, 1–25. 0066-4308 (Print) Case Reports Journal Article.

Tulving, E. & Markowitsch, H. J. (1998). Episodic and declarative memory: role of the hippocampus. Hippocampus, 8, 198–204. 1050-9631 (Print) Journal Article Research Support, Non-U.S. Gov't Review.

Turrigiano, G. G. (1999). Homeostatic plasticity in neuronal networks: the more things change, the more they stay the same. Trends Neurosci, 22, 221–7. 0166-2236 (Print) Journal Article Research Support, U.S. Gov't, P.H.S. Review.

Turrigiano, G. G. & Nelson, S. B. (2004). Homeostatic plasticity in the developing nervous system. Nat Rev Neurosci, 5, 97–107. 1471-003X (Print) Journal Article Review.

Vetter, P., Roth, A., & Hausser, M. (2001). Propagation of action potentials in dendrites depends on dendritic morphology. J Neurophysiol, 85, 926–37. 0022-3077 (Print) Journal Article Research Support, Non-U.S. Gov't.

Wei, D. S., Mei, Y. A., Bagal, A., Kao, J. P., Thompson, S. M., & Tang, C. M. (2001). Compartmentalized and binary behavior of terminal dendrites in hippocampal pyramidal neurons. Science, 293, 2272–2275.

Williams, S. R. & Stuart, G. J. (2000). Site independence of epsp time course is mediated by dendritic i(h) in neocortical pyramidal neurons. J Neurophysiol, 83, 3177–82. 0022-3077 (Print) In Vitro Journal Article.

Williams, S. R. & Stuart, G. J. (2002). Dependence of epsp efficacy on synapse location in neocortical pyramidal neurons. Science, 295, 1907–10. 1095-9203 (Electronic) Journal Article Research Support, Non-U.S. Gov't.

Williams, S. R. & Stuart, G. J. (2003). Role of dendritic synapse location in the control of action potential output. Trends Neurosci, 26, 147–154.

Wilson, H. R. & Cowan, J. D. (1972). Excitatory and inhibitory interactions in localized populations of model neurons. Biophys J, 12, 1–24. 0006-3495 (Print) Journal Article.

Wilson, M. A. & McNaughton, B. L. (1993). Dynamics of the hippocampal ensemble code for space. Science, 261, 1055–8. 0036-8075 (Print) Journal Article.

Wood, E. R., Dudchenko, P. A., Robitsek, R. J., & Eichenbaum, H. (2000). Hippocampal neurons encode information about different types of memory episodes occurring in the same location. Neuron, 27, 623–33. 0896-6273 (Print) Journal Article.

Yu, F. H. & Catterall, W. A. (2003). Overview of the voltage-gated sodium channel family. Genome Biol, 4, 207. 1465-6914 (Electronic) Journal Article Review.